ANALYTICAL INVESTIGATIONS OF LAMINAR SEPARATIONS USING THE "CROCCO-LEES MIXING PARAMETER" METHOD

By

ALEXANDER ROBERT PETERS

Bachelor of Science
University of Nebraska
Lincoln, Nebraska
1959

Master of Science
University of Nebraska
Lincoln, Nebraska
1963

Submitted to the Faculty of the Graduate College of
the Oklahoma State University
in partial fulfillment of the requirements
for the degree of
DOCTOR OF PHILOSOPHY
May, 1967

ANALYTICAL INVESTIGATIONS OF LAMINAR SEPARATIONS USING THE "CROCCO-LEES MIXING PARAMETER" METHOD

Thesis Approved:

Donald R. Haworth
Thesis Adviser

Glen W. Zumwalt

J. Paul Hartzer

Ladislaus J. Fila

D. D. Durham
Dean of the Graduate College

ACKNOWLEDGMENTS

I would like to express my appreciation to my wife, Jane, for being understanding and patient during my years of graduate study. Her encouragement was a great help during the moments of frustration and discouragement which accompany work of this type.

A special note of thanks goes to my principal adviser, Dr. D. R. Haworth, for the many hours of consultation and assistance which he devoted to this topic. Dr. Haworth's foresight and guidance was of great help in the overall investigation. The cooperation given by others on my committee, Dr. G. W. Zumwalt, Professor L. J. Fila, and Dr. J. P. Devlin, is gratefully acknowledged.

The author is indebted to Mrs. Barbara Fluent for her assistance in typing the rough draft and final copy of the manuscript.

As a final note, I would like to acknowledge the sincere and professional manner in which the graduate program in the Mechanical Engineering Department is administered. The availability of a fine library, an accessible computing center, and a realistic set of departmental ground rules were certainly instrumental in my progress.

TABLE OF CONTENTS

Chapter Page

LIST OF TABLES

LIST OF FIGURES

NOMENCLATURE

A	momentum parameter = 0.44
a	speed of sound
$C, C(K)$	mixing rate correlation function
$\overline{C}, C_1, C_2$	average values of C(K)
c_f	skin friction coefficient
$D, D(K)$	skin friction correlation function
f	defined in equation (2)
$F, F(K)$	defined in equation (3)
I	momentum flux = $\int_o^\delta \rho\ u^2\ dy$
k	$(d\delta/dx) - \theta$
k_1, k_2, k_3, k_4	terms in Runge-Kutta method
$\overline{m}$	mass flux in the x-direction = $\int_o^\delta \rho\ u\ dy$
m	$\overline{m}\ a_t$
M	Mach number
$M_{e1}, M_{e2}, M_{e3}, M_{e4}$	terms in Runge Kutta method, Mach numbers
p	pressure
q_0, q_1, q_2, q_3, q_4	terms in Runge-Kutta method
R	gas constant
Re	Reynolds number
Re_δ^{**}	$\simeq \sqrt{A}\ \sqrt{Re_{x_b}}$
T	temperature
t	$T_e/T_t = (1 - \frac{\gamma-1}{2} w_e^2)$

u	velocity in x-direction
w	u/a_t
x,y	coordinates along and normal to the wall
γ	ratio of specific heats
Δ	incremental step
δ	boundary layer thickness
δ^*	displacement thickness
δ^{**}	momentum thickness
ε	$M_e - M_\infty$
ζ	$m/\mu_t a_t$
θ	streamline direction relative to the wall at $y = \delta$
K	Crocco-Lees velocity profile parameter
μ	coefficient of viscosity
ρ	density
σ	$D(K)/2(1-K)\ C(K)$
τ	shear stress
ϕ_e	$(1 - \frac{\gamma-1}{2} w_e^2)/\gamma w_e$
ϕ_1	$(T_1/T_t)\ (1/\gamma w_1)$

Subscripts:

b	Blasius flat plate conditions
c	plate-ramp corner
e	conditions at $y = \delta$
i	incompressible conditions
o	conditions at start of interaction region
p	plateau
r	beginning of reattachment
s	conditions at separation

t	free stream stagnation conditions
w	wall
x	at location x
l	mean value of viscous region
∞	free stream conditions

CHAPTER I

INTRODUCTION

The purpose of this thesis is to provide an analytical method for calculating the pressure distribution which results from a two-dimensional separation interaction. Because of its allied practical applications, the model used is the two-dimensional flat plate with an attached deflected flap. The flow throughout the entire compression process is assumed to be laminar and in the supersonic-hypersonic regime.

At present, the techniques for obtaining an engineering solution to this problem are virtually non-existent. The limitation which is characteristic of most solutions previously proposed is that the engineer must use information which he does not have available. For example, if the separation point is known, the entire pressure distribution may be obtained. These become merely methods for reproducing an experimental pressure distribution once some characteristic of the flow has been found experimentally.

The technique which is developed in this thesis makes use of the Crocco-Lees mixing theory. Because this theory is semi-empirical, the correlations which are developed represent an extension in the present understanding of how the parameters behave downstream from separation. By utilizing these correlations and employing a model which incorporates a straight dividing streamline, the complete separation-reattachment interaction is solved for the resulting surface pressure distribution.

This pressure field is obtained by making use only of the free stream conditions ahead of the interaction and the model geometry.

The Separated Flow Problem

Since separated and reattaching flows can occur under a variety of circumstances, an understanding of these phenomena are of great importance in the solution of many engineering design problems. The flow may be laminar, transitional, or turbulent; steady or unsteady; and subsonic or supersonic. In all cases, the main cause of the phenomenon of separation can be traced to the inability of the low energy viscous region adjacent to a body to adjust to the imposed inviscid pressure distribution.

Current interest in high velocity flight, whether aircraft or suborbital vehicles, has stimulated considerable research in the supersonic and hypersonic separation problem. Among the problems encountered are control requirements and the prediction of pressures on the body surface. Large and often unpredictable changes in aerodynamic control characteristics result when an airflow separates from the body surface. These control complexities become more severe at high velocities due to the energy level of the flow. In the design of future hypersonic vehicles, separated flows and their effects on the control characteristics must be well-understood.

Effective aerodynamic controls usually involve compressions of the local stream flow. This is because the pressure loads produced by compression surfaces are considerably larger than those produced by expansion surfaces. Separations which result from this type of compression turn have received the most attention because of their probable use in

hypersonic flight controls. This application provides justification for the analytical and experimental interest in the two-dimensional plate and ramp model.

The adverse pressure gradient which causes the relatively low velocity layer near the surface to decelerate and ultimately reverse may result from several causes. In general, it usually results from the effect of body geometry on the inviscid stream, or it may be caused by a shock wave impinging on the boundary layer, or both. The thickening of the boundary layer from these various causes affects the surface pressure distribution. Despite the simple description, separation phenomena are quite complex.

Figure 1 presents the essential features of the two-dimensional free interaction separation caused by a flat plate and ramp. It should be mentioned that the separation and reattachment shocks coalesce into a single shock at a distance above the boundary layer. The fluid near the body passes through a succession of weak shocks, while the flow well out into the inviscid layer passes through only a single shock.

Scope of Investigation

Considering this separation problem from the perspective of the engineer who in the end must apply the theories to hardware applications, the problem becomes clouded with complications. The flow conditions ahead of the interaction and the geometry are the only quantities which are known in advance. The locations of separation and reattachment, and the distribution of pressure throughout the interaction region are not known initially. This is one important class of problems in which the static pressures are not given, but must be determined by the

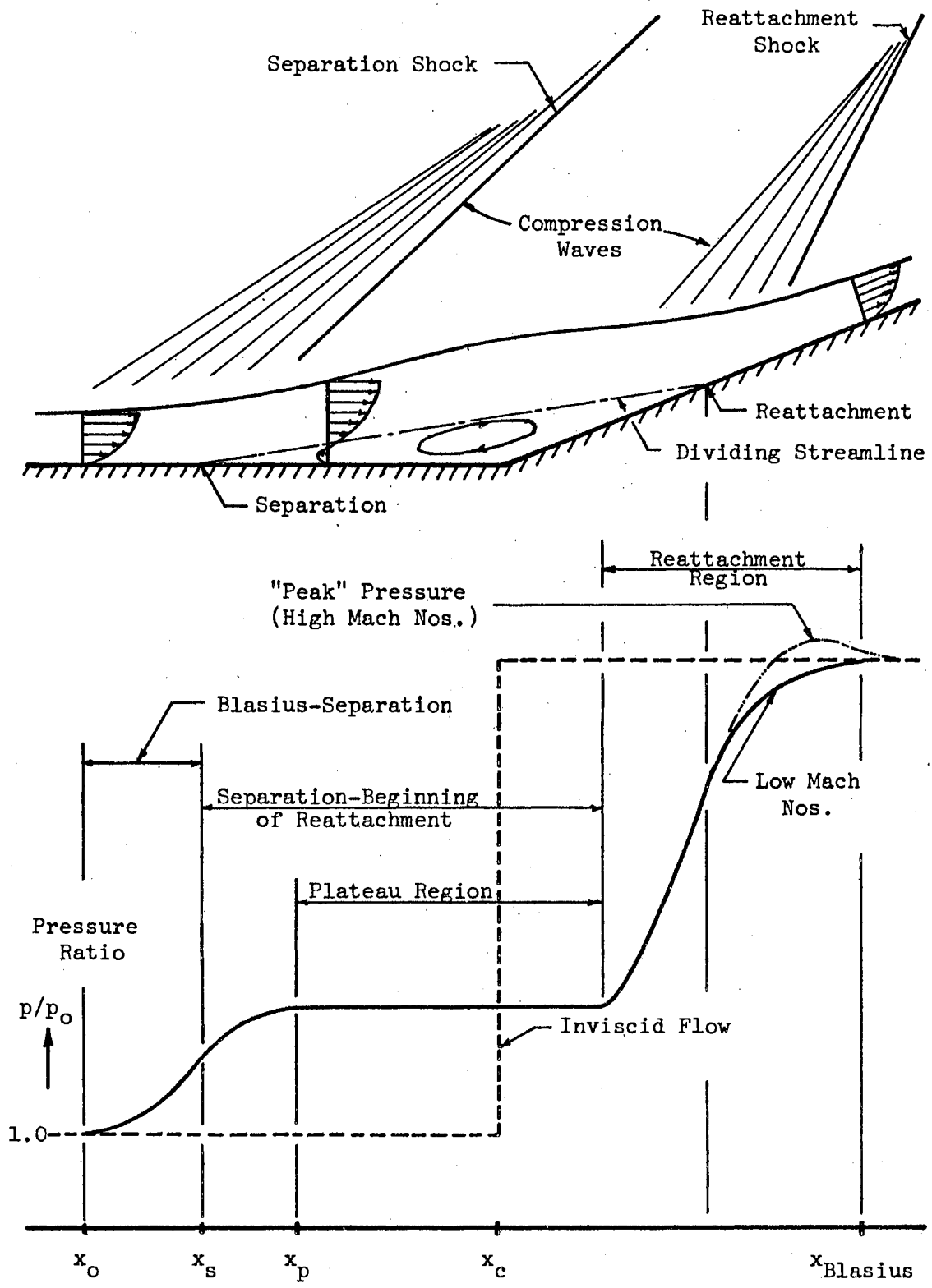

Figure 1. Shock Wave-Laminar Boundary Layer Interaction, Shock Generated by Ramp

interaction between the "external" inviscid flow and the viscous layer near the surface.

The Crocco-Lees method is capable of embracing the entire separated interaction within a single framework once the semi-empirical features have been reasonably well defined. The problem is analyzed by breaking the interaction region into three distinct parts. These parts include: 1.) flat plate Blasius type flow to separation, 2.) separation to pressure plateau to beginning of reattachment, and 3.) reattachment and transition to downstream conditions. By utilizing an empirical pressure plateau correlation and the downstream pressure ratio calculated from inviscid theory, the three segments are tied together. A straight dividing streamline which connects the separation and beginning of reattachment points is assumed. The inviscid turning angle dictated by the empirical plateau pressure is used to approximate the breakaway angle which this streamline makes with the plate. By first guessing a separation point, the beginning of reattachment point becomes fixed. By working through the interaction up to the beginning of reattachment, it is determined if sufficient mixing has occurred in the plateau region to accomplish reattachment at the known higher pressure downstream.

If the length of the mixing region (pressure plateau) is too short to accomplish the inviscid reattachment pressure rise, a new separation location farther forward on the plate must be selected. Iteration will produce the proper location for the separation point and will give the pressure distribution throughout the entire interaction.

In considering the foundation upon which to base the separation development, the design engineer was kept uppermost in mind. Simplicity

of use, conceptual understanding, and accuracy were given prime consideration.

CHAPTER II

REVIEW OF PREVIOUS WORK

In early attempts by Howarth (1)*, and others, to solve this supersonic interaction problem, the interaction between the adjacent subsonic and supersonic layers within the boundary layer was considered as the important mechanism. It was reasoned that a small disturbance in the supersonic flow is propagated upstream in the subsonic flow, causing the boundary layer thickness to change and to deflect the free stream. Such methods were restricted by the assumption of small perturbations and by the fact that viscosity effects were neglected. This technique has been unsuccessful in assessing the effects of boundary layer separation.

In 1952, a mixing theory developed by Crocco and Lees (2) appeared. They considered the interaction between the dissipative flow and the nearly isentropic outer stream as a flow model. In their model, it was the mixing, or the transport of momentum from the free stream to the dissipative layer, that was the fundamental mechanism in the growth of the boundary layer. The theory accounts for viscosity through a boundary layer velocity profile parameter. The skin friction, mixing rate, and mean boundary layer temperature are estimated in terms of this parameter. The analysis treats both separation and reattachment without

---

*Numbers in parentheses indicate references in the bibliography.

placing any restriction on the size of the disturbance. The concept of mixing between the viscous and inviscid layers has become the standard physical model used to analyze separated flows.

Another significant contribution to the understanding of separation has been presented by Chapman, Kuehn, and Larson (3). This work was primarily an experimental investigation, but it has helped considerably in ascertaining the general characteristics of flow separations and in crystallizing the notion of a dividing streamline. The dividing streamline may be thought of as an artificial boundary which separates the trapped circulating inner flow from the outer stream.

By using the physical model described by Crocco-Lees, the method for solution of this problem usually follows either a semi-empirical or an analytical approach. The original theory was developed in such a manner that it was semi-empirical. Three correlation parameters, dependent upon the velocity profile parameter, were needed in order to describe the flow. Other researchers have chosen to develop theories which are capable of including the entire separated flow within a single framework, without introducing these semi-empirical features. This is accomplished by assuming a form for the velocity profile as it traverses the interaction region. Regardless of which of these approaches is selected, nearly all of the solutions make use of the von Karman integral momentum technique as a means of simplifying and handling the boundary layer equations. It should also be noted that all the methods mentioned apply only to ideal gases and two-dimensional geometries. All employ the usual compressible boundary layer assumptions which are: Prandtl number of unity, viscosity proportional to temperature, no heat transfer at the wall, and zero pressure gradient normal to the wall.

The original Crocco-Lees theory has been examined and extended by Cheng and Bray (4), Cheng and Chang (5), Glick (6), and others. However, the semi-empirical feature and the general lack of detailed experimental data, particularly for supersonic laminar separated flows, has directed attention away from this method. This has been true because the three correlation parameters which are necessary must be derived from other sources, either theoretical or experimental. There are no theoretical solutions for separated flows so experimental values must be used entirely. Since the Crocco-Lees method is used in this investigation, its facets and details will be elaborated upon in the following chapters.

There are other possible ways to treat separated and reattaching flows. By employing the first moment of momentum in addition to the usual (zeroth) momentum integral, another relationship between the flow variables is obtained. This first moment equation is obtained by multiplying the momentum equation by u and then integrating across the boundary layer. This first moment, plus the choice of an alternate parameter that is satisfactory for the treatment of separated flows, determines the essential differences between the Crocco-Lees method and other approximate integral methods.

For example, Tani (7) used a fourth-degree polynomial to describe the velocity profile, in which the parameter has a physical meaning in that it is proportional to the shearing stress at the wall. Tani applied his method only to attached flows. Pinkus (8) extended the Tani method to separated laminar boundary layers on compression corners and curved surfaces. The chief criticism voiced against the use of polynomials to describe the separated flow is that they are not capable of

describing the constant pressure plateau region which is characteristic of laminar separations. Due to the mass entrainment (or mixing) which takes place in the plateau region, a similar profile throughout this region cannot be justified.

In an attempt to avoid some of the difficulties encountered with polynomials, Lees and Reeves (9) have elected to use the Stewartson (10) reversed-flow profiles. As in the Pinkus method, the successful application of this method to separated and reattaching flows hinges on the proper choice of the one-parameter family of velocity profiles which is utilized to determine the integral properties of the viscous flow. The single independent parameter is not explicitly related to the local static pressure gradient. They found in their development that the Stewartson reversed-flow profiles had the qualitatively correct behavior while polynomials did not. The Lees and Reeves method does raise some complications in that these profiles are not available in the form of analytical expressions. The velocity profiles which are used have never been substantiated by experimental measurements. Also, no constant pressure plateau region can ever be reached except in an asymptotic sense.

Makofski (11), like Tani and Pinkus, has elected to represent the velocity profile with a polynomial. He uses a fifth-degree polynomial and two undetermined parameters instead of the usual one. One of the parameters is related to the skin friction at the wall, while the other is proportional to the imposed pressure gradient. As with other methods which use polynomials, the primary difficulty lies in its application to the constant pressure plateau region downstream of separation. There are additional mathematical complexities introduced by the second

parameter, the only justification being the possibility of obtaining significantly better results.

Two methods which differ somewhat from the usual pattern of those already mentioned include the "free interaction" theory by Erdos and Pallone (12) and the "method of integral relations" which is being actively pursued by Nielsen, Lynes, Goodwin, and Holt (13).

The free interaction concept may be applied to both laminar and turbulent flows. This analysis treats the complex separation phenomenon in two phases: 1.) A study of shock-boundary layer interaction (without specification of the location of the interaction with respect to the compression corner). 2.) Application of the results of the first phase to the problem of flow separation in a compression corner, and determination of the location of the separation and reattachment interaction.

In the first phase, semi-empirical equations are developed for the determination of the pressure distribution in the free interaction. In the second phase, the location of the separation and reattachment points has been fixed by an empirical correlation formula. With the correlation formula and the free interaction equations, it is possible to predict the complete pressure distribution for a shock-separated flow. However, this correlation formula is based upon very meager data, a single experiment, and is only a first approximation. Additional data is needed to confirm and extend the results.

The "method of integral relations" has been mentioned with increased frequency as a new and promising analytical method for handling the separation problem. This technique, a general method of numerical solution for nonlinear fluid-dynamic problems, has the important

advantage of being well-suited for digital computation. The approach was first introduced by Dorodnitsyn (14). Principal among the inherent difficulties is the fact that the one-parameter family of velocity profiles used does not represent accurately all the possible velocity profiles that can be developed in separated and attached flows.

The review of literature makes one cognizant of the similarities which exist among the different methods. All techniques employ basically the same physical model and assumptions. The chief difference which appears is whether semi-empirical correlations are used to represent the velocity profile changes or whether some velocity profile shape must be assumed.

To attain the goal of an engineering solution to this interaction problem, the Crocco-Lees semi-empirical approach was selected. The velocity profile changes are absorbed in the correlation parameters, without becoming involved in the detailed changes in the velocity profile shape. It was felt that the requirements of simplicity, conceptual understanding, and accuracy could be best satisfied by using this method of attack.

CHAPTER III

DEVELOPMENT OF THE CROCCO-LEES METHOD

The so-called free interaction type of boundary layer separation is the classification which is of interest in this study. In a free interaction the pressure distribution of the outer flow is considered to be the result of a mutual interaction between the boundary layer and the inviscid flow. In a free interaction the flow is independent of the direct influence of the downstream configuration and is also independent of the manner of inducing the separation.

The original Crocco-Lees paper dealt with flows up to the point of separation for compression corners and for the aft flow over a supersonic airfoil with a blunt trailing edge. The original concepts which apply up to the point of separation have remained essentially unchanged except for the behavior of the mixing rate parameter (C(K)). Glick (6) has extended the technique to include the separated region and has cleared-up some troublesome details near separation, such as the correct behavior of C(K).

Velocity Profile Parameters

The Crocco-Lees method is based upon the assumptions that the parameters describing the boundary layer are dependent upon the rate of entrainment of fluid into the boundary layer from the external stream and that there exist certain universal correlation functions which

relate these parameters. The boundary layer profiles are absorbed in the definition of a new velocity profile parameter. The analytical development for the method hinges on the velocity shape parameter, K, which is non-dimensional and is defined as the ratio of the momentum flux to the product of mass flux and local external velocity. It may be expressed as

$$K = \frac{I}{\bar{m}\, u_e} = \frac{\text{momentum flux}}{\text{mass flux} \times u_e} ,$$

where

$$I = \int_0^\delta \rho u^2 \, dy$$

$$\bar{m} = \int_0^\delta \rho u \, dy \quad .$$

Different K's are associated with different velocity profiles. This gives a conceptual feeling for the changes which occur without becoming involved in the mathematics which describe the actual profile shape. This method is consistent with the concepts that the velocity profile is dependent upon its previous history and that K at separation can differ from K at reattachment.

This basic parameter which characterizes the flow in the viscous region may be defined in terms of either compressible or incompressible boundary layer variables (2, 6) as

$$K = \frac{\delta - \delta^* - \delta^{**}}{\delta - \delta^*} = \frac{\delta_i - \delta_i^* - \delta_i^{**}}{\delta_i - \delta_i^*} \quad . \tag{1}$$

The Stewartson (15) transformation, which assumes a Prandtl number of unity and viscosity proportional to the absolute temperature, is utilized to transform a compressible boundary layer into its equivalent incompressible form. It may be observed that K is not determined solely by δ, and it is not explicitly related to the free stream velocity gradient along the plate outside the viscous layer.

By dividing the momentum flux by the mass flux, a mean velocity (u_1) is obtained for the viscous region. Also, without attaching any physical significance to the definition, one can think of a mean-temperature (T_1) across the viscous region and a mean-density (ρ_1). These are related by the perfect gas law as

$$T_1 = p/\rho_1 R \quad .$$

The ratio of the mean-temperature to the temperature at the edge of the boundary layer is called f. This parameter, defined in terms of the incompressible boundary layer variables, can be shown to be

$$f = \frac{T_1}{T_e} = \frac{(\delta_i - \delta_i^* - \delta_i^{**})\delta_i}{(\delta_i - \delta_i^*)^2} = \frac{K\,\delta_i}{(\delta_i - \delta_i^*)} \quad . \qquad (2)$$

In a sense, the deviations of f and K from unity measure the non-uniformity of the velocity profile. For every incompressible boundary layer flow, f and K can be related to each other. Compressible boundary layers may be expressed in an equivalent incompressible form. Once transformed, each streamline location in the flow region corresponds to a point in the f-K plane, and the whole class of flows (attached, separating, separated, etc.) is represented by a single locus of points in the f-K plane.

For convenience, an alternate mean-temperature parameter, F, is defined as

$$F = \left(\frac{f}{K^2} - 1\right) = \frac{\delta_i^* - \delta_i^{**}}{(\delta_i - \delta_i^* \quad \delta_i^{**})} \quad . \tag{3}$$

F and K, just as f and K, are defined by incompressible boundary layer parameters and are uniquely related.

Equations Which Define the Flow

For mathematical solution, a model must be selected to represent the physical phenomenon. For purposes of analysis, the flow is divided into two parts -- an outer region which is assumed to be essentially nondissipative, and an inner region in which the viscosity is assumed to play an important role. Figure 2 expresses the separated region in terms of the Crocco-Lees model. The extent of the viscous region is measured by the length, δ, which for the case of a body in a high-Reynolds-number stream is the usual boundary layer thickness. The definition of the length δ is artificial. Physical quantities, such as pressure and interaction distance, only depend to a small degree on the definition adopted for δ.

The definition for laminar boundary layer thickness (δ) is the distance above the surface at which the velocity ratio $u_{(\delta)}/u_e$ has a particular value. Because of the way in which it is defined, it is a hard quantity to measure experimentally. Small changes in the definition of δ do not modify the character of the final results, but they do alter the intermediate numerical values. Any reasonable value of δ should give qualitative agreement with experimental results.

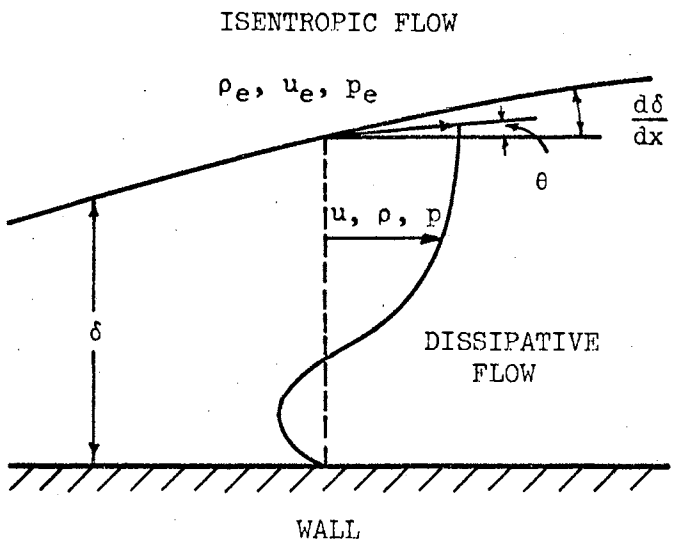

Figure 2. Flow Regions as Described by Crocco-Lees

The variations in the velocity profile parameter, K, besides being dependent on the profile shape are also dependent on the definition used for δ. If $u_{(\delta)}/u_e$ is taken as 1.0, the whole f-K curve reduces to a single point, and in terms of the shape parameter, all profiles are the same. If a $u_{(\delta)}/u_e$ of .82 is selected as the definition used, all profiles between the flat-plate-type flow and separation have nearly the same K.

As a criterion for the optimum selection of a definition for δ, $\Delta K = K_b - K_s$ should be selected as a maximum. It was found that this ΔK maximum requirement resulted in a definition of approximately $u_{(\delta)}/u_e = .96$. Also observed was the fact that ΔK was almost constant between $\delta = .94$ and .98, and any value within these limits is the most desirable. In this investigation, the value used for $u_{(\delta)}/u_e$ is the same as the one used by Glick and has a numerical value of approximately .95. By using the same boundary layer thickness definition, it was felt that a more meaningful extension of the method could be obtained.

The Navier-Stokes equations are unwieldy and have not been used successfully in the interaction solution. In order to permit a meaningful mathematical analysis, several simplifying assumptions must be employed. The principal assumptions which have been employed may be grouped into the following three categories:

1. The usual boundary layer equations describe the viscous region. The boundary layer equations have evolved from the Navier-Stokes equations by assuming a.) the gradients of viscous stresses in the flow direction are negligible in comparison with the static pressure gradient in that direction, b.) the pressure gradient normal to the surface is zero, and c.) by making an order-of magnitude comparison to

eliminate terms. The second restriction, zero pressure gradient, does not hold in actual practice for some cases. For example, in the supersonic part of a boundary layer the pressure is nearly constant along Mach waves, which at higher Mach numbers could introduce appreciable pressure gradients. Also, in the vicinity of the point where a shock wave impinges on the boundary layer, large pressure gradients normal to the wall must exist.

In this analysis the static pressure across the internal viscous region is taken as being equal to the local pressure in the outer inviscid region. The analysis is further restricted to flows over adiabatic walls. This simplifies the viscous equations since no energy is transferred at the wall.

2. The boundary layer is assumed to remain laminar throughout the entire interaction. In this study, only boundary layers which are relatively well understood are included. The present formulation, while qualitatively capable of handling transitional and turbulent interactions, will not be applied to these cases. In addition, the flow is steady with a constant stagnation temperature throughout the entire interaction region.

3. The fluid (air) is assumed to be thermally and calorically perfect. The flow in the outer inviscid region is supersonic and isentropic. This means that the Prandtl-Meyer relationship may be used to determine the flow direction as it proceeds through the interaction compression. As already mentioned, a Prandtl number of unity and viscosity proportional to the absolute temperature is required in order to determine the equivalent incompressible boundary layer for each compressible boundary layer.

The flow within the viscous region is described by the momentum and continuity equations which can be written in the following form:

$$\frac{dI}{dx} = u_e\left(\frac{d\bar{m}}{dx}\right) - \delta\left(\frac{dP}{dx}\right) - \tau_w \tag{4}$$

$$\frac{d\bar{m}}{dx} = \rho_e u_e \left(\frac{d\delta}{dx} - \tan\theta\right) \tag{5}$$

where θ is the streamline direction angle at $y = \delta$ relative to the wall. (A complete development of the equations used in this chapter is given in Appendix A.) In all previous work using this model, it has been the practice to replace tan θ by θ. In order to obtain as accurate values as possible, tan θ will be used throughout in this analysis. The magnitude of errors introduced by the various approximations which have frequently been employed will be discussed later in this chapter.

Equations (4) and (5) may be written in the following form:

$$\frac{d}{dx}(m K w_e) = w_e\left(\frac{dm}{dx}\right) - \frac{P w_e c_f}{2\phi_e} - \delta\left(\frac{dP}{dx}\right) \tag{6}$$

$$\frac{dm}{dx} = \left(\frac{P}{\phi_e}\right)\left(\frac{d\delta}{dx} - \tan\theta\right) \tag{7}$$

where

$$\phi_e = \frac{\left(1 - \frac{\gamma-1}{2} w_e^2\right)}{\gamma w_e} \quad ,$$

$$w_e = u_e/a_t \quad ,$$

and

$$a_t = \sqrt{\gamma R T_t} \quad .$$

In addition to these two equations for the viscous region, the Bernoulli equation is used to describe the external inviscid flow. It can be shown that this equation may be expressed as

$$\frac{dp}{p} = \frac{-dw_e}{\Phi_e} \quad . \tag{8}$$

In addition to these three equations, (6), (7), and (8), the mass flux in the viscous region can be expressed as

$$\bar{m} = \rho u_1 \delta = \frac{P \delta u_1}{T_1 R} \quad . \tag{9}$$

Since $m = \bar{m}\, a_t$, equation (9) is used to obtain the following expression:

$$m = \frac{P \delta}{\Phi_1} \quad ,$$

where

$$\Phi_1 = \frac{T_1}{T_t \gamma w_1} \quad .$$

The Prandtl-Meyer relationship used to express the flow angle θ, can be expressed in terms of w_e, i.e., $\theta = \theta(w_e)$, giving another independent equation.

This system of five equations involves eight unknowns (δ, m, K, w_e, c_f, ϕ_1, p, and θ). To account for the three remaining unknowns and thus complete the mathematical formulation of the method, semi-empirical coefficients are introduced. These account for the mean temperature, the skin friction, and the mixing in the viscous region. These additional parameters, all dependent upon the velocity profile shape parameter K, are defined as F(K), D(K), and C(K). F(K) is related to the mean temperature-mean velocity correlation; D(K) is the skin friction

correlation function; and C(K) is the mixing rate correlation function. F(K) has already been described in terms of the velocity profile variables. In terms of the eight variables, these new correlation functions are expressed as follows:

$$F(K)=F=\frac{\phi\gamma w_1}{K^2}-\left(1-\frac{\gamma-1}{2}w_e^2\right)=\frac{\phi\gamma w_1}{K^2}-t \tag{10}$$

$$D(K)=D=\frac{c_f m}{\mu_e a_t} \tag{11}$$

$$C(K)=C=\frac{m\left(\frac{d\delta}{dx}-\tan\theta\right)}{\mu_e a_t}=\frac{mk}{\mu_e a_t} \tag{12}$$

In the solution of the interaction problem, the functional dependence of these empirical coefficients must be obtained through correlation with experiments.

With these definitions of F(K), D(K), and C(K), the system of equations may be solved simultaneously to obtain the following set of non-linear first order ordinary differential equations:

$$\frac{dK}{d\xi}=\frac{-KF\left\{\frac{c}{5}\left[t-K(F+t)-\frac{(1-K)(1-\sigma)}{KF}\left[K(F+t)\left(1-\frac{3\gamma-1}{2}M_e^2t\right)+KM_e^2t^2(\gamma-1)\right]\right]+\tan\theta\right\}}{C\left\{K(F+t)\left(1-\frac{3\gamma-1}{2}M_e^2t\right)+K(\gamma-1)M_e^2t^2-KF\left(F+t+K\frac{dF}{dK}\right)\right\}} \tag{13}$$

and

$$\frac{dM_e}{d\xi}=\frac{-M_e\left\{\frac{c}{5}\left[t-K(F+t)-(1-\sigma)(1-K)\left(F+t+K\frac{dF}{dK}\right)\right]+\tan\theta\right\}}{C\left\{K(F+t)\left(1-\frac{3\gamma-1}{2}M_e^2t\right)+K(\gamma-1)M_e^2t^2-KF\left(F+t+K\frac{dF}{dK}\right)\right\}} \tag{14}$$

These two general equations describe the flow and are basic to the Crocco-Lees method. By proper selection of the parameters C(K), D(K), and F(K), these equations may be specialized to the various flow regions within the interaction. In these two equations, several terms have been combined and written as new quantities which are defined as follows:

$$\sigma = \frac{D(K)}{2(1-K)\,C(K)}$$

$$t = \frac{T_e}{T_t} = \left(1 - \frac{\gamma-1}{2} W_e^2\right) = \frac{1}{\left(1 + \frac{\gamma-1}{2} M_e^2\right)}$$

$$\varsigma = \frac{m}{a_t \mu_t} = \frac{\bar{m}}{\mu_t} \quad .$$

The quantity ζ which appears in the above general system of equations behaves like a Reynolds number. It may also be written

$$\varsigma = \frac{\int_0^\delta \rho u \, dy}{\mu_t} \quad ,$$

which is dimensionless and has all the terms that appear in a Reynolds number. Conceptually, it is evident that ζ should increase with distance down the plate because it is related to the boundary layer growth. In the separated flow region, ζ would be expected to grow more rapidly than in a normal flat plate case, due to the large changes in boundary layer thickness. The rate at which ζ grows is related to the mixing. The more vigorous the mixing, the faster the rate at which ζ and boundary layer thickness increase.

A discussion of how the two general equations, (13) and (14), have been modified or adapted to each of the three regions will now be given.

Blasius to Separation

In the region upstream of separation the boundary layer is attached. The correlation parameters which are used in this region have been developed by Glick (6), and while not optimum, they do give qualitatively correct pressure distributions. The parameters which were obtained have been derived from both detailed theoretical and experimental data. It was found that all three of these parameters varied in this region. In the interest of simplicity, linear or other simple variations were selected for each parameter.

F(K) was obtained from a maximization method which was found to be in fair agreement with the curve based on the Falkner-Skan solution. This maximum method leads to a simple expression and in this form is helpful in obtaining the mixing rate correlation function from the experimental studies.

The D(K) relationship that was used in this region was based upon the Falkner-Skan solution. The D(K) correlation is probably the best understood of the three parameters. It is related to the skin friction and is the easiest to measure experimentally.

The C(K) correlation was obtained from detailed analytical and experimental Schubauer ellipse data. The C(K) variation differs appreciably from the correlation curve which was used previously. The early workers had used a relationship derived from the Falkner-Skan solution. This curve was found to be qualitatively different from the curve based on experimental results.

The correlation parameters which are used in equations (13) and (14) for the Blasius to separation region are:

$$F(K) = \frac{2\,(1-K)}{(2K-1)}$$

$$D(K) = 22.2\,(K - .63)$$

$$C(K) = 36.2\,(K - .63) \quad .$$

It should be noted that the method for defining the boundary layer thickness is artificial and will lead to different numerical values for F(K), C(K), and D(K) when some other definition is assumed. The above parameters may be used only with the δ definition which has been adopted.

Separation to Beginning of Reattachment

Beyond the separation point the flow is detached. Since there are no detailed theoretical studies which apply to separated and reattaching flows, this region must be handled differently than the attached region. It is assumed that the skin friction at the wall is sufficiently reduced so that it can be neglected in this region. D(K) is taken as zero rather than trying to approximate the average negative value which this parameter would have. As a first approximation, F(K) is taken as constant and equal to the value at separation. The mixing rate correlation function, C(K), is more elusive and must follow a trajectory such that the correct pressure distribution results. The shape and dependence of this trajectory will be discussed in the next chapter.

By taking

$$D(K) = 0 \quad ,$$

$$F(K) = F_s \quad ,$$

and

$$C(K) = C \quad ,$$

the generalized equations may be written in a simpler form as

$$\frac{dK}{ds} = \frac{-KF\left\{\frac{C}{\delta}\left[t - K(F+t) - \frac{(1-K)}{KF}\left(K(F+t)\left(1-\frac{3\gamma-1}{2}M_e^2 t\right) + KM_e^2 t^2(\gamma-1)\right)\right] + \tan\theta\right\}}{C\left\{K(F+t)\left(1-\frac{3\gamma-1}{2}M_e^2 t\right) + K(\gamma-1)M_e^2 t^2 - KF(F+t)\right\}} \qquad (15)$$

and

$$\frac{dM_e}{ds} = \frac{-M_e\left\{\frac{C}{\delta}\left[t - K(F+t) - (1-K)(F+t)\right] + \tan\theta\right\}}{C\left\{K(F+t)\left(1-\frac{3\gamma-1}{2}M_e^2 t\right) + K(\gamma-1)M_e^2 t^2 - KF(F+t)\right\}} \qquad (16)$$

Mixing in this region is of paramount importance. After separation the flow is essentially divided into two parts by the dividing streamline. The fluid along the dividing streamline is accelerated by viscous momentum transfer in the region between separation and the beginning of reattachment. The fluid is thereby prepared for the reattachment pressure rise which occurs on the ramp when this streamline is stagnated.

Reattachment

It has been previously noted that the skin friction is probably the best understood of the three correlation parameters. In the reattachment region, the skin friction has a negative value ahead of and a positive value downstream from the reattachment point. To simplify the analysis of this region, the positive and negative regions offset one another, and may be taken as negligible over the entire region. Just as in the separation to beginning of reattachment region, D(K) will be taken as zero.

The mixing rate correlation, C(K), must come principally from experiment. The experiments of Chapman, Kuehn, and Larson (3), using

a special model to study the reattachment process, has helped to substantiate the belief that mixing is negligible in the reattachment process. It has been pointed out that the most important phenomena in the reattachment process are the deceleration of the flow and the contraction of the viscous region, and not mixing. In the spirit of simplicity, C(K) has been taken as zero in this region.

The only parameter left to be defined is F(K). This parameter is the hardest to determine because it is dependent upon velocity profile measurements, which are virtually nonexistent for separated flows of this type. F(K) is used to correlate the flow behavior throughout the reattachment region since it is closely allied with the actual profile changes. It seems apparent that the deceleration and contraction of the viscous region can be easily associated with the various changes in F(K) values. The character of a particular reattachment pressure rise can be related to changes in F(K). A discussion on how F(K) has been correlated, using experimental data, is deferred until the next chapter.

The general equations, (13) and (14), are not altered to handle this region. Since ζ is dependent on the amount of mixing (related to the boundary layer growth), and does not vary in the reattachment region, it is simpler to develop a new set of equations which relate changes in K to the change in M_e and x-distance.

Starting with the basic momentum and $\frac{d\delta}{dx}$ equations which are given in Appendix A,

$$\frac{dK}{dx} - \frac{KF}{M_e}\frac{dM_e}{dx} = (1-\sigma)(1-K)\left(\frac{1}{m}\frac{dm}{dx}\right) \qquad \text{(A-12)}$$

$$\left[F+t+K\frac{dF}{dK}\right]\frac{dK}{dx}-\left[K(F+t)\left(1-\frac{3\gamma-1}{2}w_e^2\right)+Kt(\gamma-1)w_e^2\right]\frac{1}{M_e}\frac{dM_e}{dx}$$

$$=\frac{\rho_e u_e}{\mu_e}\frac{1}{\zeta}t^2\left[\tan\theta+\frac{c}{\zeta}\left(t-K(F+t)\right)\right], \qquad (A\text{-}15)$$

two ordinary differential equations may be obtained. The two relationships which are desired are dM_e/dK and dx/dK. From (A-12), by taking $dm/dx = 0$ (zero mixing),

$$\frac{dM_e}{dK}=\frac{M_e}{K\,F(K)} \qquad (17)$$

is obtained, where the F(K) behavior has not yet been defined. From the $d\delta/dx$ equation, by taking C(K) and D(K) zero, and making the substitutions

$$\frac{dM_e}{dx}=\frac{M_e}{KF}\frac{dK}{dx} \quad \text{and} \quad w_e^2=M_e^2 t \quad ,$$

the following equation is obtained:

$$\frac{dx}{dK}=\frac{x_s\left[F+t+K\frac{dF}{dK}-\left(\frac{F+t}{F}\right)\left(1-\frac{3\gamma-1}{2}M_e^2 t\right)-\left(\frac{\gamma-1}{F}\right)M_e^2 t^2\right]}{Re_{x_s}\frac{t^2\tan\theta}{\zeta}} \qquad (18)$$

The method of numerical solution for these three regions will be discussed in the following chapter.

Transformation to Real Plane

No mention has been made yet on how the generalized differential equations are transformed into a meaningful pressure versus distance distribution along the plate. The transformation back to the physical plane is made by using the continuity equation. The separation point

is taken as a reference and the continuity equation is integrated. The resulting expression may be written in the form

$$\frac{x_s - x}{x_s} = \frac{1}{Re_{x_s}}\left(1+\frac{\gamma-1}{2}M_\infty^2\right)^2 \int_{\zeta}^{\zeta_s} \frac{\zeta\, d\zeta}{C(K)} \frac{M_\infty}{M_e}\left[\frac{1+\frac{\gamma-1}{2}M_e^2}{1+\frac{\gamma-1}{2}M_\infty^2}\right]^{\frac{3\gamma-1}{2(\gamma-1)}} \tag{19}$$

This equation is used in the entire region from the Blasius point to the beginning of reattachment.

The pressure corresponding to a given point is obtained directly from the isentropic relationship

$$\frac{p}{p_o} = \left[\frac{1+\frac{\gamma-1}{2}M_{e_b}^2}{1+\frac{\gamma-1}{2}M_e^2}\right]^{\frac{\gamma}{\gamma-1}} \tag{20}$$

where M_{e_b} is the reference local Mach number at the point where the pressure first starts to increase. This pressure relationship is used throughout the entire interaction.

How K Changes With Velocity Profile Changes

One value of the velocity profile shape parameter K, because of the way it is defined, can describe many different profile shapes. It is noteworthy to point out that in particular, a given value can describe both an attached and a separated profile shape or two different separated profiles. With the definition for δ which has been selected, the flat plate Blasius type profile is represented by $K = 0.693$ and the separation profile by $K = 0.63$. K is a minimum at the separation point and must increase again with the presence of a reversed flow adjacent to the surface. K reaches a maximum value which is larger than the

Blasius value somewhere in the separated region. In the reattachment, since the experimental profiles have not been determined accurately, it will be assumed that the Blasius value of K is approached from the positive side, rather than traversing first through a trajectory which leads to K-separation. The arguments here become heuristic in nature. From schlieren photographs of the flow downstream from reattachment, there is observed a "necking down" in boundary layer thickness. After this, the boundary layer appears to grow in a normal fashion and would be expected to correspond to the Blasius K. In the vicinity of reattachment, because the flow impinges on the surface, the boundary layer can be thought of as more nearly resembling a slug type flow. In other words, the displacement thickness might be thought of as being a minimum at reattachment and then increasing to the Blasius value.

Figure 3 illustrates approximately how K and the velocity profile shapes are assumed to vary, starting from a Blasius profile and then traversing the entire interaction region. All of the boundary layer details have not been preserved in this illustration. For example, the free stream velocity u_e and the boundary layer thickness δ would both change from location to location.

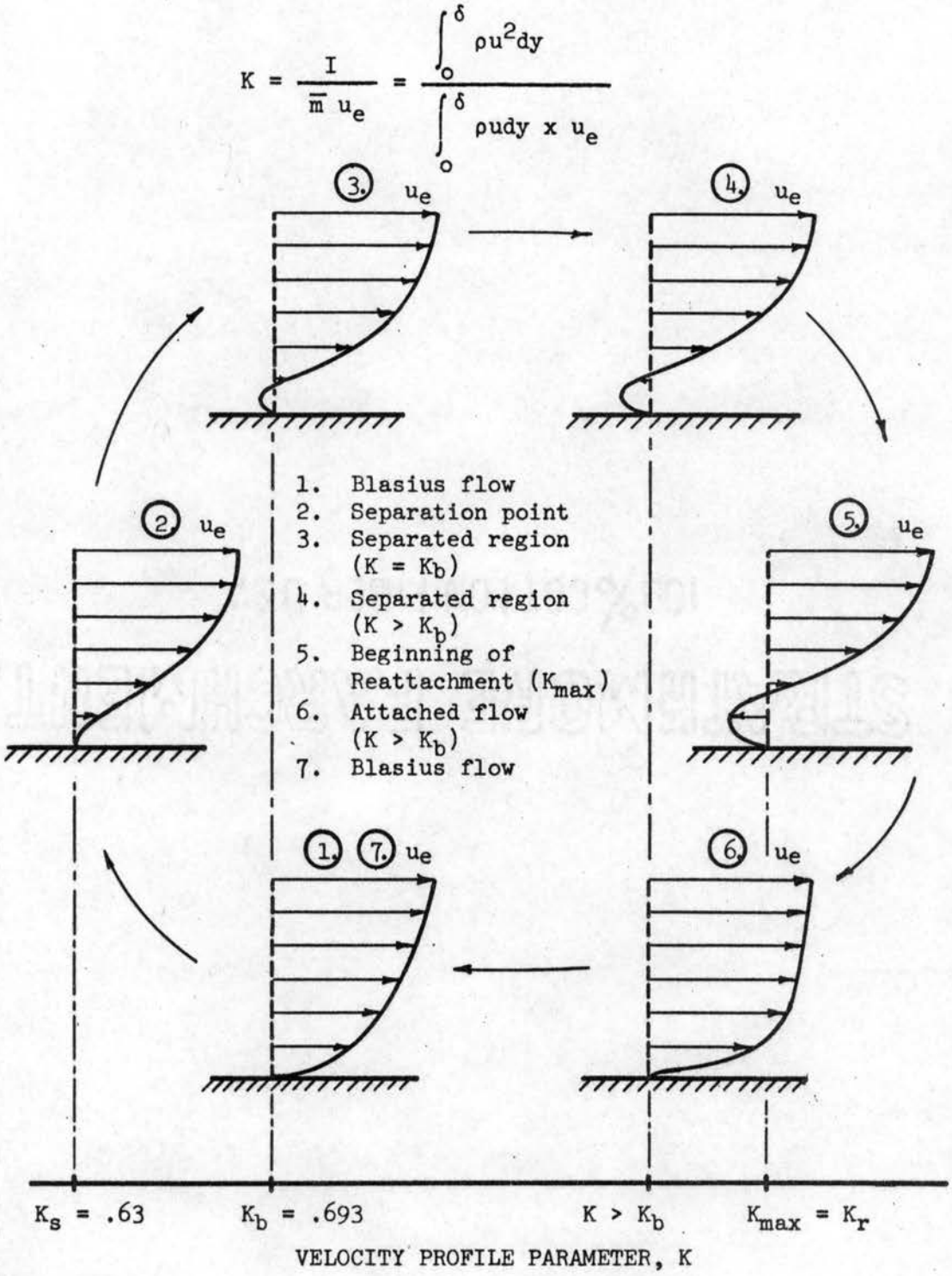

Figure 3. Approximate Velocity Profile and K Changes Throughout a Free Interaction

CHAPTER IV

SOLUTION IN THE INTERACTION REGION

This chapter discusses how the equations are solved and the manner in which the required correlations with experimental data were obtained. The solution of the entire interaction is handled in the same three segments or regions as described previously. A subroutine was written for each of these three regions and incorporated in a general program. The general program was solved using an IBM 7040 digital computer. A discussion of the complete interaction and general program, each subroutine, and the experimental data selected is given.

General Solution-Complete Interaction

Before discussing the complete computer solution, it should prove beneficial to discuss details which are characteristic of laminar separation-pressure distributions. In laminar separations, the pressures along the plate and ramp surfaces are influenced over a considerably larger region than for turbulent separations on a similar geometry. Figure 4 illustrates the details of the various surface pressure distributions which can be obtained by making various assumptions for supersonic and hypersonic flows.

The simplest example is explained by Figure 4-a, which is the idealized inviscid flow model. No boundary layer exists, and the shock originates at the juncture of the plate and ramp. This idealized model

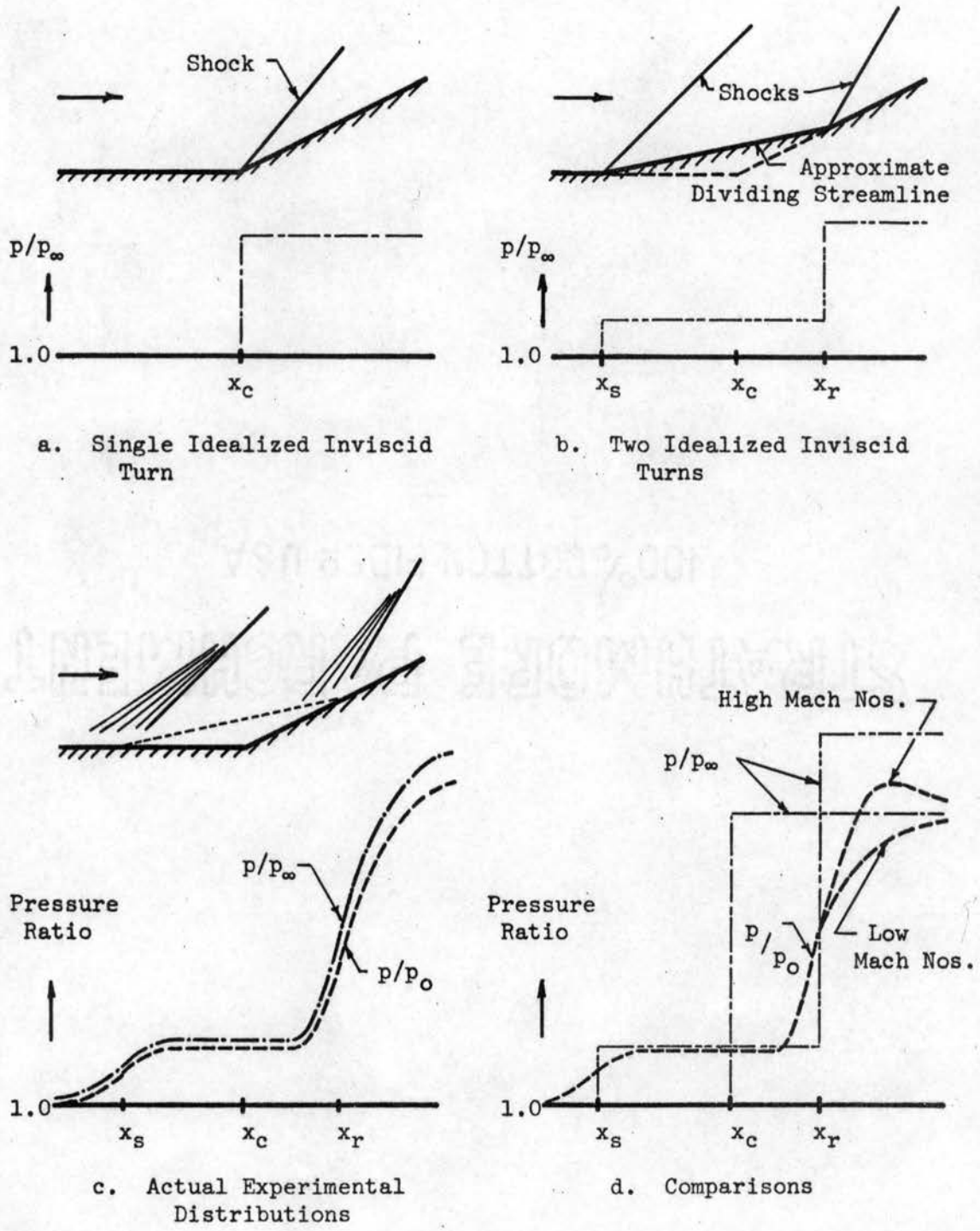

Figure 4. Pressure Distributions for a Flat Plate and Attached Flap

has the pressure distribution indicated in which a single discontinuous pressure rise occurs at the ramp corner.

The next configuration illustrated, Figure 4-b, is a two-ramp configuration in which the straight dividing streamline is replaced by a solid surface. In this case the flow must negotiate two idealized inviscid turns with the two pressure discontinuities as indicated. The two surface discontinuities can be used to correspond to the separation and reattachment points respectively. There is no way to know in advance how to approximate the separation and reattachment points, and hence, to approximate the location of the intermediate ramp.

The actual pressure distribution is shown in Figure 4-c. Note that the pressure decreases to a minimum at the beginning of the interaction, rises to a constant plateau value which extends to or beyond the ramp corner, and then rises rather sharply to a final value. In actual experimental tests, the pressure ratio may reach a peak value after reattachment and then decrease slightly. The Mach number at the beginning of the interaction is less than the free stream Mach number. This results in a pressure ratio greater than one at the start of the interaction, when based on the free stream pressure. This decrease in Mach number results from the viscous interaction effects caused by the plate leading edge. If the reference pressure is taken as the pressure at the beginning of the interaction (p_o), the resulting pressure distribution is shifted downward as shown.

The last part of Figure 4 shows how the pressure distributions from the previous three parts appear when they are superimposed on one another in the same figure. In this figure, all curves except (p/p_o) are dependent upon the free stream reference conditions. As a general

rule the final downstream pressure ratio predicted by the single inviscid turn, does not differ greatly from the final p/p_o ratio.

In the literature on separated flows, it has become standard practice to use the pressure at the beginning of the interaction as the reference value. This study also follows the standard convention by selecting p_o as the reference pressure.

To tie the complete interaction together within a single framework, and to obtain the necessary semi-empirical correlations, it becomes necessary to make some assumptions regarding the resultant pressure distribution. First, it is assumed that the final pressure on the ramp corresponds with the same pressure ratio which would be obtained if the free stream flow negotiated the single inviscid turn as shown in Figure 4-a. This compromise was imposed as a result of experimental pressure measurements on the ramp surface at different Mach numbers. At low Mach numbers (2-5) it appears to give good correlation, while at higher Mach numbers it is below the peak pressure in many instances.

Additional assumptions regarding the plateau pressure ratio and its typical behavior are made. On the basis of the observed experimental pressure distributions, it is assumed that once the plateau region is reached, the pressure ratio remains fixed until the beginning of reattachment. Figure 5 presents a plot showing how the experimental plateau pressure ratios appear when compared with the correlation equation selected. This equation is the same as the one presented by Sterrett and Holloway (16), except that the numerical coefficient was changed. The plateau pressure ratio has been approximated by the following expression:

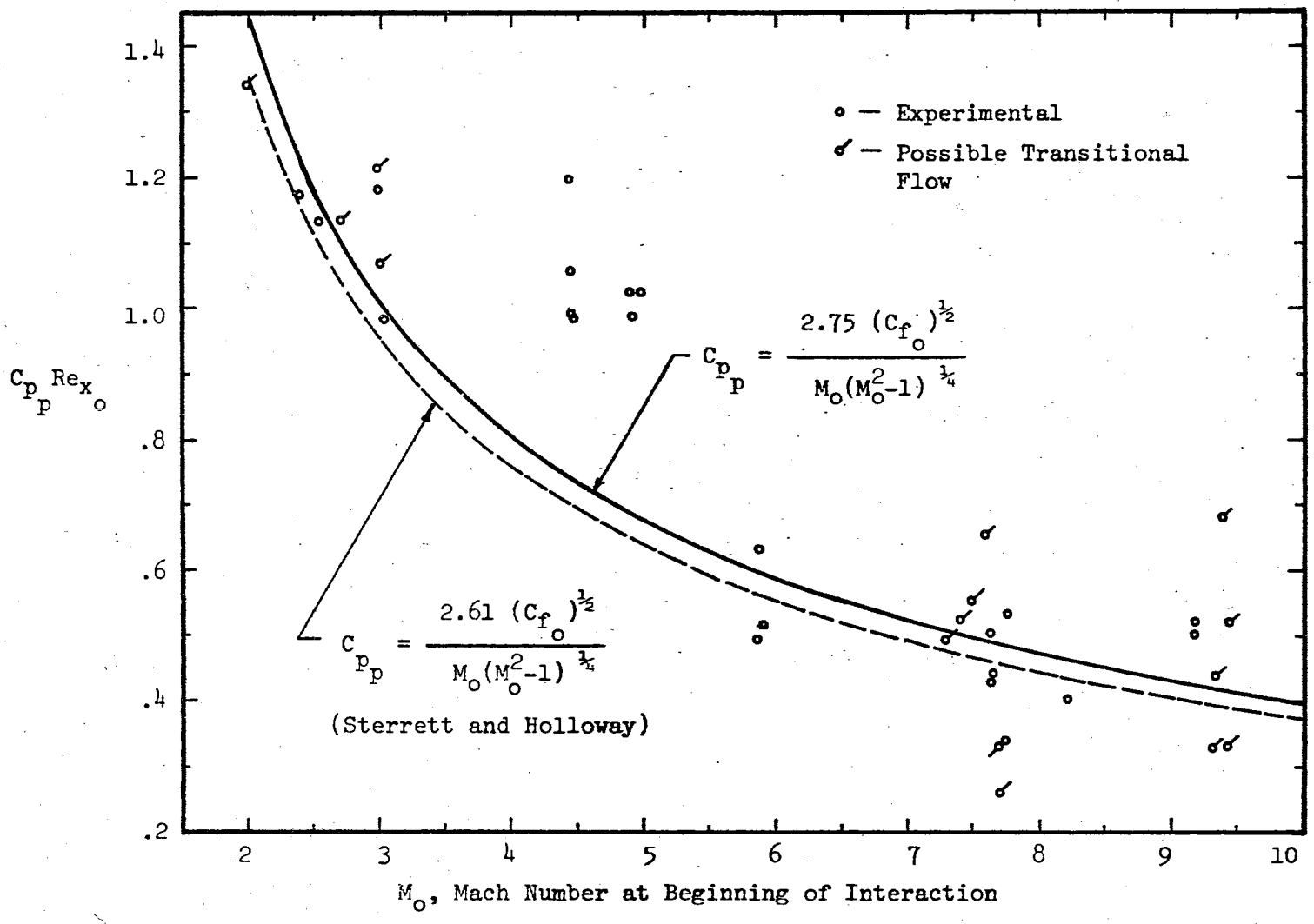

Figure 5. Plateau Pressure Correlation

$$\left(\frac{P}{P_o}\right)_p = 1.0 + \frac{1.1207\ \gamma\ M_o^2}{\left[M_o\left(M_o^2-1\right) Re_{x_o}\right]^{1/4}} \quad . \tag{21}$$

This equation normalizes the spread in the experimental variation and provides a closed mathematical expression for calculation purposes. It should be noted that the dependent parameters are the Mach and Reynolds numbers at the beginning of the interaction.

This plateau pressure equation differs from the one Chapman, Kuehn, and Larson (3) developed in that a $(M_o^{1/4})$ term appears in the denominator. Other semi-empirical correlations (17, 18) were tried, but the expression selected gave the best fit of the data.

The breakaway angle which the dividing streamline makes with the plate was assumed to be the inviscid turn angle which would be necessary to reach the calculated plateau pressure. At low Mach numbers, this technique gives angles which correspond closely with the measured angles in the schlerien photographs. However, at higher Mach numbers these angles were smaller than the measured angles. For a fixed geometry, experimental observations indicate that the plateau pressure ratio increases rather slowly with increasing Mach number, while the overall pressure ratio increases rapidly.

Since the goal of this thesis is to predict the entire pressure interaction, a "beginning of reattachment" must be specified. The scheme being discussed requires that the location where the reattachment pressure rise first starts must be known, and, of course, the resultant pressure distribution should be in good agreement with experimental measurements. Several previous investigators (6, 8, 9) have considered

that the reattachment pressure rise begins at the ramp corner, while Erdos and Pallone (12) use the dividing streamline to locate the reattachment pressure rise. In their solution, Erdos and Pallone assume that the reattachment of the dividing streamline on the ramp corresponds with the mid-pressure point of the reattachment pressure rise. The merit of either of these techniques rests in its correlation with the observed experimental data used. The first procedure, where the pressure rise begins at the corner, has been compared principally with low Mach number data, while Erdos and Pallone have used but a single experiment at Mach 2.0. In this thesis, a general technique was sought. After examining considerable experimental data, a fair approximation for the beginning of reattachment in the Mach 2-10 range, is to consider that the reattachment process begins at the point where the dividing streamline impinges on the ramp. This gives considerable deviation from selected experiments at the lower Mach numbers used (2.0-3.0), but the correlation was found to be quite satisfactory above this range.

The technique for solving the complete interaction pressure distribution is schematically outlined by the computer flow diagram in Figure 6. The only program inputs are free stream Mach and Reynolds numbers, the location of the ramp corner and end of ramp, the ramp angle, an approximate value of the Mach angle which corresponds with the known ramp angle and Mach number, the ratio of specific heats, the ΔK increment used in the numerical integration, an accuracy term, and the $F(K)$ value which correlates the reattachment process. Program inputs also included an estimated value for the location of the separation point and a term which specifies the maximum number of iteration loops allowed before the solution is automatically terminated. The latter

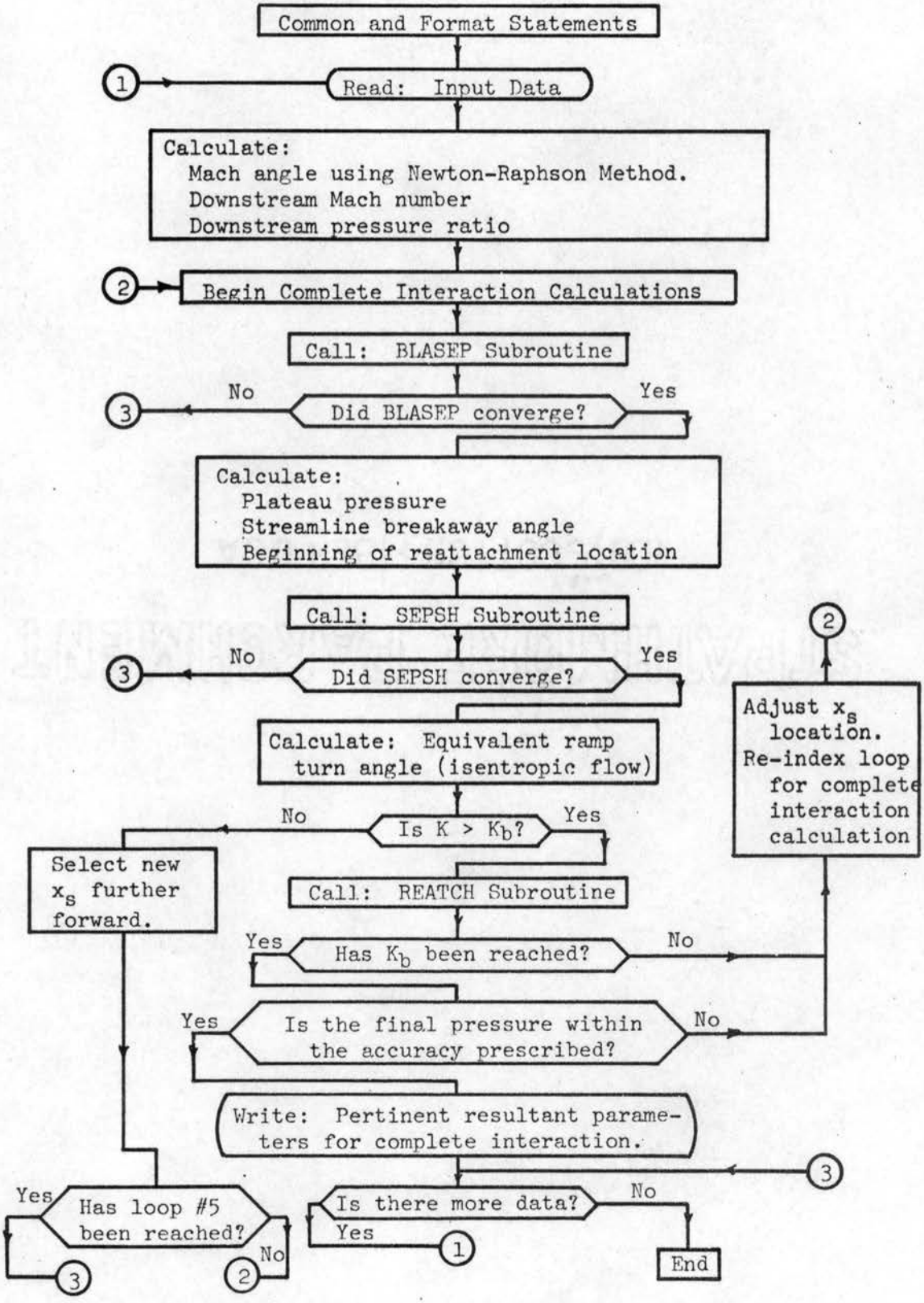

Figure 6. Computer Flow Diagram for Complete Interaction

of these last two terms is used to safeguard against the use of too much computer time when a slow convergence is encountered. An estimated value for the location of separation was used to start the calculations. This very probably could have the effect of reducing the time required to obtain a solution. The value 1.4 has been used throughout this work as the ratio of specific heats, γ. This quantity was assigned a variable name to permit the use of different γ's, had the need arisen. The approximate value for the Mach angle was input to start the Newton-Raphson calculations. This insures that the method will converge on the correct angle. All of the remaining input quantities are obtained directly from the known flow and geometry except for the ΔK increment, accuracy, and F(K) terms. The ΔK increment and accuracy terms are chosen arbitrarily while F(K) comes from a previously determined correlation curve.

Figure 7 explains some of the solution particulars which, together with the flow diagram (Figure 6), will be helpful in the discussion that follows. Note that the location of the separation point controls the whole solution. A change in the location of separation affects the plateau pressure ratio, the dividing streamline breakaway angle, the location of the beginning of reattachment, and hence, the whole pressure distribution. The computational requirements necessitate that the correct downstream Mach number be reached at the same time the Blasius value of K is reached. By adjusting the location of the separation point it is possible to match the downstream requirements and also to have the correct final velocity profile shape.

After reading the input values, the general program first calculates the downstream Mach number and pressure ratio by using the

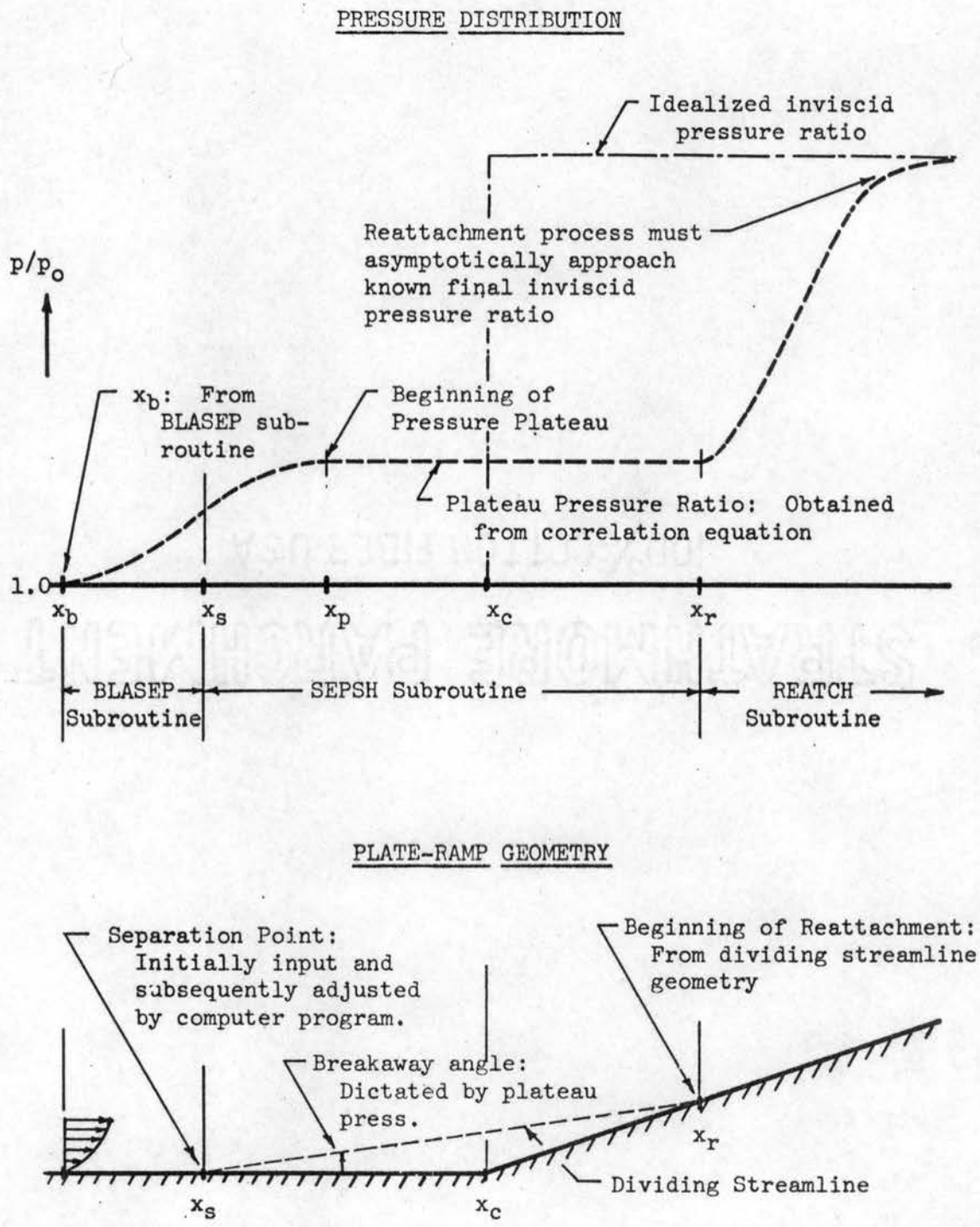

Figure 7. Pictorial Explanation of Complete Interaction Solution

inviscid flow relationships. The pressure ratio becomes the final value which must be matched at the end of the reattachment portion of the solution. The next step in the solution is to solve for the pressure distribution between the beginning of the interaction (Blasius point) and the separation point. The BLASEP subroutine is called for in these calculations.

From the conditions which are found at the Blasius point, the plateau pressure ratio, streamline breakaway angle, and the beginning of reattachment location are determined. Next the pressure distribution between the separation point and the beginning of reattachment is found, using the SEPSH subroutine. This subroutine calculates a pressure distribution ahead of the pressure plateau and maintains a constant pressure ratio throughout the plateau.

The x-distance measurements are made along the surface of the plate and ramp, rather than along the axis. The direction of the streamline at the edge of the boundary layer, θ, is measured with reference to the plate and ramp surfaces. At the ramp corner this reference changes and necessitates a compensation in the reattachment portion of the solution. The angle θ is calculated using the Prandtl-Meyer relationship. Since the local free stream Mach number does not change in the plateau region, the direction of streamline at the edge of the boundary layer remains fixed. As far as the pressure in the outer inviscid flow (outside the boundary layer) is concerned, the change in the direction of the plate and ramp boundary is not realized until the beginning of the reattachment pressure rise. For this reason, no change in the value of θ has been incorporated prior to the beginning of reattachment. For calculation purposes, the measured value of the ramp angle cannot be used for

this turn. Instead, an equivalent turn angle obtained from the Prandtl-Meyer relationship must be used. This is necessary because the incremental changes in the outer streamline direction have been approximated by using the Prandtl-Meyer equation. By such a procedure, the downstream Mach number and streamline direction may be matched for all flows, once the correct separation point location has been obtained.

The next step in the computer program is to solve the reattachment region. For this, the REATCH subroutine is called. The solution in this region starts at the last point in the SEPSH solution and works toward the Blasius-profile flow. The correct overall solution is obtained when the downstream pressure ratio and Blasius K value are reached simultaneously. When this desired end result occurs, the pressure distributions found by the BLASEP, SEPSH, and REATCH subroutines give the correct overall pressure distribution. When a satisfactory match in the reattachment region is not obtained, a new location for the separation point must be selected and the entire cycle of calculations repeated, starting with the BLASEP subroutine.

Two corrections are possible in repositioning the separation point. The separation point must move either upstream or downstream with respect to its previous location. This adjustment can be determined from the way K and the pressure ratio behave near the end of the REATCH solution. In the case where the Blasius value of K is reached before attaining the desired pressure ratio, the separation point must be moved forward of its previous location. When the final pressure ratio is reached before the Blasius K value is reached, the pressure distribution will intercept rather than asymptotically approach the final downstream pressure. This signifies that the mixing region was too large and that

the separation point should move closer to the ramp corner. Figure 8 illustrates the characteristic behavior of the pressure distribution when the separation point is forward, aft, and at the correct location. Another point to be noted in this figure is that the plateau pressure ratio decreases as the separation point moves closer to the corner.

The general program adjusts the separation point location in accordance with the checks mentioned. The magnitude of the adjustment is controlled by how closely the final end conditions are matched. In general, it takes only a few steps for the solution to converge on a separation point which will satisfy the end conditions downstream.

An item which has not been previously discussed and which has considerable affect on the speed of convergence is the use of accuracy terms. This value, like the size of the integration increment, is arbitrary. The accuracy term is used in both the BLASEP and SEPSH subroutines and in the general program. In the BLASEP subroutine it is used in determining when the correct ε_s and ζ_s have been found, and in the SEPSH subroutine it is used in matching the calculated plateau pressure ratio. Its use in the two subroutines will be discussed in the following two sections. In the general program it is used in a check to see if the calculated final pressure ratio is close enough to the inviscid final value to allow the solution to be concluded. Figure 9 illustrates how the accuracy term is used in specifying the band of values which constitute an acceptable solution. In all cases, K must reach the final Blasius value before the check is performed. This means that the final pressure cannot be greater than the final inviscid value, but it can be in the range determined by the accuracy term.

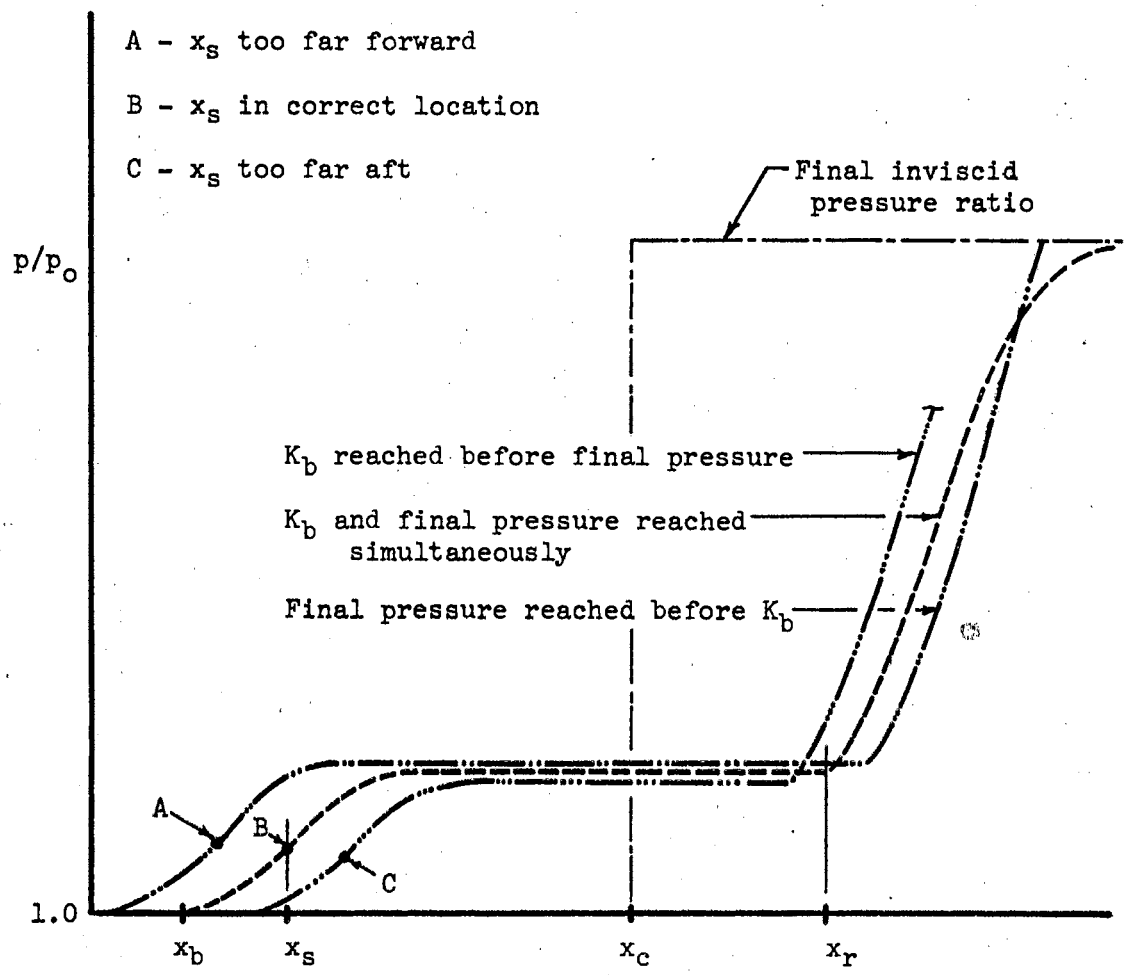

Figure 8. The Effect of Separation Point Location on the Interaction Pressure Distribution

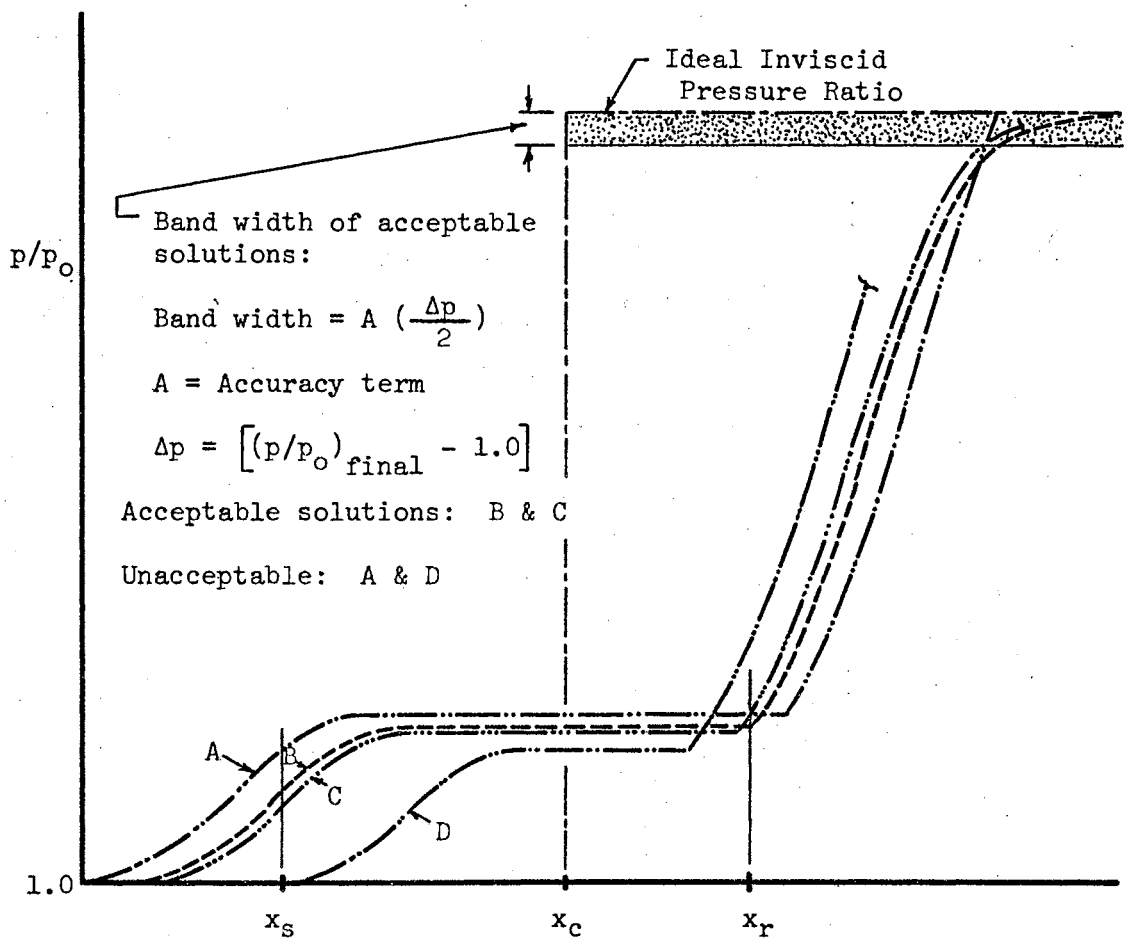

Figure 9. Use of Accuracy Term in Determining an Acceptable Solution in the General Program

An accuracy term of .05 has been used throughout this investigation. This value is used in the general program and both subroutines. In preliminary calculations, values larger and smaller than .05 were used. It was found that the number of steps needed to obtain the desired convergence increased with smaller accuracy terms, while the overall accuracy decreases rapidly with larger values. For an engineering solution, .05 was found to give good results.

The ΔK increment used in the numerical integrations likewise has some bearing on the overall accuracy. After trying several values, .003 was selected and used throughout.

Blasius Point to Separation (BLASEP Subroutine)

The semi-empirical correlation parameters mentioned in Chapter III are the same as those developed by Glick in the region upstream of separation where the boundary layer is attached. The differential equations (13) and (14), incorporating these semi-empirical parameters, were programmed as the BLASEP subroutine. A flow diagram for this subroutine is given in Figure 29 of Appendix C, and the Fortran listing is given in Appendix D.

This subroutine requires that values of ε and ζ, analogous to Mach and Reynolds numbers, be chosen at the separation point. Once selected, these values are used to start the step-by-step calculations which move upstream in ΔK increments to the Blasius point. The solution in this subroutine involves trying repeated choices of ε and ζ at the separation point in order to end with the correct values at the Blasius point.

The values corresponding to the Blasius point which must be matched are obtained by assuming that the weak hypersonic pressure interaction

solution applies along the plate. These quantities are calculated by using the following two equations:

$$\zeta_b = \frac{t\sqrt{A}\sqrt{Re_{x_b}}}{(1-K_b)} \tag{22}$$

and

$$\varepsilon_b = \frac{M_\infty\left(1+\frac{\gamma-1}{2}M_\infty^2\right)C(K)(1-K)^2}{\sqrt{M_\infty^2-1}\sqrt{A}\sqrt{Re_{x_b}}}\left[1-\frac{KF}{1-K}\left(1+\frac{\gamma-1}{2}M_\infty^2\right)\right]\Bigg|_{K=K_b} \tag{23}$$

where A = 0.44. (An explanation and derivation of these expressions is given in Appendix A.) The quantity ε_b may also be written in a linearized form by making the assumption that $M_\infty >> 1$. However, this form of the equation was not used in the BLASEP subroutine, because there are large differences between the exact and linearized values at low Mach numbers.

The solution which was obtained between the Blasius and separation points differs from Glick's work in that the exact form rather than linearized form of the differential equations have been used. This point, while not terribly important at lower Mach numbers, does make an appreciable difference in the results obtained at higher Mach numbers. It is interesting to note that all the methods which were mentioned in Chapter II make use of the assumption that $\varepsilon << M_\infty$, implying that $M_e \approx M_\infty$. With this approximation, the differential equations are expressed in their linearized form.

From equation (23) it is noted that the value of ε_b increases as a function of M_∞^4. Therefore, as the Mach number increases, the assumption that $\varepsilon << M_\infty$ becomes more subject to question. Figure 10 illustrates the magnitude of error involved in this assumption. The absolute value of the ratio ε_b/M_∞ has been plotted as a function of both Mach

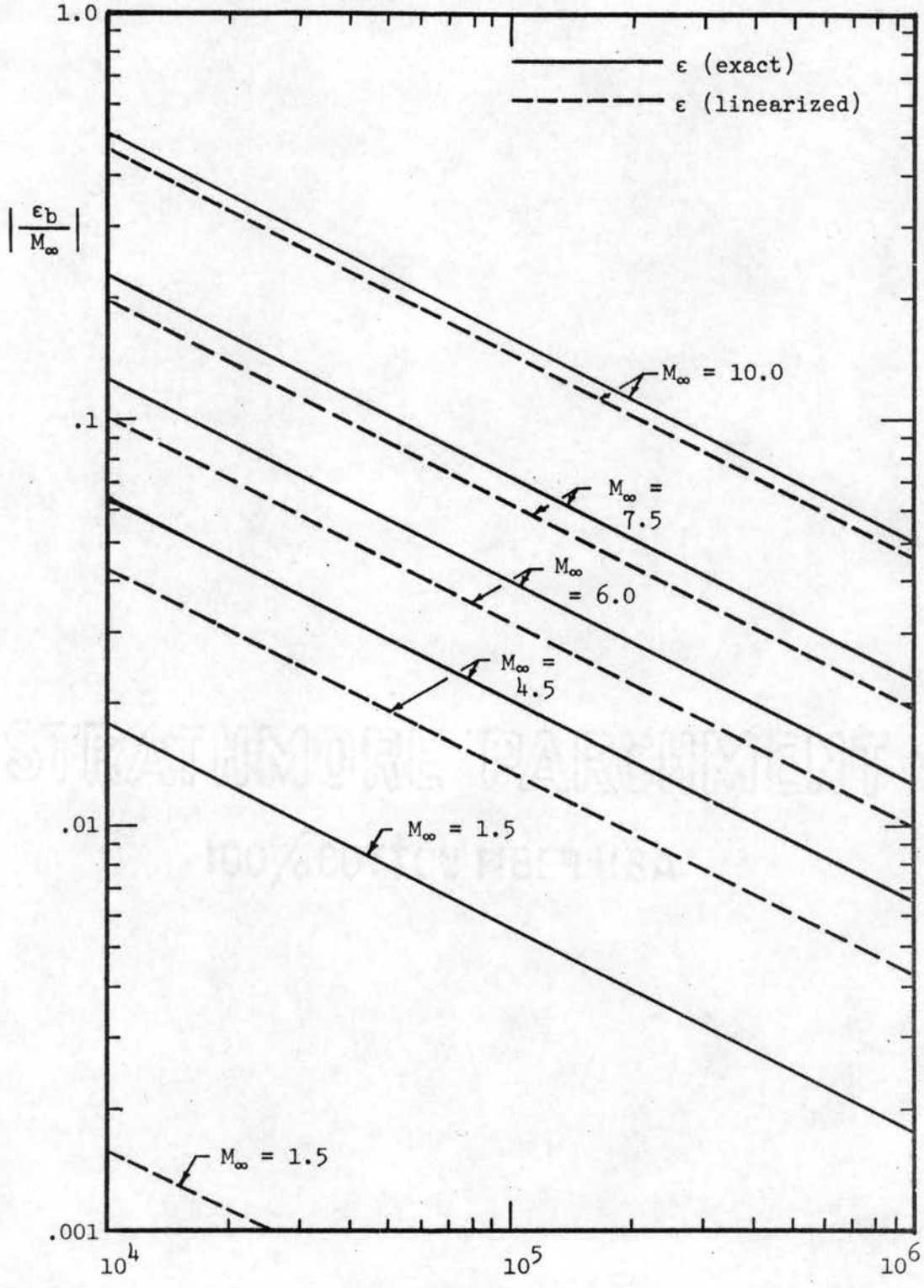

Figure 10. $\left|\frac{\varepsilon_b}{M_\infty}\right|$ as a Function of M_∞ and Re_b

and Reynolds numbers. The values of ε_b used in plotting this figure have been found by using both the exact and linearized form of the ε_b equation. It is observed that the linearized and exact values approach each other at higher Mach numbers, and that the ε_b/M_∞ ratio increases with increasing Mach number when the Reynolds number is held fixed.

The relationship illustrated in Figure 10 applies only to the ε value calculated at the Blasius point. Since the magnitude of ε increases throughout the interaction, the ε/M_∞ ratio would be larger and raise even more doubt about the use of the linearized equations. For this reason, the exact form of the differential equations and the exact Prandtl-Meyer relationship have been used in preference to the linearized forms. This involves no added complexities as far as the computer solution is concerned.

The numerical solution performed by the computer makes use of a refined Runge-Kutta method devised by Gill (19, 20). The discussion and explanation of these calculations is given in Appendix B. All calculations have been incremented with K as the independent variable.

The correct solution requires that ε and ζ must be matched at the Blasius point. This is complicated by the fact that changes in either ε_s or ζ_s will cause changes in the location found for x_b. This causes ε_b and ζ_b to take on ever-changing values as the convergence progresses. It was found that during the convergence, ε was the more sensitive of the two variables. As a result, it was convenient to first converge on the correct ε_s, and then to work on ζ_s, rather than to converge on both values simultaneously. The convergence scheme which was finally used evolved largely from the trial-and-error approach. Often a technique which works well at low Mach numbers will converge very slowly at

higher Mach numbers, and conversely. The system which was finally adopted gave satisfactory convergence speed over the entire Mach 2-10 range. However, it was not the optimum solution in some regions of this range.

The accuracy term was employed in the check to see if satisfactory ε_s and ζ_s values had been found. Here, as in the matching of the final pressure ratio in the general program, the accuracy term is used to specify the band of values which constitutes an acceptable solution. The smaller the accuracy term; the narrower the band; the larger a number of trials needed to reach convergence.

Separation to Beginning of Reattachment (SEPSH Subroutine)

In this region, equations (15) and (16) were programmed for computer solution as the SEPSH subroutine. The flow diagram which illustrates the computational procedure is given by Figure 30 in Appendix C, and the Fortran listing is given in Appendix D. The ε and ζ values which have been found at the separation point are used to start the solution.

The only semi-empirical parameter to be handled in this region is the C(K) or mixing term. The mixing is of paramount importance and as a result is dominant over the effects any changes in F(K) and D(K) may have. Glick has proposed two techniques for treating the C(K) values in this region. He conjectures that C(K) rises from zero at the separation value of K to some maximum value at the beginning of the plateau, and that C(K) remains constant after this point. He offers a simplified and refined approach as an approximation for this distribution of C(K). In the simplified case, C(K) takes on a constant value

$\overline{C}$ throughout the whole region. In the refined case, C(K) has a value of C_1 between separation and the plateau, and a value of C_2 throughout the plateau region. The values of $C_1 = 11.0$ and $C_2 = 15.0$ presented by Glick were obtained from one set of experimental data (Mach 2.45). These values were suggested as universal for all separations. Figure 11 illustrates the various C(K) trajectories from Glick's work.

In this study it was found that C(K) takes on a behavior different from that specified by Glick. First, C_1 does not universally equal 11.0 but has a dependency on the Mach and Reynolds numbers at the beginning of the interaction. Also, a constant value for C_2 was found to produce a decreasing rather than constant pressure ratio in the plateau. If a constant pressure ratio is to be maintained, C(K) must continually increase with increasing K values. The definition for C(K),

$$C(K) = \frac{\overline{m}}{\mu_e \rho_e u_e} \frac{d\overline{m}}{dx} \quad ,$$

points out the inconsistency in fixing C_2 as a constant. The only way that C(K) may be constant in the plateau region, according to the definition, is for $\overline{m}$ to be constant and hence $d\overline{m}/dx$ to be zero. However, this results in a value of zero for the mixing parameter.

In the SEPSH subroutine, C(K) is assumed to have a constant value of C_1 between separation and plateau, and then to follow a trajectory such that the pressure remains constant in the plateau. Since C_1 is not a universal value, the subroutine has a built-in convergence scheme for finding the correct C_1 value. The subroutine calculates an initial C_1 and then makes subsequent adjustments until the plateau pressure ratio determined by equation (21) is reached. The accuracy term is used in specifying the range of values for an acceptable matching of

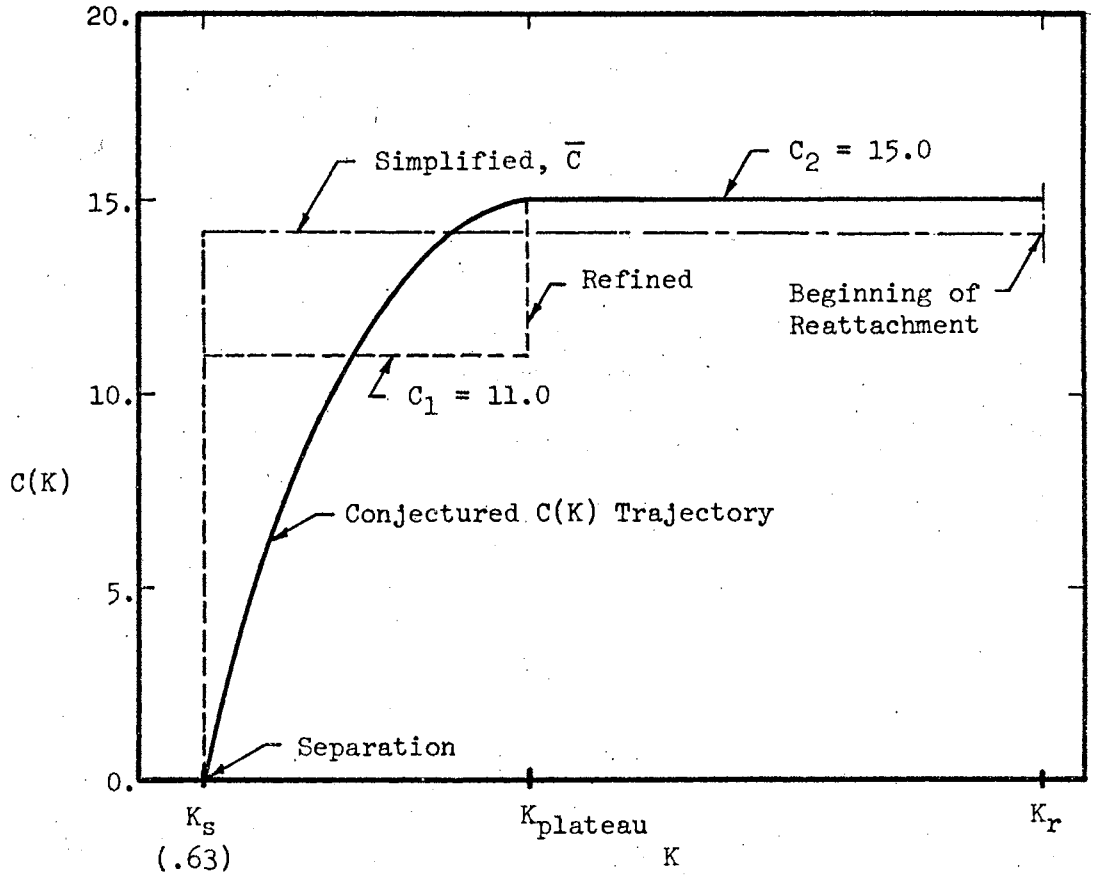

Figure 11. Glick's C(K) Trajectories Between Separation and Shock Impingement

the plateau pressure ratio. Figure 12 illustrates how C_1 affects the pressure distribution between separation and the plateau and how the accuracy term is employed.

With C_1 a fixed constant, the program simply marches in ΔK steps from the separation point to the plateau, calculating the corresponding pressure ratio and x-location value for each step. The beginning of the plateau is reached when the pressure gradient (dp/dx) equals zero. This portion of the calculations is repeated until a C_1 is found which gives a correct matching of the plateau pressure ratio. From this point on to the beginning of reattachment, C(K) is calculated in each ΔK step such that the pressure gradient remains equal to zero. When the known x-location that corresponds to the beginning of reattachment is reached, the SEPSH subroutine is completed, and control is returned to the general program.

Figure 13 illustrates the C(K) behavior for this region. In all cases C(K) increases with K in the pressure plateau -- serving as an indication that the mixing becomes more vigorous with increased distance down the plateau, rather than remaining constant as Glick assumed. The length of the plateau, K_p to K_r, is determined in part by the overall magnitude of the reattachment pressure rise. At a given Mach number, the length of the region increases with the increase in pressure rise. The numerical values which K_p and K_r assume are not fixed, but vary, depending on the flow and geometry. In general, K_p has values in the vicinity of 0.70 - 0.77. The value of the corresponding K_r is larger than or equal to K_p and must have a value greater than 0.693 (the Blasius value) if the REATCH subroutine is to work. When K_r is less than or equal to K_b, this indicates that the separation point

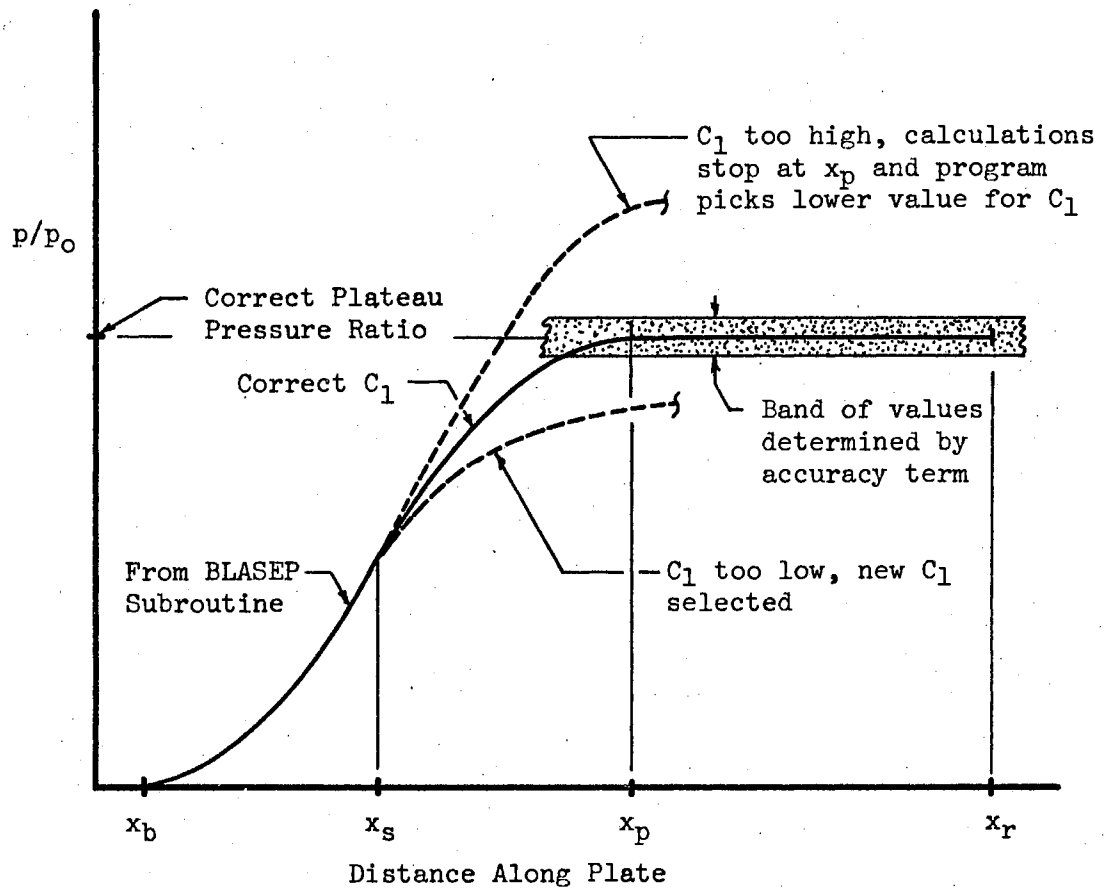

Figure 12. Solution in the SEPSH Subroutine

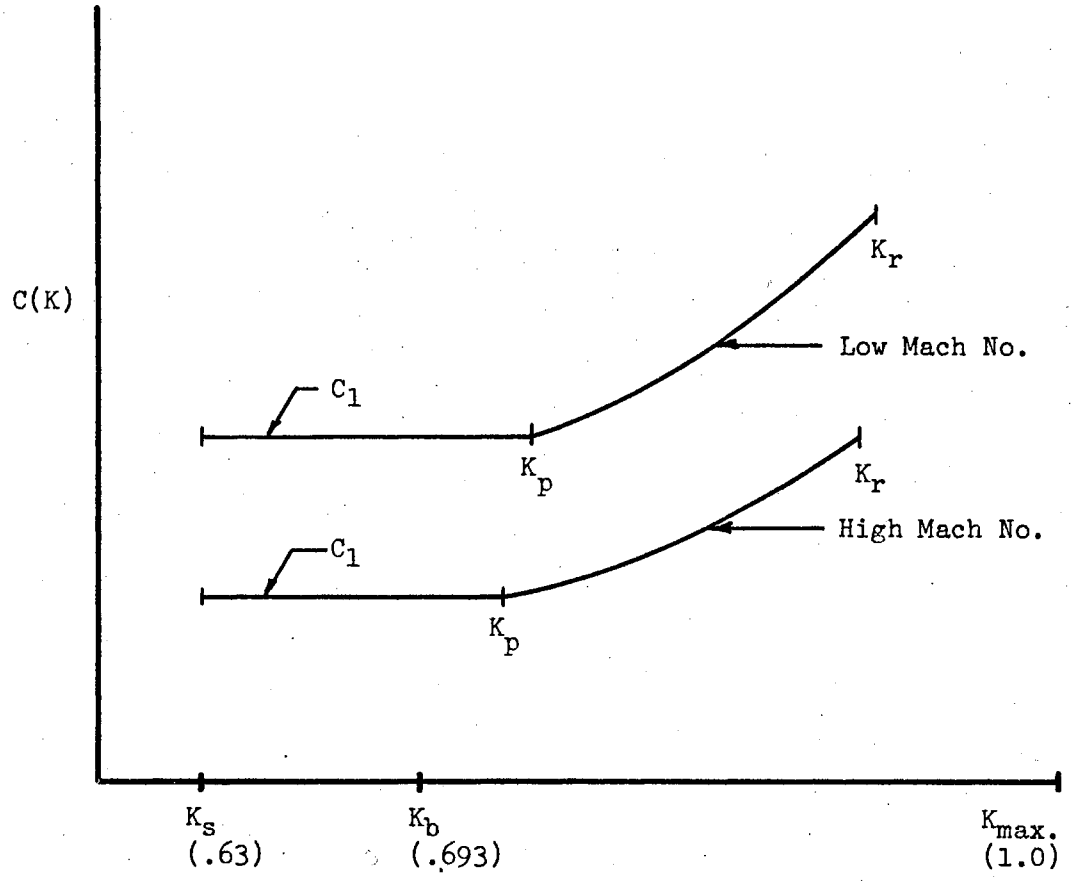

Figure 13. C(K) in the Separation to Beginning of Reattachment Region

should be moved forward to obtain a workable solution. If this condition occurs within the first five loops in the calculation procedure (see Figure 6), a new x_s further forward is automatically selected. Beyond the fifth loop, the solution is terminated when K_r is less than K_b.

Reattachment (REATCH Subroutine)

The reattachment process starts at the point where the dividing streamline impinges on the ramp. Equations (17) and (18), which were derived for this region, are solved in the REATCH subroutine. A schematic representation of the computational details is given in the flow diagram which appears as Figure 31 in Appendix C. A complete Fortran listing for this program is given in Appendix D.

The solution in this region must begin with the values of K, ζ, and M_e which were found for x_r in the SEPSH subroutine. The numerical value of these three quantities for a given set of flow conditions and geometry is affected by the length of the mixing region. The K and ζ values at the start of reattachment increase while M_e decreases slightly as the separation point is moved forward. One other parameter, F(K) must be considered. It has been assumed that this quantity has a constant value throughout the reattachment process, and that this value is dependent on the size of the ramp angle and the free stream Mach number. These values were determined from correlation with existing experiments and are discussed in the next chapter. The parameter F decreases with increasing Mach number. For a given Mach number F decreases with increasing ramp angles as shown.

The direction of the streamline at the edge of the boundary layer, θ, is measured with reference to the ramp surface in the reattachment region. Ahead of the reattachment region this angle is measured with the plate as the reference. This angle starts from a small positive value at the start of the interaction and increases continually until a constant angle is reached at the beginning of the pressure plateau. In the reattachment region the measurement reference changes, and θ assumes negative values until the end of reattachment. As the solution progresses through the reattachment region the free stream Mach number continually decreases, causing the outer streamline direction to rotate in a counter-clockwise direction. At the end of the reattachment process this outer streamline is parallel with the ramp, corresponding to the initiation of Blasius-type flow downstream of reattachment.

The Prandtl-Meyer relationship has been used to calculate an equivalent turn angle for the ramp deflection angle, and this assures that the correct downstream Mach number, pressure ratio, and streamline direction must all be reached simultaneously. However, it does not assure that K_b and the downstream pressure ratio will be reached together. This latter match is possible only in one case, when x_s is at the correct location.

Figures 8 and 9 illustrate the general requirements for a satisfactory solution. The REATCH calculations proceed in ΔK steps, working from K_r to K_b. The subroutine continues until either the final pressure ratio or K_b is reached. When the pressure ratio is reached first, this signals the general program that an unsatisfactory reattachment was made and that a new separation point must be selected. If K_b is reached first, the general program performs a check to see if the

pressure is within the band set by the accuracy term. If it is not, a new separation point must be tried and the calculations must be repeated.

Experimental Data

The previous sections in this chapter have been devoted to explaining the computer solution of the complete interaction. This section discusses the type of experimental data needed, limitations which have been imposed as a result of the data which were available, and the manner in which the data have been employed in the overall study. The purpose in using this experimental data was to obtain a F(K) correlation for the reattachment region.

A sequence of data was needed at several uniformly-spaced Mach numbers between 2 and 10, in which the Reynolds number and ramp angle were varied independently. This permits a discrimination between the effects of Mach number, Reynolds number, and the strength of the interaction (ramp angle). To obtain an optimum correlation of the semi-empirical parameters, a wind tunnel test program would have been desirable. Since this was not feasible, data which were currently available had to be utilized.

The whole method is dependent upon the location of the separation point. This point should be located with as much precision as possible in order to obtain a good semi-empirical correlation. In addition to the separation point, closely-spaced pressure measurements along the plate and ramp are highly desirable. The plateau pressure ratio and beginning of reattachment are determined from this distribution. Schlieren photographs, when used in conjunction with the pressure

distribution, are extremely helpful in locating the separation point and in determining whether the flow remains laminar throughout the entire interaction region.

A current problem common to the study of high velocity laminar separated flows is that only a limited amount of experimental data is available. An effort was made to obtain and use data taken under a wide variety of flow conditions and from a variety of tunnel facilities. Much of the data used had not been previously published in the open literature. If it had, it was generally of recent origin. A total of 38 cases with Mach numbers between 2 and 10 were selected for analysis. The ramp angle in these selected experiments ranged from 5 to 30 degrees. Because of the general scaracity of data, some experiments which normally would be of marginal value were used. A complete tabulation of this data, together with some of the results which were obtained, is given in Table I of the next chapter.

The Reynolds numbers at the start of the interaction varied between 10^5 and 10^6, with a few exceptions. If plotted, the Mach and Reynolds number values give a good scatter of data between Mach 2 and 10 and Reynolds numbers 10^5 and 10^6.

Much of the unpublished data was of limited value, because there were no accompanying schlieren photographs or supplementary information. The separation point location was not given in much of the data. In the cases where it was not specified, the separation point was assumed to lie at the point where the slope of the pressure distribution curve was a maximum in the region ahead of the plateau. This technique introduces chance for appreciable errors, particularly in the case where the surface pressure measurements are not spaced close to one another.

Without a photograph, there is no way of knowing whether the reattachment was transitional or laminar. The nearly constant plateau region was taken as an indication that the flow remained laminar through most of the interaction.

Another problem which was encountered is that it is possible that three-dimensional effects become appreciable at higher Mach numbers. Putman (21) and other experimentalists have noted that two-dimensional flow cannot be obtained at higher Mach numbers, i.e., above Mach 8 to 10. Even two-dimensional models with end plates do not aleviate this difficulty. As a result, only three-dimensional type flows can be obtained at higher Mach numbers. Due to this problem, this study has been limited to Mach numbers below 10.

The Mach 10 data had only limited pressure measurements on the ramp surface and did not afford an opportunity to make a good comparison between the calculated reattachment pressures and the experimental measurements. Analysis of Mach 16 data by Miller et al (22) was attempted, but the leading edge interaction effects were such that it was not possible to make a satisfactory correlation. Another problem at high Mach numbers is that the normal pressure gradient across the boundary layer is no longer zero.

The data used in this investigation was utilized in a manner which will be described.

The BLASEP and SEPSH subroutine portions of the general program were used to calculate the pressure distribution in the region ahead of the beginning of reattachment. The separation point, which had been determined experimentally, was used in these computations. The final values of K, ζ, and M_e from these calculations correspond with the

start of reattachment. These are used to start calculations in the reattachment region. In addition, many other intermediate parameters are calculated by these subroutines. Several of these have been tabulated and are given in Table I in the subsequent chapter.

The F value necessary for the correct reattachment pressure rise must be found. To do this, the REATCH subroutine was modified into a F-Calculation program. The flow diagram and listing for this program is given in Appendix C and Appendix D respectively.

Through repeated choices, the correct value of F is found so that the correct downstream pressure ratio and K_b are reached simultaneously. In this convergence on F, an accuracy term is employed. The accuracy term is employed in the same manner as has previously been illustrated for the C_1 convergence in the SEPSH subroutine. Figure 14 illustrates how the behavior of F influences the correct matching of the downstream pressure ratio.

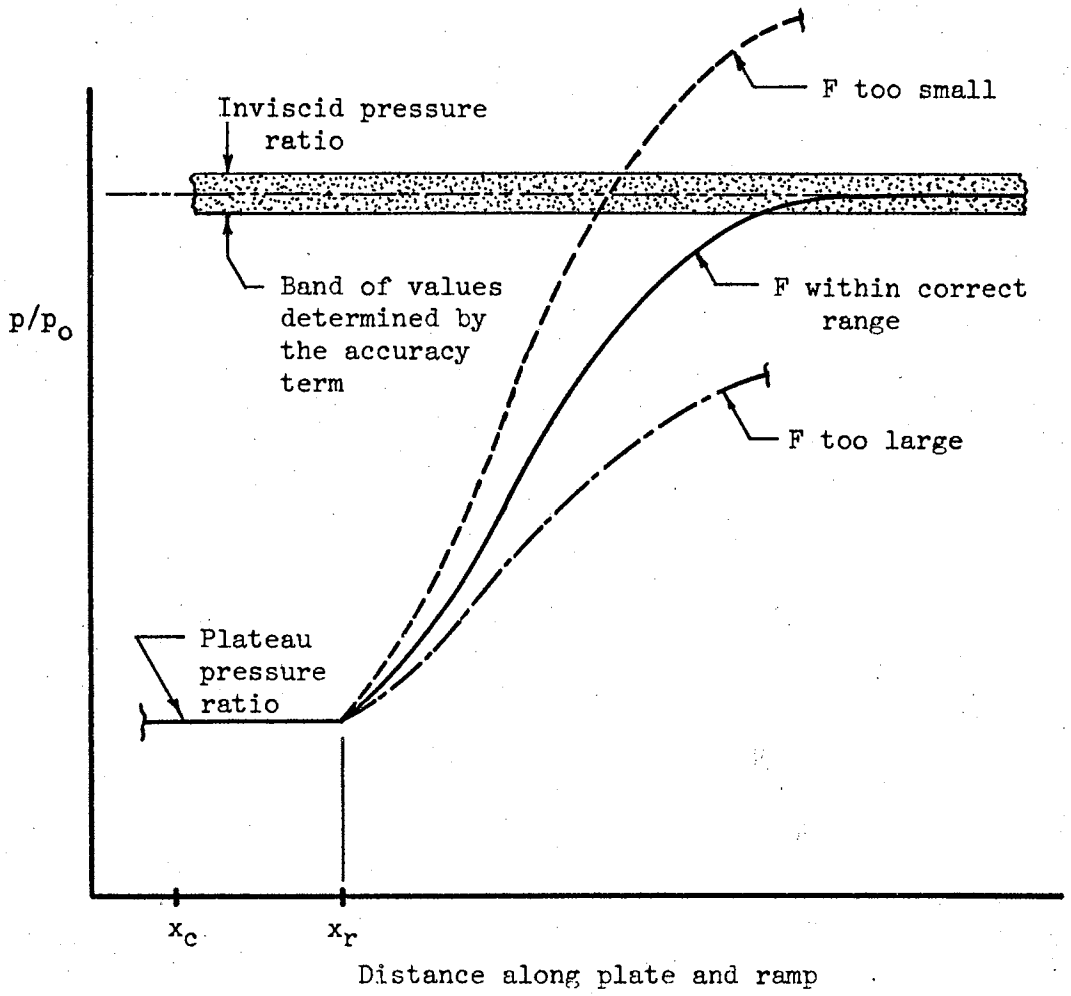

Figure 14. F Behavior in Reattachment Region (F-Calculation Program)

CHAPTER V

DISCUSSION OF RESULTS

This chapter details the experimental data which were reduced and used in determining the C_1 and F(K) correlations. The F(K) values are needed to obtain a solution for the complete pressure distribution in the interaction region. Also included are examples showing the comparison between the general program calculations and experiment.

Reduction of Experimental Data

The data assembled for use in determining the needed correlations were analyzed in the manner described in the previous chapter. The principal data and results collected during the course of this investigation are presented in a concise form in Tables I through IV.

Table I lists the pertinent parameters which were taken directly from the experimental data. With the exception of x_s and $(p/p_o)_p$, this table lists the quantities which the design engineer would have at his disposal for determining the interaction solution. The $(p/p_o)_p$ values given in Table I have been plotted in Figure 5 and show the comparison between the approximate experimental plateau pressure ratio and the value obtained from the correlation equation (21).

The x_s values given in Table I were of paramount importance in finding the C_1 and F correlation values. In the cases where x_s was approximated by the maximum slope technique, the value in Table I has

TABLE I

EXPERIMENTAL DATA USED IN THE CORRELATION

No.	Mach No.	Source	Re/In	Ramp Angle	x_c,In	x_s,In	$(p/p_o)_p$ [c]
1	2.00	3,6	151,000.	6.50[c]	1.962	1.515	1.18
2	2.45	3,6	60,000.	13.00[c]	.900	.315	1.46
3	2.55	23	70,800.	10.00	2.280	1.050[c]	1.33
4	2.70	28	467,000.	10.00	2.250	1.643	1.20
5	3.00	24	34,000.	10.00	8.000	5.700	1.37
6	3.00	24	95,000.	20.00	8.000	6.250	1.25
7	3.00	24	34,000.	30.00	8.000	4.790	1.40
8	3.06	23	109,100.	10.00	2.280	1.120[c]	1.36
9	4.50	25	120,000.	15.00	8.000	5.660	1.50
10	4.50	25	89,000.	30.00	8.000	3.400	1.75
11	4.50	25	88,000.	15.00	8.000	5.500	1.55
12	4.50	25	120,000.	30.00	8.000	3.660	1.60
13	5.00	24	93,000.	15.00	8.000	4.450	1.70
14	5.00	24	280,000.	15.00	8.000	4.460	1.55
15	5.00	24	97,000.	30.00	8.000	2.390	1.85
16	6.00	a	103,300.	14.00	6.000	4.000[c]	1.50
17	6.00	b	83,500.	20.00	12.000	6.750[c]	1.60
18	6.00	b	83,590.	10.00	12.000	9.300[c]	1.45
19	8.00	a	18,330.	20.00	10.000	7.120	2.05
20	8.00	a	24,200.	20.00	10.000	7.500	2.05
21	8.00	a	35,000.	20.00	10.000	7.250	2.05
22	8.00	a	54,200.	20.00	10.000	6.750[c]	2.15
23	8.00	b	85,670.	20.00	12.000	6.500[c]	1.70
24	8.00	26	250,000.	15.00	7.250	4.600[c]	1.65
25	8.00	26	250,000.	22.50	7.250	3.400[c]	1.50
26	8.00	b	85,210.	5.00	12.000	11.000[c]	1.20
27	8.00	b	85,280.	10.00	12.000	9.250[c]	1.40
28	8.00	b	86,350.	10.00	12.000	9.450[c]	1.50
29	8.00	b	86,800.	15.00	12.000	7.300[c]	1.70
30	8.00	b	87,580.	20.00	12.000	5.350[c]	1.85
31	8.45	a	590,000.	14.60	6.000	3.250[c]	1.55
32	10.00	b	82,820.	10.00	12.000	9.000[c]	1.75
33	10.03	27	126,000.	10.00	8.725	8.000[c]	1.70
34	10.03	27	126,000.	20.00	8.725	5.800[c]	2.00
35	10.03	27	126,000.	30.00	8.725	3.850[c]	2.20
36	10.03	21	127,000.	10.00	8.750	8.250[c]	2.10
37	10.03	21	127,000.	20.00	8.750	6.500[c]	2.50
38	10.03	21	127,000.	30.00	8.750	3.750[c]	2.25

a Unpublished NASA Langley Research Center data (29)
b Unpublished Air Force Flight Dynamics Laboratory data (30)
c Approximated from data

TABLE II

PARAMETERS DETERMINED BY BLASEP SUBROUTINE

No.	x_b, In	Re_{x_b}	M_{e_b}	ζ_b	M_{e_s}	ζ_s	$(p/p_o)_s$
1	1.2206	184,311.	1.991	517.9	1.901	558.0	1.150
2	.1880	11,280.	2.399	107.5	2.287	127.6	1.192
3	.7850	55,578.	2.525	223.9	2.406	246.3	1.203
4	1.4809	691,580.	2.692	733.8	2.568	758.8	1.211
5	4.6236	157,202.	2.978	309.2	2.840	330.8	1.232
6	5.4281	515,669.	2.988	557.2	2.853	584.6	1.226
7	3.6943	125,606.	2.975	276.4	2.840	301.6	1.226
8	.8788	95,877.	3.030	236.1	2.888	255.0	1.240
9	4.7991	575,892.	4.462	329.4	4.256	347.1	1.300
10	2.6630	237,007.	4.441	212.8	4.238	230.9	1.295
11	4.4898	395,102.	4.454	273.5	4.251	292.3	1.296
12	3.0018	360,216.	4.452	261.4	4.245	278.4	1.301
13	3.5600	331,080.	4.929	212.2	4.699	227.8	1.316
14	3.8383	1,074,724.	4.961	378.5	4.733	397.0	1.312
15	1.7606	170,778.	4.901	154.0	4.680	170.5	1.304
16	3.1186	322,151.	5.865	155.6	5.588	168.6	1.342
17	5.1855	432,989.	5.884	179.6	5.616	195.8	1.327
18	7.4887	625,980.	5.903	214.6	5.628	229.8	1.337
19	5.4072	99,114.	7.306	58.3	6.971	64.0	1.348
20	5.6212	136,033.	7.407	66.6	7.068	73.5	1.349
21	5.3876	188,566.	7.496	76.7	7.154	84.5	1.349
22	5.0548	273,970.	7.582	90.9	7.234	100.1	1.352
23	4.8239	413,264.	7.660	109.1	7.311	120.2	1.349
24	3.5614	890,350.	7.768	156.0	7.408	169.7	1.357
25	2.5768	644,200.	7.727	134.0	7.372	146.7	1.354
26	8.4190	717,383.	7.742	141.0	7.386	154.2	1.353
27	7.0918	604,789.	7.719	130.1	7.360	142.2	1.358
28	7.1551	617,843.	7.722	131.4	7.366	143.9	1.354
29	5.5683	483,328.	7.685	117.2	7.327	128.4	1.359
30	4.0288	352,842.	7.632	101.5	7.278	111.6	1.356
31	2.5824	1,523,616.	8.232	183.3	7.843	197.2	1.370
32	6.9053	571,897.	9.327	88.8	8.895	97.1	1.367
33	6.1253	771,788.	9.444	100.8	9.012	110.4	1.363
34	4.4182	556,693.	9.340	87.4	8.914	95.6	1.362
35	2.9746	374,800.	9.190	74.2	8.770	80.9	1.361
36	6.2452	793,140.	9.452	102.0	9.020	111.7	1.363
37	4.9711	631,330.	9.382	92.3	8.947	100.8	1.369
38	2.9009	368,414.	9.182	73.6	8.761	80.2	1.362

TABLE III

PARAMETERS DETERMINED BY SEPSH SUBROUTINE

No.	x_p,In	K_p	M_{e_p}	ζ_p	C_1	K_r	ζ_r
1	1.656	.702	1.878	737.8	15.32	.867	1570.5
2	.439	.750	2.149	265.0	12.17	.946	1125.1
3	1.285	.735	2.336	403.8	12.43	.935	1515.9
4	1.722	.687	2.558	915.7	17.63	.880	2262.4
5	6.568	.720	2.797	474.9	11.81	.852	870.8
6	6.655	.690	2.840	713.9	13.78	.820	1194.4
7	5.651	.729	2.783	460.6	12.25	.867	907.0
8	1.358	.735	2.821	404.6	11.53	.924	1320.6
9	6.513	.717	4.214	478.5	9.65	.824	758.0
10	4.288	.744	4.142	379.9	9.73	.905	990.5
11	6.602	.732	4.183	441.2	9.94	.829	680.9
12	4.417	.732	4.181	418.5	9.45	.899	1077.0
13	5.642	.744	4.598	372.8	9.12	.869	715.3
14	5.025	.708	4.701	521.7	9.31	.882	1257.3
15	3.255	.759	4.529	316.0	9.12	.932	1079.2
16	5.518	.759	5.421	308.3	8.14	.811	391.2
17	9.090	.756	5.461	348.6	8.50	.849	557.7
18	11.949	.744	5.515	372.5	8.13	.776	424.9
19*	10.712	.761	6.523	148.4	8.01	.761	148.4
20*	10.583	.745	6.648	153.6	8.10	.745	153.6
21*	10.602	.755	6.761	179.4	7.74	.755	179.4
22*	10.661	.776	6.878	224.6	7.49	.776	224.6
23	10.211	.780	6.993	263.6	7.45	.835	349.3
24	6.647	.765	7.178	321.3	7.27	.808	392.6
25	5.090	.771	7.111	293.0	7.21	.862	482.8
26*	13.285	.707	7.130	237.7	8.36	.707	237.7
27*	13.127	.754	7.097	265.4	7.18	.754	265.4
28*	13.039	.747	7.105	260.1	7.23	.747	260.1
29	11.217	.774	7.044	265.6	7.13	.813	320.6
30	8.478	.780	6.950	247.4	7.40	.868	410.4
31	4.546	.759	7.635	354.0	7.15	.847	553.2
32*	13.190	.756	8.444	201.4	7.18	.756	201.4
33*	8.994	.684	8.587	167.7	11.67	.684	167.7
34*	9.217	.776	8.450	219.0	7.10	.776	219.0
35	6.645	.795	8.265	210.4	7.27	.858	303.6
36*	8.934	.672	8.607	161.6	14.64	.672	161.6
37*	9.120	.745	8.506	197.7	7.27	.745	197.7
38	6.466	.795	8.256	208.8	7.27	.863	311.8

*A constant pressure plateau region was not reached.

TABLE IV

PARAMETERS DETERMINED BY GENERAL PROGRAM
AND BY F-CORRELATION PROGRAM

No.	$(p/p_o)_p$	$(p/p_o)_{final}$	x_r,In	F(K)
1	1.193	1.390	2.390	4.070
2	1.477	2.170	1.433	2.548
3	1.339	1.897	3.266	3.005
4	1.195	1.960	2.458	1.917
5	1.318	2.055	9.322	1.897
6	1.237	3.783	8.288	.578
7	1.336	6.333	8.486	.503
8	1.367	2.103	3.079	2.741
9	1.374	4.224	8.564	.797
10	1.464	11.050	8.629	.633
11	1.410	4.224	8.667	.843
12	1.420	11.050	8.538	.610
13	1.485	5.226	9.002	.973
14	1.364	5.226	8.734	.961
15	1.569	13.000	8.832	.712
16	1.606	5.531	6.624	.733
17	1.564	9.268	12.987	.651
18	1.517	3.668	13.107	.738
19*	2.067	16.590	10.712	.266
20*	2.003	16.590	10.583	- -
21*	1.938	16.590	10.602	.236
22*	1.867	16.590	10.661	.314
23	1.792	14.870	13.027	.536
24	1.665	9.443	7.836	.547
25	1.716	18.310	7.824	.559
26*	1.699	2.556	13.285	.298
27*	1.727	5.241	13.127	.466
28*	1.723	5.241	13.039	.395
29	1.765	9.443	13.195	.585
30	1.820	14.870	13.283	.653
31	1.625	9.685	6.553	.705
32*	1.933	7.067	13.190	- -
33*	1.879	7.067	8.994	- -
34*	1.941	22.420	9.217	.291
35	2.018	45.410	9.292	.426
36*	1.874	7.067	8.934	- -
37*	1.917	22.420	9.120	.186
38	2.021	45.410	9.333	.435

*A constant pressure plateau region was not reached.

been given a superscript. There were instances in the data where x_s was specified, but no mention was made as to how this location was determined. The confidence vested in a specified x_s location was enhanced when a schlieren photograph accompanied the pressure distribution.

Using the x_s values given in Table I, the correlation procedure was begun by solving the BLASEP subroutine. This subroutine establishes the correct ε and ζ values at the separation point and also gives the location and parameters at the start of the interaction. The important parameters from this subroutine, together with the calculated Blasius point Reynolds number, are given in Table II. This Reynolds number and the Mach number at the start of the interaction (M_{e_b} or M_o) are used to determine the plateau pressure ratio. The calculation of the plateau pressure ratio is performed by the general program, and the results have been tabulated in Table IV. The point at which the reattachment process begins, x_r, is also determined by the general program and is presented in Table IV.

The SEPSH subroutine is solved in the region between separation and the beginning of reattachment using the ε and ζ values at the separation point as the starting conditions. A satisfactory solution is obtained by selecting C_1 in such a manner that the calculated plateau pressure ratio is reached. The SEPSH solution terminates when x_r is reached, which corresponds with the location of the start of reattachment. Of the 38 cases analyzed, there were twelve in which x_r was reached before a plateau region was established. In these cases, C_1 was selected such that the final pressure at x_r matched the plateau pressure ratio determined by the general program. The cases where no

plateau was established have been noted in Table III and IV. The use of these data will be discussed later in this chapter.

A final correlation for F(K) was made by solving the F-Calculation program. This F value must be selected such that the final downstream pressure ratio is matched at the completion of the reattachment process. The final pressure ratio and the calculated F values are given in Table IV.

Determination of Universal C_1 and F Relationships

The data in Tables I through IV must be analyzed and a F correlation established. In keeping with the simplicity desired, this F correlation must be presented in such a manner that the designer can find F for a given configuration without performing preliminary calculations. In order to meet this requirement, F has been found and presented such that it is a function of the free stream Mach number and the ramp angle.

As a logical extension to the Crocco-Lees method, the inclusion of a C_1 correlation has also been developed. This correlation is a by-product of this study and extends the general understanding of the Crocco-Lees mixing theory. Since C_1 was calculated prior to F for each case, this correlation will be discussed first.

Because of the way it is related to the plateau pressure ratio, parameter C_1 also depends on the location of the separation point. To present a desirable C_1 correlation, certain data had to be eliminated from consideration. It is known that transition in the reattachment region causes the separation point to move closer to the ramp corner. Table V was prepared to aid in determining which of this data should

TABLE V

EVALUATION OF EXPERIMENTAL DATA

No.	Was x_s given in the data?	Was Schlieren photo given?	lam. or trans. reattachment?	Was plateau reached in calculations?
1	yes	no	transitional	yes
2	yes	yes	laminar	yes
3	no	no	laminar	yes
4	yes	yes	transitional	yes
5	yes	yes	laminar	yes
6	yes	yes	transitional	yes
7	yes	yes	transitional	yes
8	no	no	unknown	yes
9	yes	yes	laminar	yes
10	yes	yes	laminar**	yes
11	yes	yes	laminar	yes
12	yes	yes	laminar**	yes
13	yes	yes	laminar	yes
14	yes	yes	laminar	yes
15	yes	yes	laminar	yes
16	no	no	unknown	yes
17	no	no	unknown	yes
18	no	no	unknown	yes
19	yes	no	unknown	no
20	yes	no	unknown	no
21	yes	no	unknown	no
22	no	no	unknown	no
23	no	no	unknown	yes
24	no	no	unknown	yes
25	no	no	unknown	yes
26	no	no	unknown	no
27	no	no	unknown	no
28	no	no	unknown	no
29	no	no	unknown	yes
30	no	no	unknown	yes
31	no	no	unknown	yes
32	no	no	unknown	no
33	no	yes*	unknown	no
34	no	yes*	unknown	no
35	no	yes*	unknown	yes
36	no	yes*	unknown	no
37	no	yes*	unknown	no
38	no	yes*	unknown	yes

*Of marginal value
**Probably laminar

be eliminated. This table indicates the known cases in which transition occurs during the reattachment process.

At the onset it was not known whether or not the transition in the reattachment region would have an appreciable affect on the F correlation. For this reason, some transitional data were included among the 38 cases considered. Table V also indicates those cases in which x_r was reached prior to establishing a plateau region.

Figure 15 presents the C_1 versus free stream Mach number correlation which was found in this study. In this plot, the 12 cases where a plateau had not been established and the four known transitional cases were eliminated from consideration. It is probable that the 12 cases in which the plateau was not reached were also transitional flows. This is merely a conjecture without the benefit of additional information. The remaining 22 C_1 values have been plotted and show that C_1 decreases with increasing Mach number. The C_1 values at $M_\infty = 10.03$ are of uncertain accuracy because the pressure data offers a poor approximation in locating x_s. Errors in the selected location for x_s introduce errors in C_1 and F.

The results in Figure 15 show no discernible relationship between C_1 and the Reynolds number. C_1 depends only on the Mach number and is independent of Reynolds number in the range from 10^5 to 10^6.

The F correlation values depend on the solution in the plateau region. The 16 cases which had been previously eliminated in the C_1 correlation are of no value in the F correlation. Table VI has been prepared to illustrate the resulting dependence of F on M_∞ and the ramp angle. These data points have been plotted in Figure 16 and illustrate that F decreases with increasing Mach number. These data

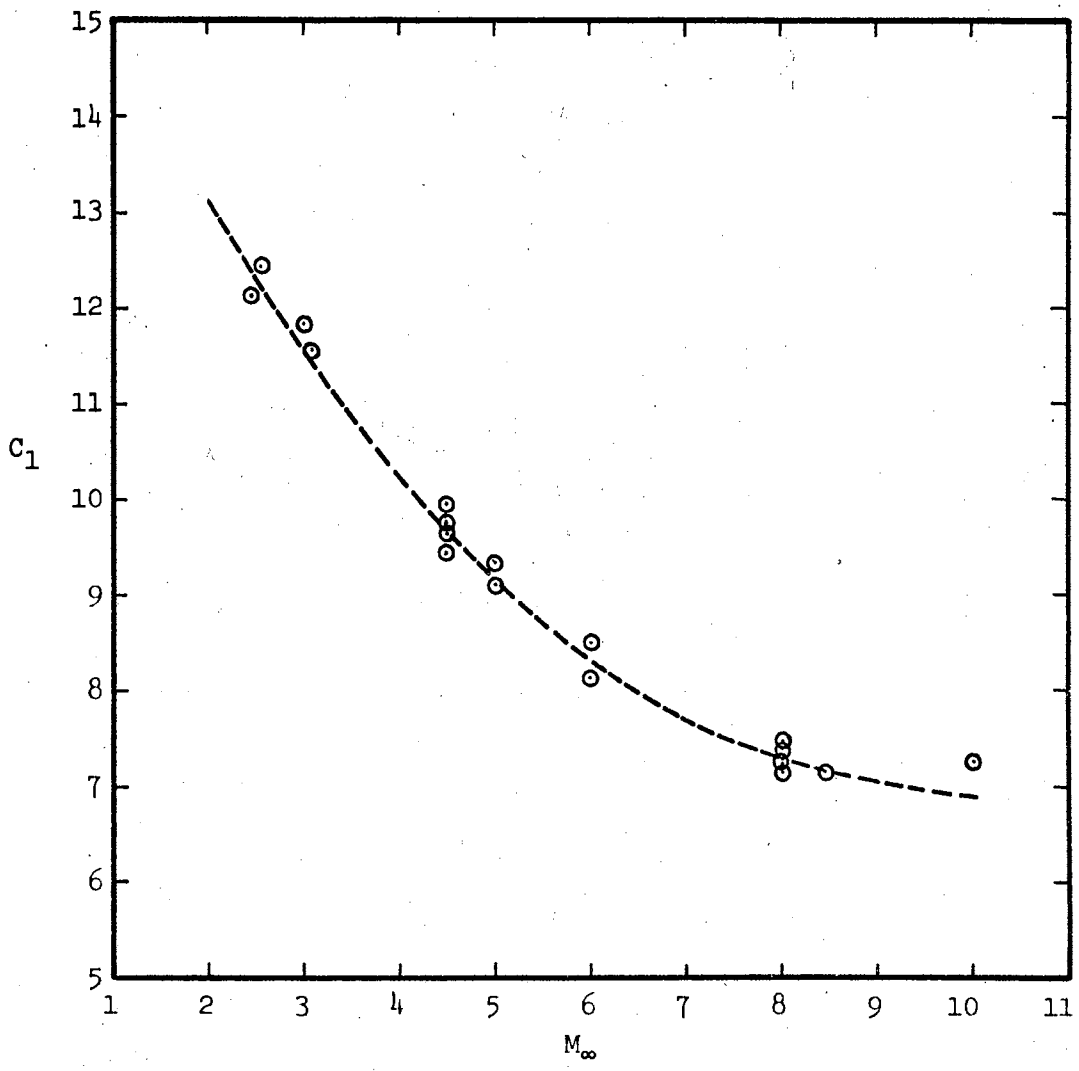

Figure 15. Correlation of C_1 vs. M_∞ in the Separation-Plateau Region

TABLE VI

SYNOPSIS OF RESULTS FOR F-M_∞-RAMP ANGLE CORRELATION

Ramp Angle = 10°

No.	M_∞	F
3	2.55	3.005
5	3.00	1.897
8	3.06	2.741
18	6.00	.738

Ramp Angle = 15°

No.	M_∞	F
9	4.50	.797
11	4.50	.843
13	5.00	.973
14	5.00	.961
24	8.00	.547
29	8.00	.585

Ramp Angle = 20°

No.	M_∞	F
17	6.00	.651
23	8.00	.536
30	8.00	.653

Ramp Angle = 30°

No.	M_∞	F
10	4.50	.633
12	4.50	.610
15	5.00	.712
35	10.03	.426
38	10.03	.435

Other Data

No.	M_∞	Ramp Angle	F
2	2.45	13.00	2.548
16	6.00	14.00	.733
25	8.00	22.50	.559
31	8.45	14.60	.705

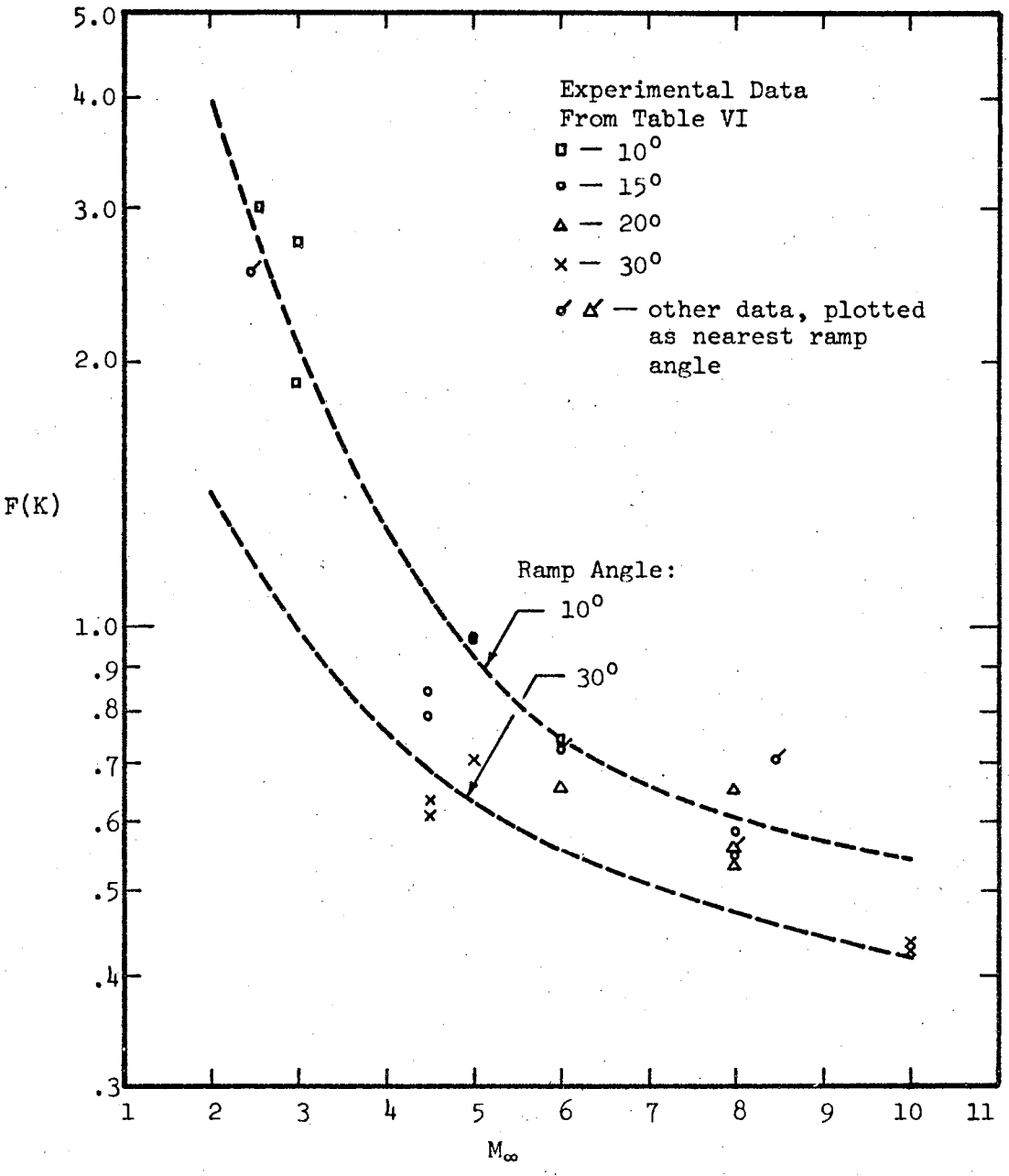

Figure 16. F-Correlation Curve

further show that F decreases with increasing ramp angle. Curves have been sketched in Figure 16 to give the values of F which are used in the program calculations.

The 16 values of C_1 and F which had been eliminated from consideration were compared with the C_1 and F correlation curves. The C_1 values which were not plotted in general lie above the curve in Figure 15. Also, the F values which were not used generally lie below the representative curves. It is evident that the presence of transition in the reattachment region has the effect of shifting the C_1 curve upward and the F curve downward. For purely laminar interactions, C_1 and F can be approximated quite well with the single curves given. A band of values is encountered when transitional effects are included, and the uniqueness of the correlation method breaks down.

The F value which is input into the general program is obtained directly from Figure 16. With the free stream Mach number and ramp angle known, it is a simple matter to interpolate F directly from the figure.

Solution of the Complete Interaction Problem

The complete computer solution has been described in Chapter IV. This section illustrates how the calculated pressure distributions compare with experimental measurements. Figure 17 illustrates how each of the three semi-empirical parameters vary throughout the interaction. The trajectories given in this figure duplicate the previous discussion, but they are helpful in illustrating the behavior of each parameter in each of the three regions.

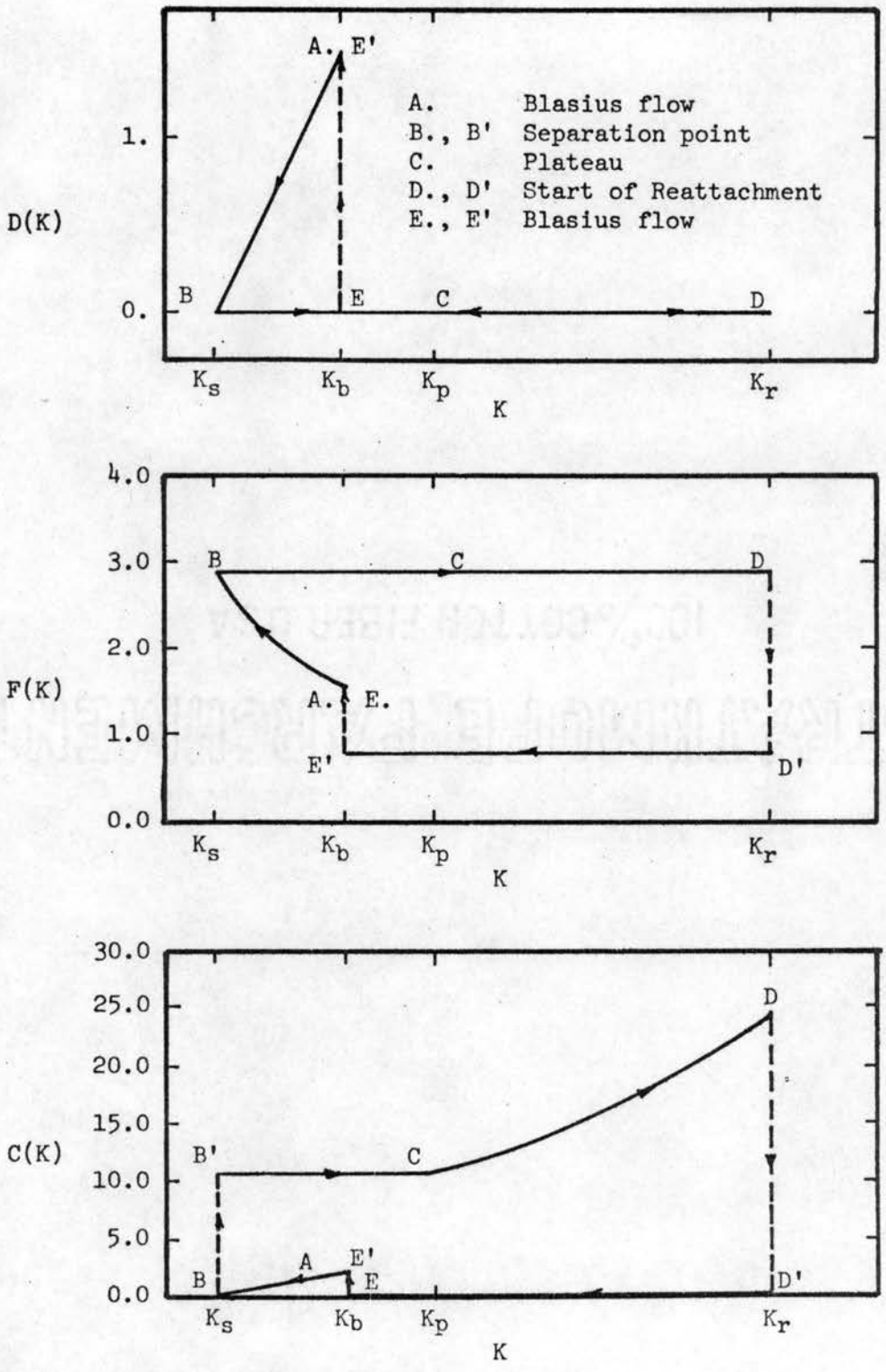

Figure 17. Trajectories of Semi-Empirical Parameters in a Shock Wave-Laminar Boundary Layer Interaction

In order to compare the calculated results with experiment, an illustrative sampling of the data is given. Figures 18 through 27 illustrate a representative sampling of data in the Mach 2.55 to 10 region. The general program calculations give a better comparison at Mach numbers above 3.0. Below Mach 3.0 the reattachment pressure rise starts too far downstream and also has a slope which is flatter than the experimental pressures. When the magnitude of the overall pressure rise on the ramp is considered, the resulting discrepancy will not introduce design errors as large as a similar discrepancy at higher Mach numbers would. The solution developed gives good agreement over the range of data (Mach 2-10).

To illustrate the program's convergence on a correct solution, Figure 28 is given. This result is the same as the one given by Figure 19 for $M_\infty = 3.0$. To start the calculation procedure, x_s was assumed to be at 4.7 inches. The convergence procedure required 4 loops to reach the desired solution. The plot for each intermediate pressure distribution has been given to show how the calculations proceed toward the correct solution. A similar set of calculations was performed by assuming that x_s was at 6.7 inches. The solution converged on a satisfactory solution in the fourth loop of calculations.

In the reattachment portion of the pressure rise, the distribution has an inflection point. This is most apparent at the higher Mach numbers. No significance is associated with this observed characteristic.

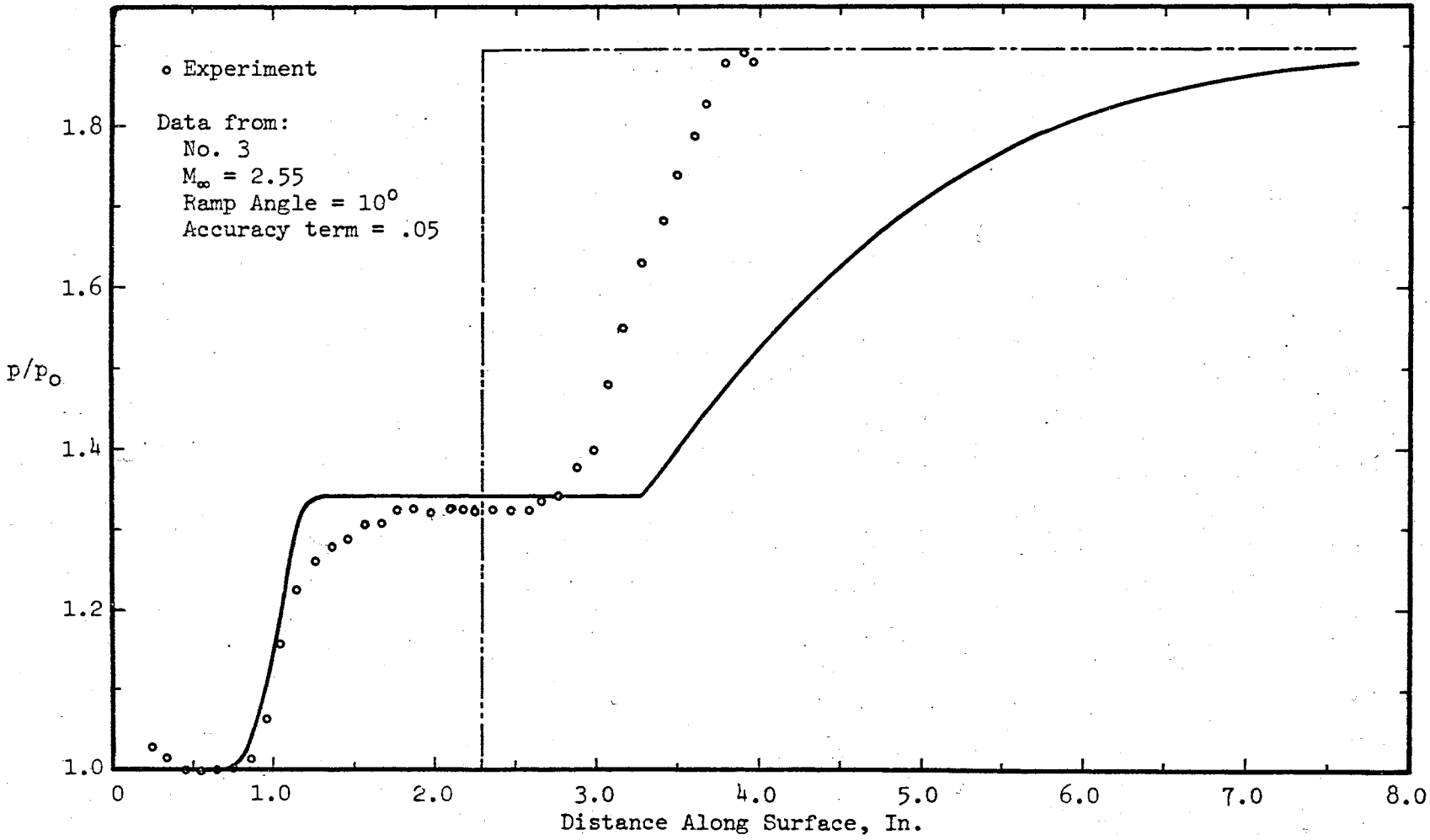

Figure 18. Correlation With Experimental Data, M_∞ = 2.55

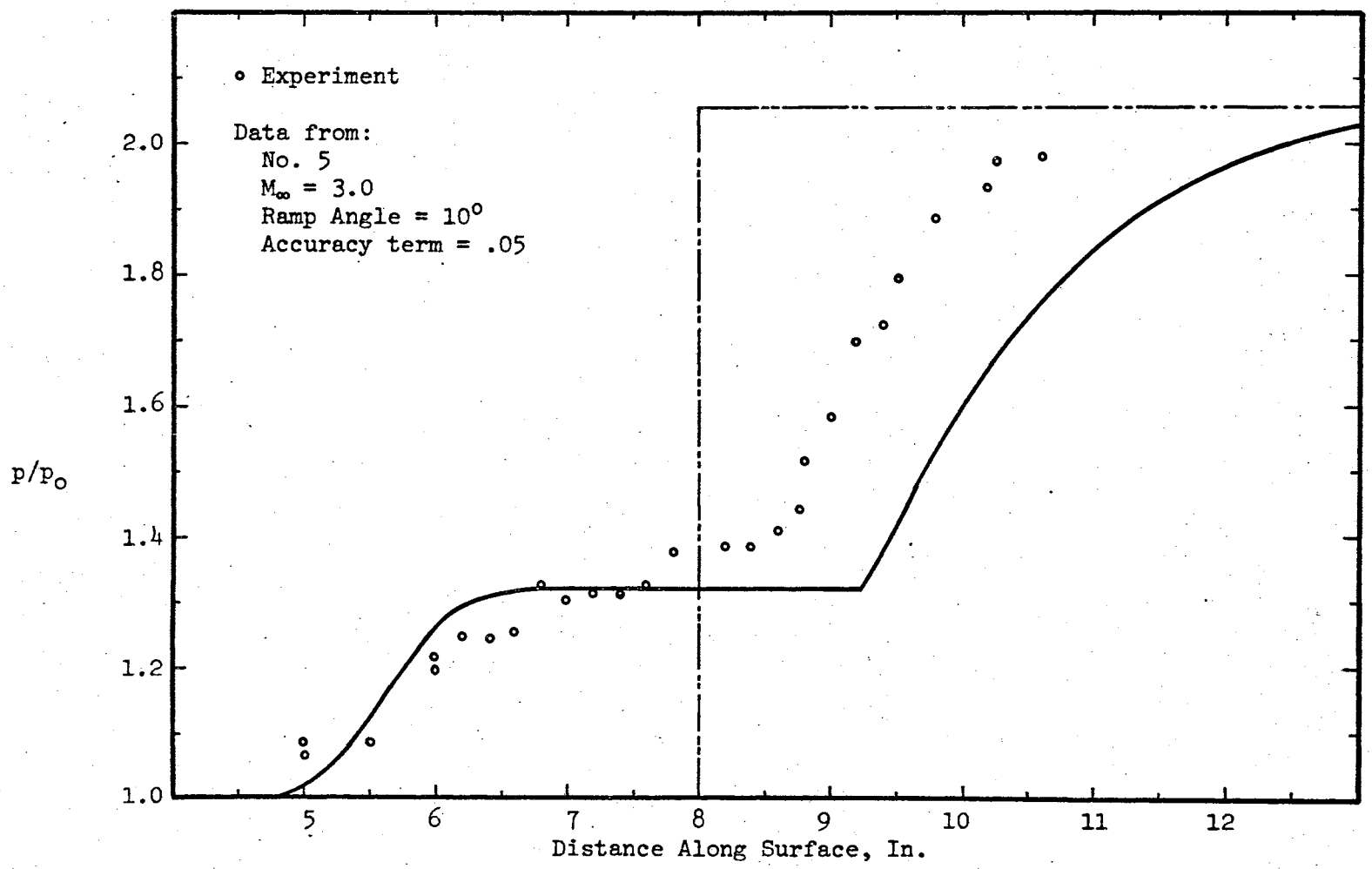

Figure 19. Correlation With Experimental Data, M_∞ = 3.0

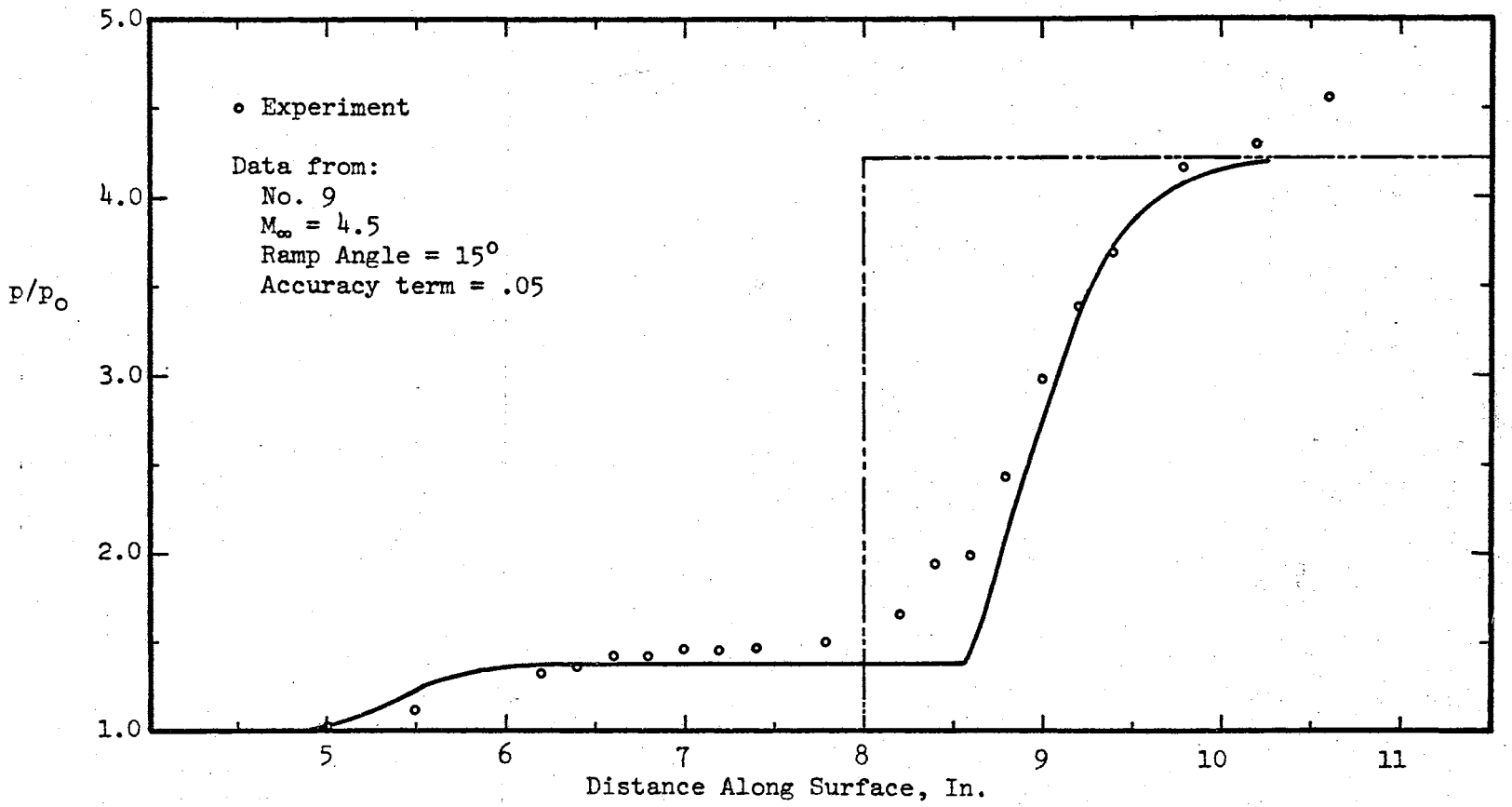

Figure 20. Correlation With Experimental Data, $M_\infty = 4.5$

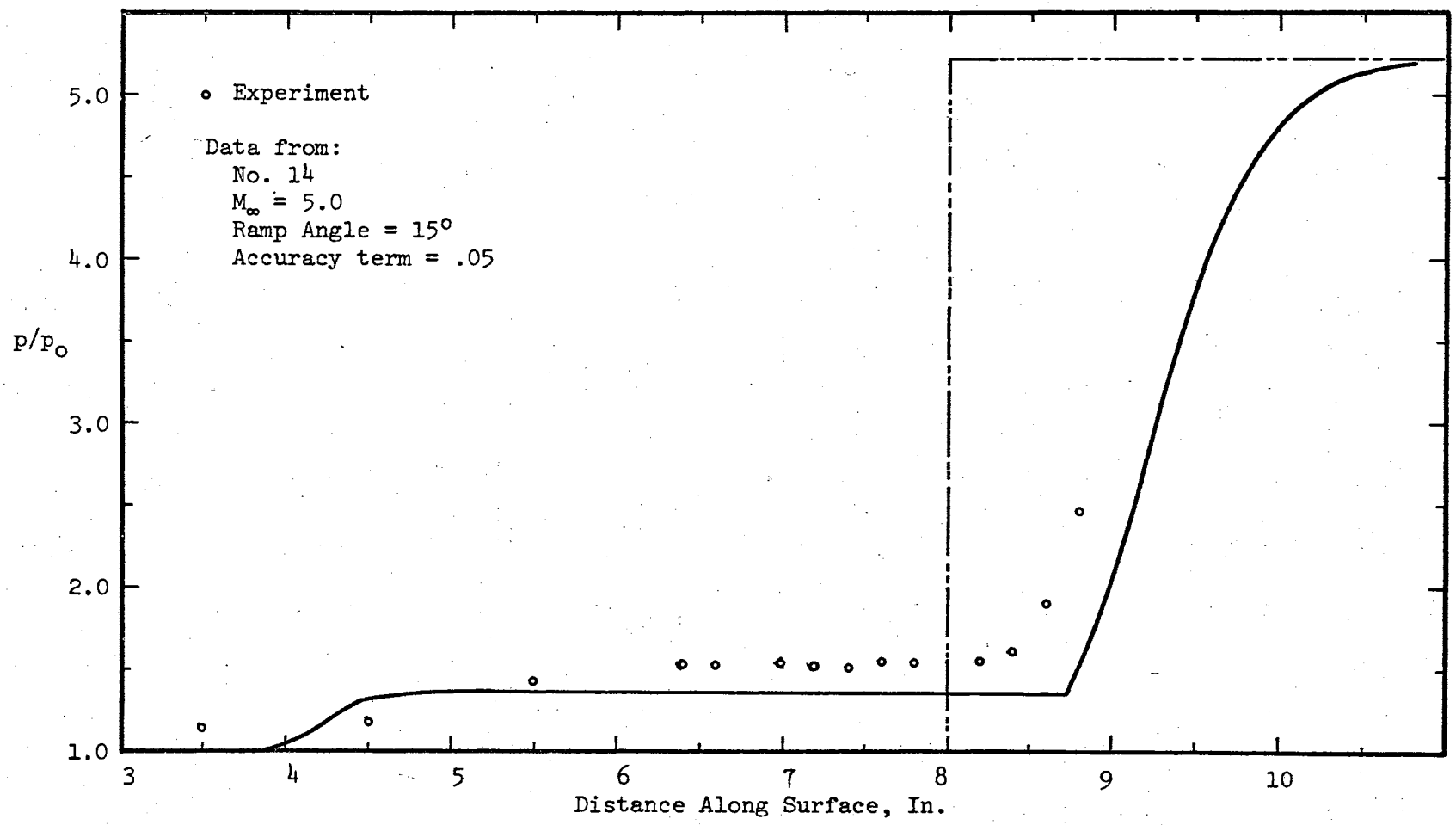

Figure 21. Correlation With Experimental Data, M_∞ = 5.0

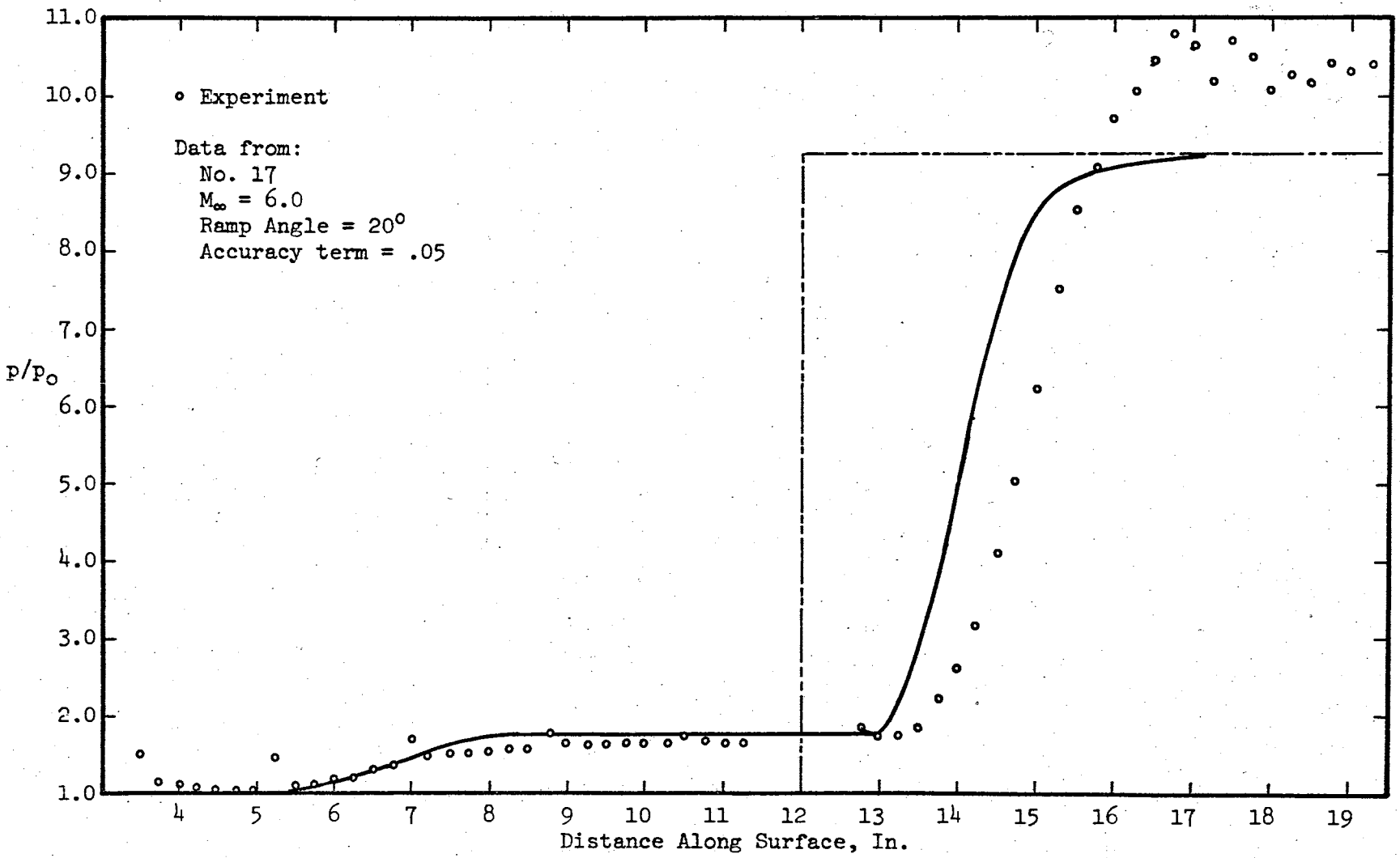

Figure 22. Correlation With Experimental Data, $M_\infty = 6.0$

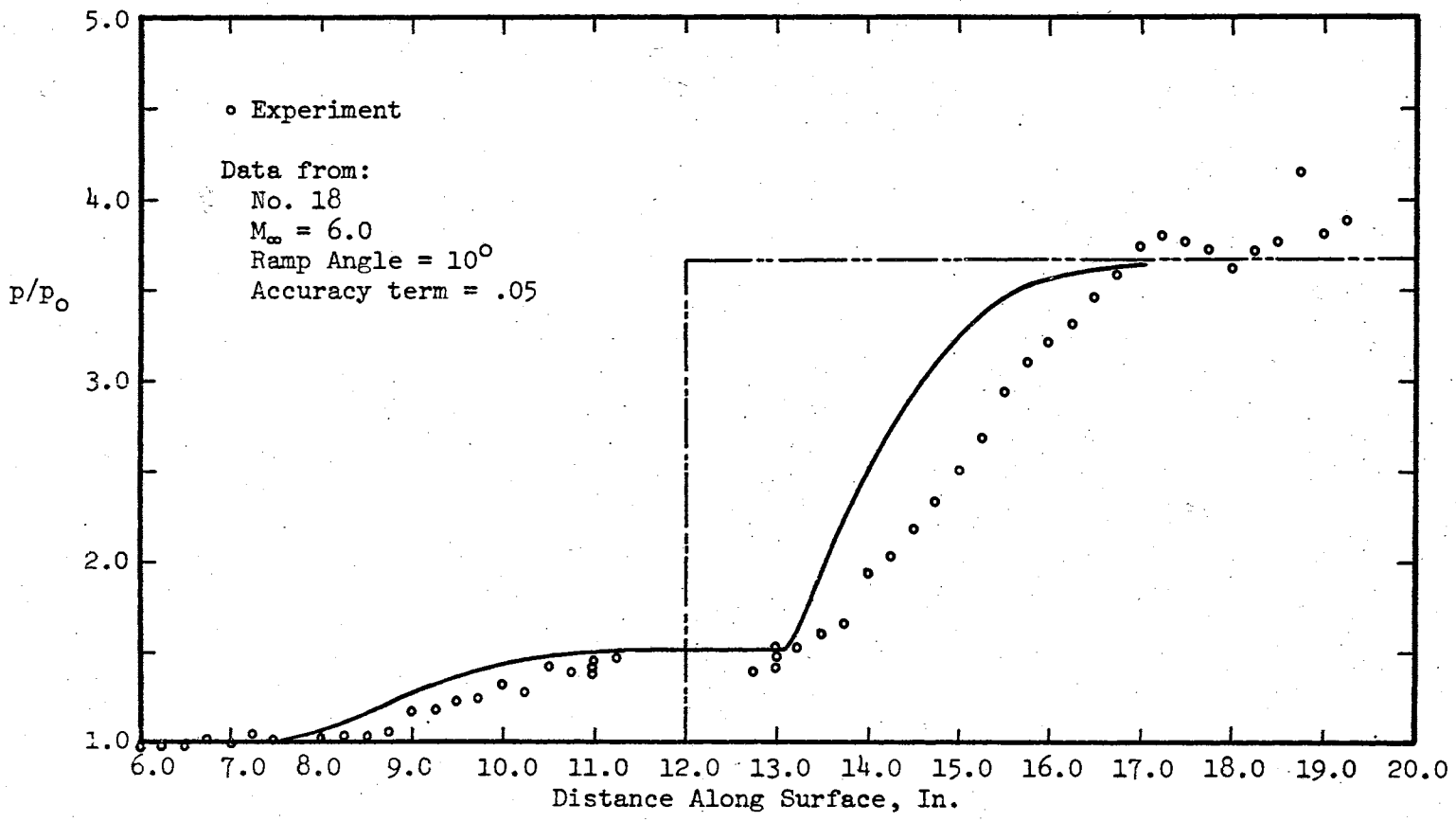

Figure 23. Correlation With Experimental Data, $M_\infty = 6.0$

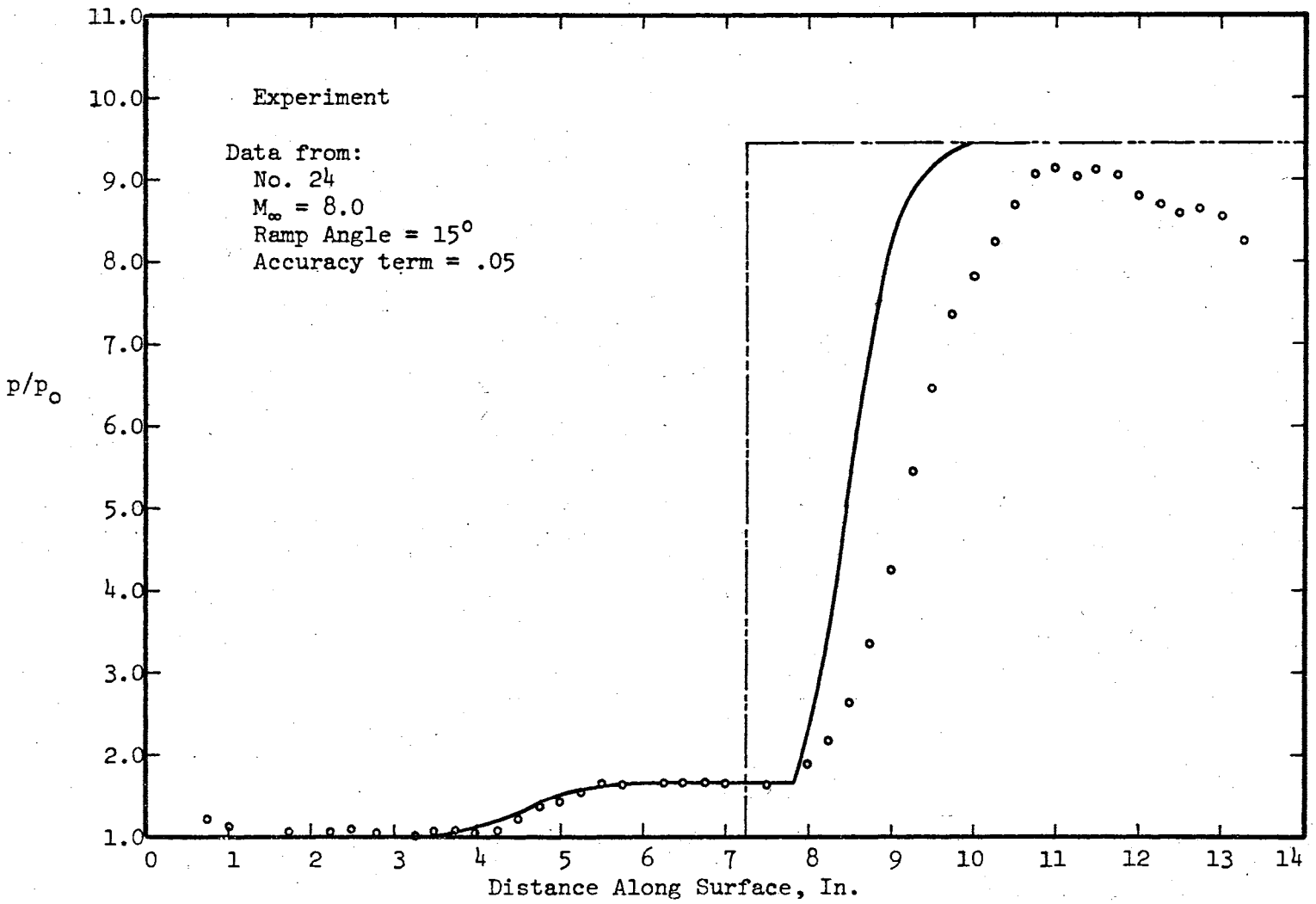

Figure 24. Correlation With Experimental Data, M_∞ = 8.0

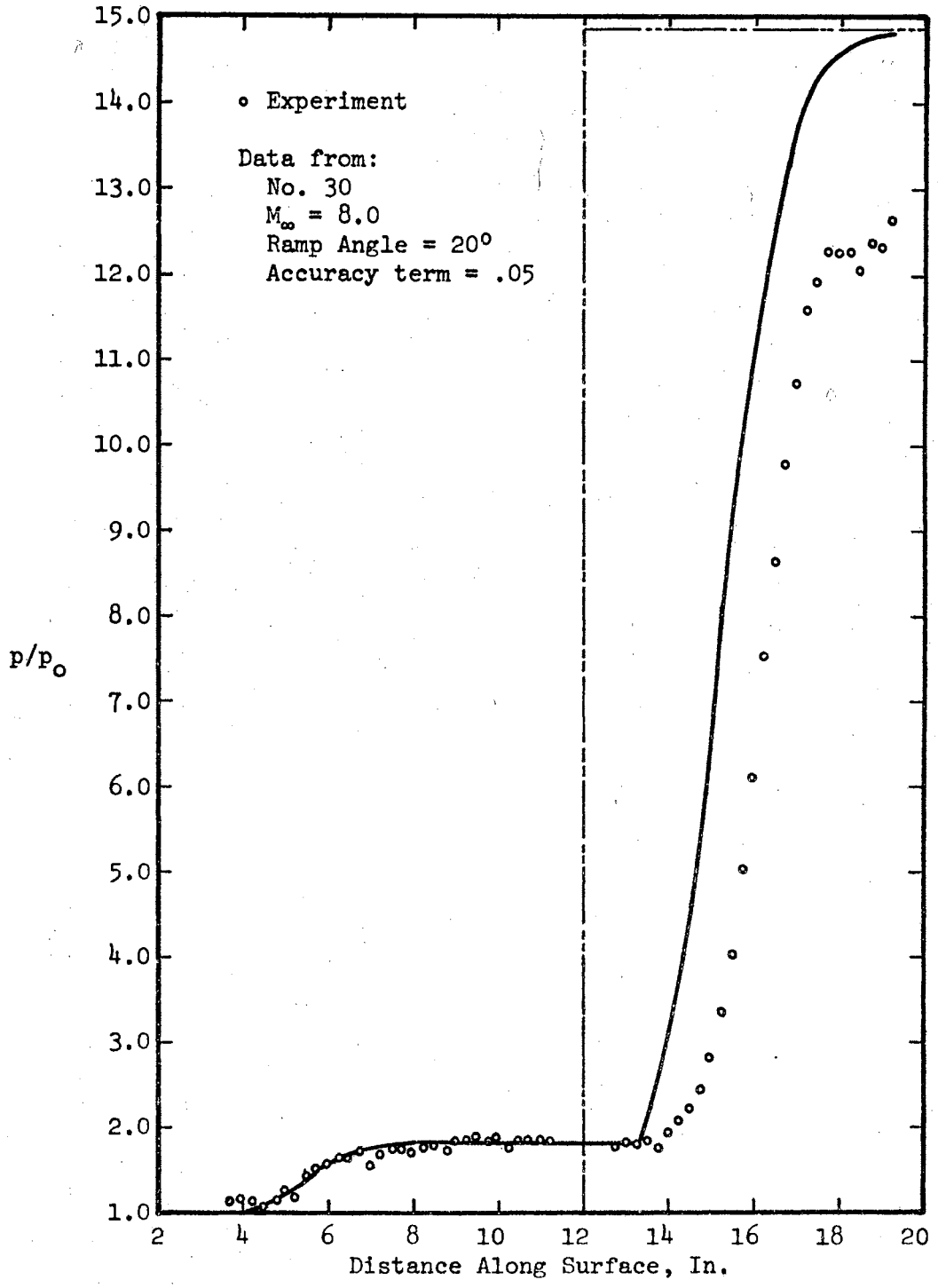

Figure 25. Correlation With Experimental Data, $M_\infty = 8.0$

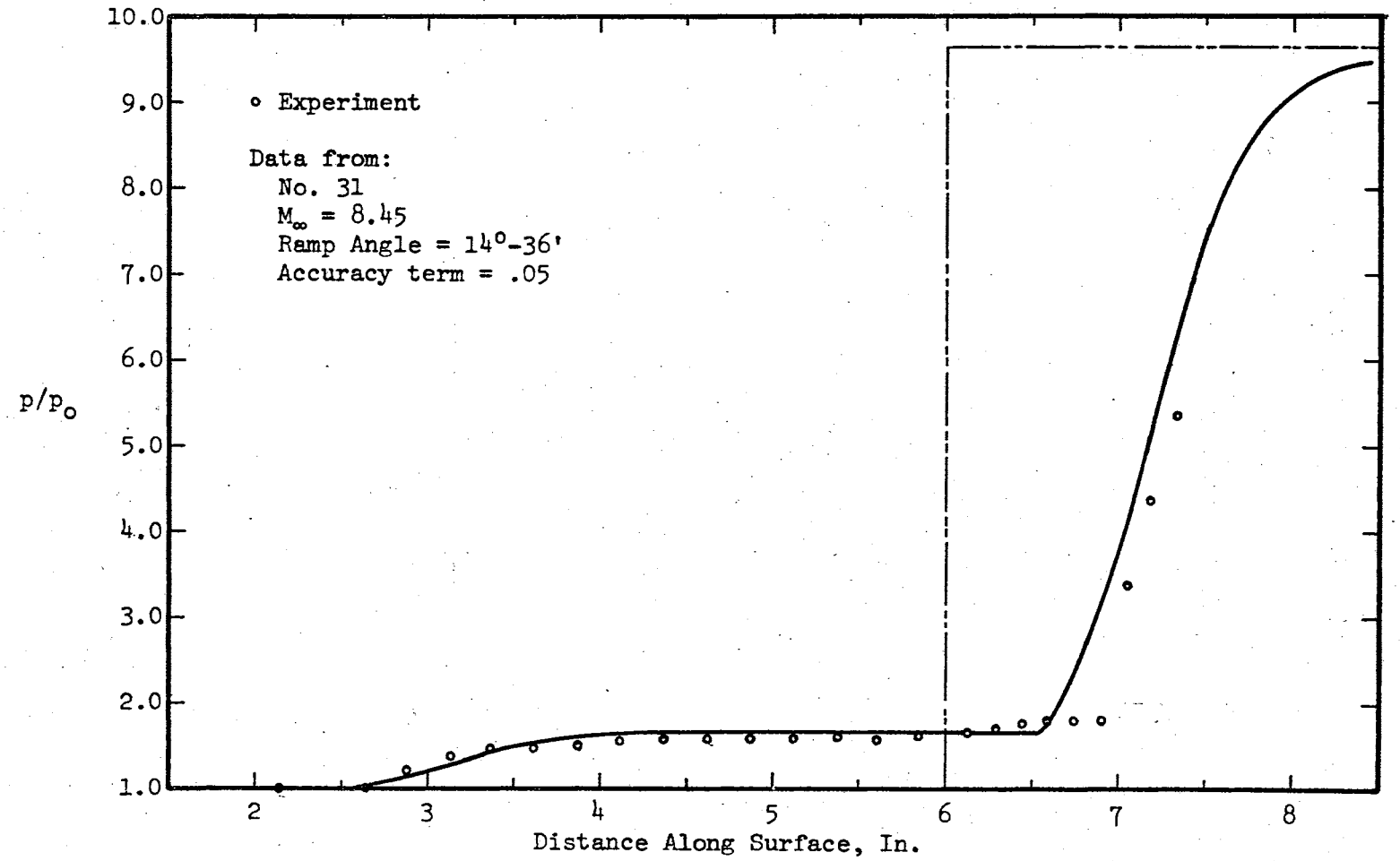

Figure 26. Correlation With Experimental Data, $M_\infty = 8.45$

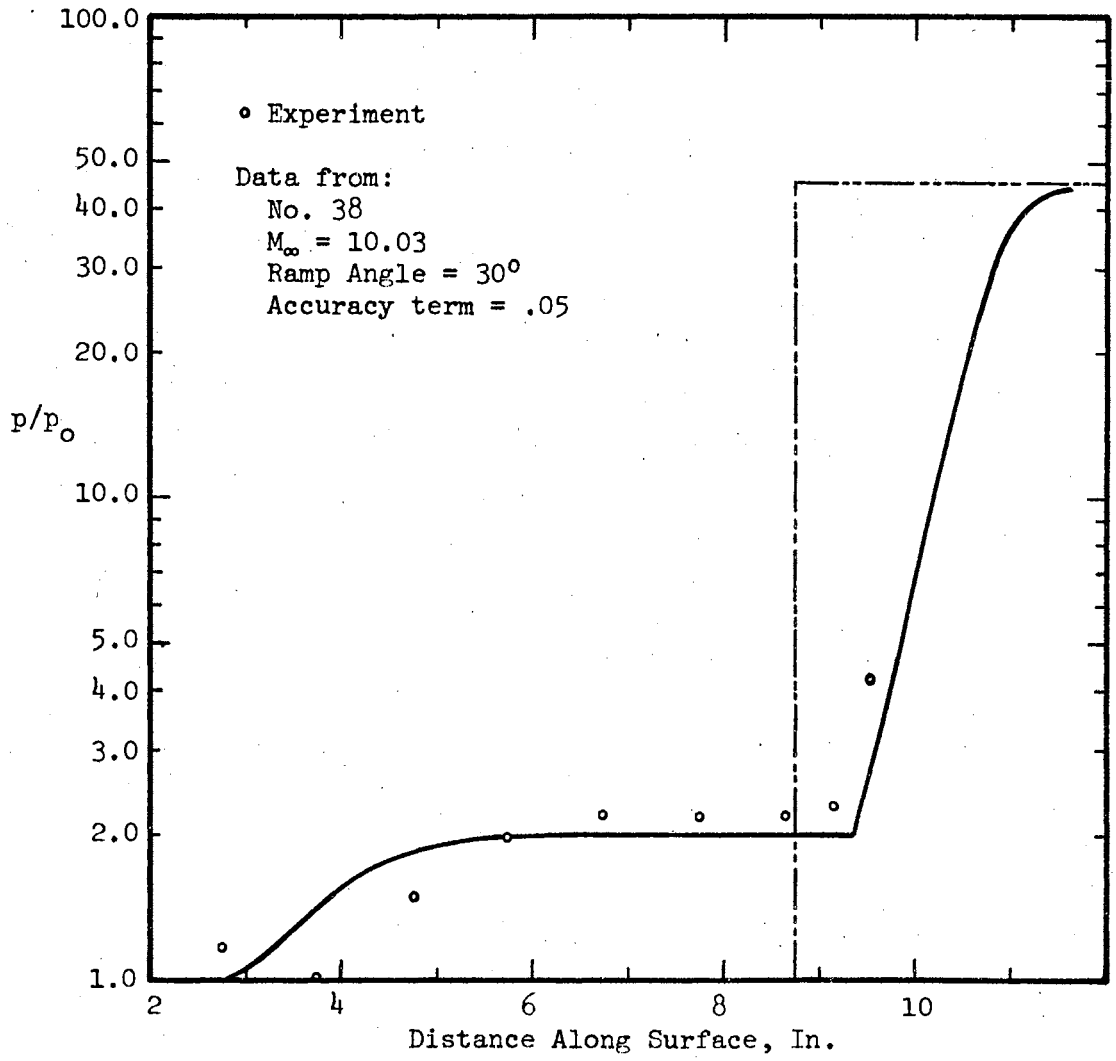

Figure 27. Correlation With Experimental Data, M_∞ = 10.03

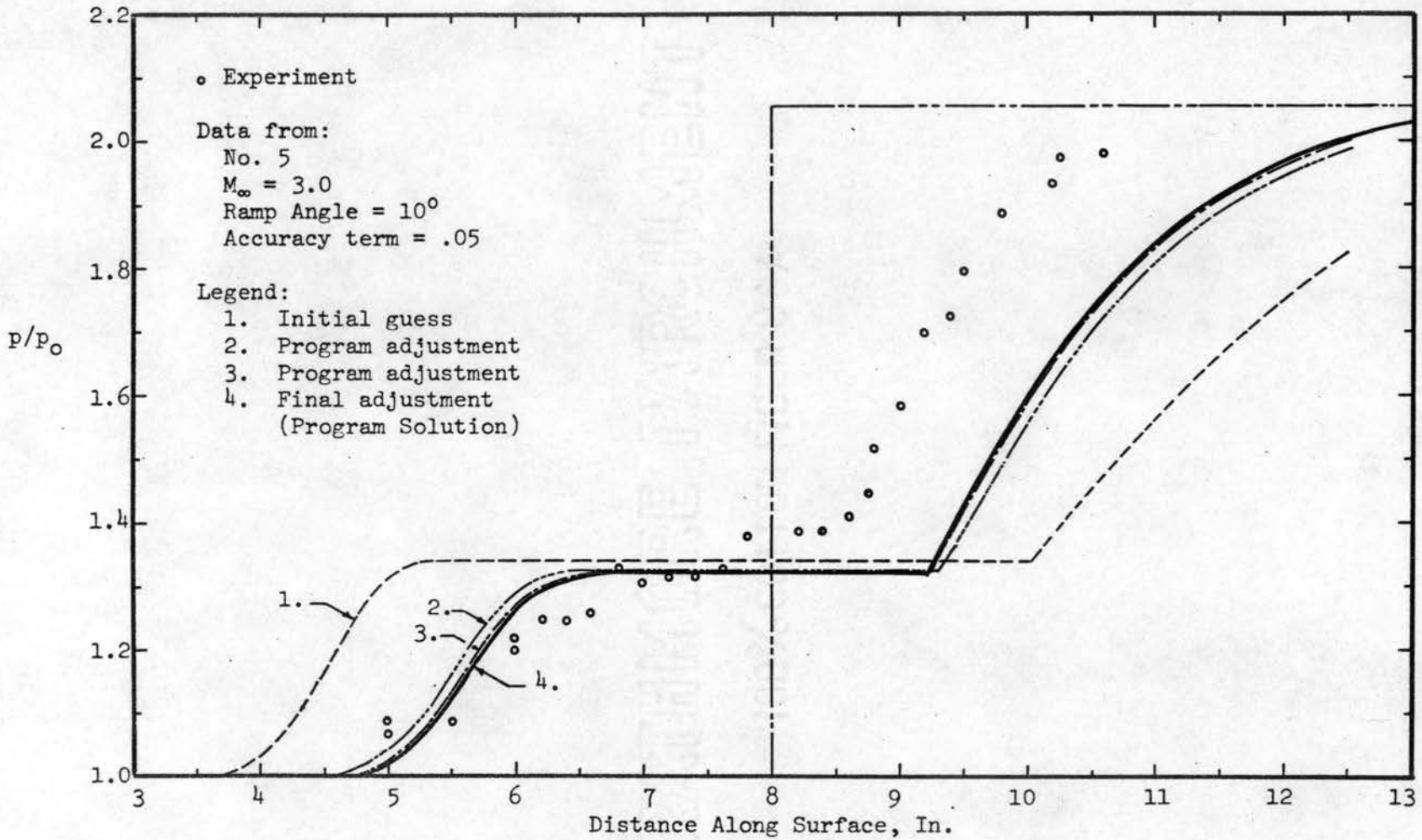

Figure 28. Illustration of Convergence on Correct Solution

CHAPTER VI

CONCLUSIONS AND RECOMMENDATIONS

Conclusions

A solution for the complete interaction-pressure distribution for laminar flows over plate and ramp combinations in the Mach 2 to 10 range has been developed. This technique is semi-empirical and makes use of the Crocco-Lees flow model. The objective of this investigation, which was to find an engineering solution for this complex interaction pressure distribution, has been fulfilled.

The three semi-empirical parameters which are used to describe the flow in each of the three regions have been defined. Further, the resultant correlations for each of the parameters are given. To obtain a solution for this problem, only the free stream flow conditions, the plate-ramp geometry, and the F(K) correlation value are necessary. This F(K) value is obtained directly from the correlation curves in Figure 16 and is based on existing experimental data.

A by-product of the method presented is that it extends the present Crocco-Lees theory by defining the correct behavior for the mixing parameter, C(K), in the region between separation and the beginning of reattachment. A C(K) correlation has been established by making use of a constant C_1 value between separation and the beginning of the plateau and a varying C(K) value from this point on. A previous hypothesis by Glick (6), that C(K) has an universal behavior in this region, was found

to be invalid. The mixing term, C_1, was found to decrease with increasing Mach number and was independent of the Reynolds number. At the outset it was felt that C_1 would depend on both the Reynolds number and the Mach number. This was not supported by the data.

In the plateau region C(K) was found to be an ever-increasing function. This study supports the conclusion that the mixing becomes more vigorous with increasing advancement into the plateau region.

The correlation parameter for the reattachment region, F, has been found to be dependent upon the free stream Mach number and the ramp angle. It was found from the correlation of results that F decreases with increasing Mach number and with increasing ramp angles. Here, too, as in the C_1 correlation, no dependence on Reynolds number was observed. On the basis of the correlation curves which were found, it is evident that F depends principally on the inviscid outer flow and to an indistinctive amount upon other effects such as the Reynolds number.

In the computer solution of the differential equations, the exact rather than the linearized form has been solved. The limitations placed on the method by the usual linearization assumption has been discussed in Chapter IV. The errors resulting from this assumption are small at low Mach numbers, but they increase rapidly with increasing Mach number.

The ultimate worth of any method rests in its comparison with experiment. The figures in Chapter V show that the correlation above Mach 3.0 is good, while the slope of the reattachment pressure rise below this value is flatter than experiment. This deviation at lower velocities may be attributed partly to the extent of the subsonic portion of the boundary layer. At higher Mach numbers the pressure clearly does not start to rise until some distance beyond the ramp corner, while

at lower Mach numbers the pressure rise appears to originate at the ramp corner. The actual reattachment point in the flow occurs somewhere downstream from the start of the reattachment pressure rise. The dividing streamline, as it has been incorporated, is used merely as a model to approximate the relative location of reattachment with respect to separation.

The chief problem encountered in this study was the collection of adequate experimental data for use in establishing the necessary F correlation. Three problems which had to be resolved before the collected data could be used were: 1.) Does the boundary layer remain laminar throughout the entire interaction?, 2.) Has the exact location of the separation point been found?, and 3.) Is the flow two-dimensional?

Transition within the reattachment region has the qualitative effect of shortening the distance between separation and reattachment. This results in a C_1 value larger than that for laminar flow at the same Mach number. A secondary result is that a smaller F is obtained in a transitional interaction. The uniqueness of the C_1 and F correlations break down when transitional flows are considered. C_1 and F may be represented by distinct curves for laminar flows, while these correlation parameters take on a band of values in transitional flows. For this reason, only laminar interactions may be treated. Transitional and turbulent flows introduce new values for the semi-empirical parameters C(K), D(K), and F(K), and for that reason, these flows cannot be incorporated within the laminar definitions used in the three regions.

In reviewing the literature on this separation-interaction problem, the similarities rather than the differences in the various methods, were most apparent. All methods make essentially the same assumptions

and incorporate the same flow model. The basic difference comes in the way the boundary layer profile is handled. Some chose to represent the boundary layer by an assumed family of profiles while others use a semi-empirical approach to represent the boundary layer. Each type of profile representation has its limitations and associated problems.

In the complete interaction solution, the initial assumptions regarding the plateau pressure ratio, the final pressure ratio, and the relative location of the dividing streamline were found to give good overall agreement. The location of x_s controls the whole interaction and is of paramount importance in this method.

Recommendations

The chief limitation recognized in this thesis was that sufficient experimental data of the type and detail needed was not available at this time. As more data becomes available, the F-correlation curves in Figure 16 should be brought up to date.

The constant-value F correlation which has been proposed for use in the reattachment region may be improved upon. This is evidenced by the fact that the slope of the pressure distribution curve is not in good agreement with experiment at low Mach numbers. An alternate method for correlating F, possibly a step function, may be needed to bring these values into better agreement. A linear variation for F throughout the reattachment process has been tried. In this case the F values became unwieldy to correlate because the starting point (K_r) was not a universal value.

A generally accepted view is that the reattachment process controls the location of the separation point and, for that matter, the behavior

of the whole interaction. Probably the most fruitful area for additional investigation in the interaction problem is to try to understand what happens in the vicinity of the reattachment point. Experimentally, detailed velocity profile measurements in the reattachment region are needed to extend the qualitative understanding of this region. Also, velocity profile measurements between separation and reattachment would be helpful in determining if K follows the trajectory which has been assumed.

BIBLIOGRAPHY

1. Howarth, L. "The Propagation of Steady Disturbances in a Supersonic Stream Bounded on One Side by a Parallel Subsonic Stream." Proceedings of the Cambridge Phil. Soc., Vol. 44, (1948), pp. 380-90.

2. Crocco, L., and Lees, L. "A Mixing Theory for the Interaction Between Dissipative Flows and Nearly Isentropic Streams." Journal of the Aeronautical Sciences, Vol. 19, (October, 1952), pp. 649-676.

3. Chapman, D. R., Kuehn, D. M., and Larson, H. K. "Investigation of Separated Flows in Supersonic and Subsonic Streams with Emphasis on the Effects of Transition." NACA Report 1356, 1958.

4. Cheng, S., and Bray, K. N. C. "On the Mixing Theory of Crocco and Lees and Its Application to the Interaction of Shock Waves and Laminar Boundary Layers, Part I." AFOSR TN 57-283, May, 1957.

5. Cheng, S., and Chang, I. D. "On the Mixing Theory of Crocco and Lees and Its Application to the Interaction of Shock Waves and Laminar Boundary Layers, Part II." AFOSR TN 58-3, November, 1957.

6. Glick, H. S. "Modified Crocco-Lees Mixing Theory for Supersonic Separated and Reattaching Flows." CAL TECH Hypersonic Research Project Memo. No. 53, May 2, 1960; also, Journal of the Aeronautical Sciences, Vol. 29, (October, 1962), pp. 1238-1249.

7. Tani, I. "On the Approximate Solution of the Laminar Boundary Layer Equations." Journal of the Aeronautical Sciences, Vol. 21, (July, 1954), pp. 487-504.

8. Pinkus, O. "A Method of Solving Supersonic Laminar Boundary-Layer Separation and Its Application to Wedges and Curved Surfaces." RAC 2232A, Republic Aviation Corp., Farmingdale, L. I., N. Y.; also, ASME Paper No. 65-APMW-19, (1965).

9. Lees, L. and Reeves, B. L. "Supersonic Separated and Reattaching Laminar Flows, I. General Theory and Application to Adiabatic Boundary-Layer/Shock Wave Interactions, AIAA Journal, Vol. 2, (Nov. 1964), pp. 1907-1920; also, GALCIT Separated Flows Research Project, Tech. Report No. 3, Oct. 1963.

10. Stewartson, K. "Further Solutions of the Falkner-Skan Equation." Proceedings of the Cambridge Phil. Soc., Vol. 50, (1954), pp. 454-465.

11. Makofski, R. A. "A Two-Parameter Method for Shock Wave-Laminar Boundary Layer Interaction and Flow Separation." Proceedings of the 1963 Heat Transfer and Fluid Mechanics Institute, Pasadena, Calif., (June 12-14, 1963).

12. Erdos, J., and Pallone, A. "Shock-Boundary Layer Interaction and Flow Separation." AVCO Technical Report RAD-TR-61-23, August 15, 1961.

13. Nielsen, J. N., Lynes, L. L., Goodwin, F. K., and Holt, M. "Calculation of Laminar Separations with Free Interaction by the Method of Integral Relations." Submitted for presentation at the AIAA 2nd Aerospace Sciences Meeting, January 25-27, 1965, in New York City, Vidya Research and Development, 1450 Page Mill Road, Palo Alto, Calif.

14. Dorodnitsyn, A. A. "General Method of Integral Relations and Its Application to Boundary Layer Theory." Advances in Aeronautical Sciences, Pergamon Press, Vol. 3, New York, 1962, pp. 207-219.

15. Stewartson, K. "Correlated Incompressible and Compressible Boundary Layers." Proceedings of the Roy Soc., London, Vol. 200, (1949), pp. 84-100.

16. Sterrett, J. R., and Holloway, P. F. "On the Effect of Transition on Parameters Within a Separation Region at Hypersonic Speeds - With Emphasis on Heat Transfer." Symposium on Fully Separated Flow, ASME, New York, 1964.

17. Wuerer, J. E., and Clayton, F. I. "Flow Separation in High Speed Flight, A Review of the State-of-the-Art." Douglas Report SM-46429, April, 1965.

18. Guman, W. J. "On the Plateau and Peak Pressure of Regions of Pure Laminar and Fully Turbulent Separation in Two-Dimensional Supersonic Flow." Journal of the Aero/Space Sci., Vol. 26, (Jan. 1959), p. 56.

19. Ralston, A. and Wilf, H. S. Mathematical Methods for Digital Computers. John Wiley & Sons, Inc., New York, (1960), Chap. IX.

20. Gill, S. "A Process for Step-By-Step Integration of Differential Equations in an Automatic Digital Computing Machine." Proceedings of the Cambridge Phil. Soc., Vol. 47, (1951), pp. 96-108.

21. Putnam, L. E. "Investigation of Effects of Ramp Span and Deflection Angle on Laminar Boundary-Layer Separation at Mach 10.03." NASA TN D-2833, May 1965.

22. Miller, D. S., Hijman, R., and Childs, M. E. "Mach 8 and 22 Studies of Flow Separation Due to Deflected Control Surfaces." AIAA Journal, Vol. 2, (February, 1964), pp. 312-321.

23. Nielsen, J. N., Lynes, L. L., and Goodwin, F. K. "Theory of Laminar Separated Flows on Flared Surfaces Including Supersonic Flow with Heating and Cooling." AGARD Conference Proceedings No. 4, Separated Flows, 1966.

24. Pate, S. R. "Investigation of Flow Separation on a Two-Dimensional Flat Plate Having a Variable-Span Trailing-Edge Flap at M_∞ = 3 and 5." Report No. AEDC-TDR-64-14, March 1964.

25. Deitering, J. S. "Investigation of Flow Separation on a Two-Dimensional Flat Plate Having a Variable-Span Trailing-Edge Flap at M_∞ = 3 and 4.5." Report No. AEDC-TR-65-59, March 1965.

26. Gulbran, C. E., Redeker, E., Miller, D. S., and Strack, S. L. "Heating in Regions of Interfering Flow Fields, Part I. Two- and Three-Dimensional Laminar Interactions at Mach 8." AFFDL-TR-65-49, Part I, July 23, 1965.

27. Townsend, J. C. "Effects of Leading-Edge Bluntness and Ramp Deflection Angle on Laminar Boundary-Layer Separation in Hypersonic Flow." NASA TN D-3290, February 1966.

28. Chapman, D. R., Kuehn, D. M., and Larson, H. K. "Investigation of Separated Flows in Supersonic and Subsonic Streams with Emphasis on the Effect of Transition." NACA TN 3869, 1957.

29. Thompson, Floyd L., Director, NASA Langley Research Center. Letter of transmittal for data, July 11, 1966.

30. Buck, Melvin L., Chief, Gas Dynamics Branch, Flight Mechanics Division, Air Force Flight Dynamics Laboratory. Letter of transmittal for data, August 12, 1966.

31. Ames Research Staff: "Equations, Tables, and Charts for Compressible Flow." NACA Report 1135, 1953.

32. Hayes, W. D., and Probstein, R. F. "Hypersonic Flow Theory." Academic Press, New York and London, (1959), Chapter IX.

33. Crocco, L. "Considerations on the Shock-Boundary Layer Interaction." Proceedings of the Conference on High-Speed Aeronautics, held at the Polytechnic Institute of Brooklyn, January 20-22, 1955.

34. Cohen, C. B., and Reshotko, E. "The Compressible Laminar Boundary Layer with Heat Transfer and Arbitrary Pressure Gradient." NACA Report 1294, 1956.

APPENDIX A

DEVELOPMENT OF EQUATIONS

This appendix supplements the development of equations which appears in Chapters 3 and 4. The two general differential equations which describe the flow are derived first, followed by the derivation of the x-length equation, the differential equations for the reattachment region, and the hypersonic limit equations.

The Crocco-Lees Differential Equations

To obtain these equations, the system of equations describing the flow are transformed into the Crocco-Lees nomenclature and then are reduced to two non-linear first order ordinary differential equations.

The momentum and continuity equations which describe the viscous region may be written directly from the flow model as

$$\frac{dI}{dx} = u_e\left(\frac{d\bar{m}}{dx}\right) - \delta\left(\frac{dP}{dx}\right) - \tau_w \qquad \text{(A-1)}$$

and

$$\frac{d\bar{m}}{dx} = \rho_e u_e\left(\frac{d\delta}{dx} - \tan\theta\right) \qquad \text{(A-2)}$$

respectively.

By using the definitions $K = I/\bar{m}u_e$ and $m = \bar{m}\, a_t$, the momentum flux, I, may be written

$$I = \frac{K\, m\, u_e}{a_t} = K\, m\, w_e \quad .$$

With this definition and the relationships $\frac{d\bar{m}}{dx} = \frac{d\left(\frac{m}{a_t}\right)}{dx} = \frac{1}{a_t}\frac{dm}{dx}$,

$C_f = \frac{\tau_w}{\frac{1}{2}\rho_e u_e^2}$, and $\phi_e = \frac{\left(1-\frac{\gamma-1}{2}w_e^2\right)}{\gamma w_e}$,

the momentum equation becomes

$$\frac{d}{dx}(mKw_e) = w_e\left(\frac{dm}{dx}\right) - \delta\left(\frac{dP}{dx}\right) - \frac{\rho w_e C_f}{2\phi_e} . \qquad (A-3)$$

In a similar manner, after making use of the definitions for m and ϕ_e, the continuity equation may be expressed as

$$\frac{dm}{dx} = \left(\frac{\rho}{\phi_e}\right)\left(\frac{d\delta}{dx} - \tan\theta\right) . \qquad (A-4)$$

The Bernoulli equation, which describes the inviscid region, is obtained in the desired form by starting from the isentropic perfect gas form which appears in Reference 31 as

$$\frac{\gamma}{\gamma-1}\left(\frac{P_t}{\rho_t}\right)\left(\frac{P}{P_t}\right)^{\frac{\gamma-1}{\gamma}} + \frac{u_e^2}{2} = \frac{\gamma}{\gamma-1}\frac{P_t}{\rho_t} . \qquad (A-5)$$

Making use of the perfect gas relationship, $\rho_t = P_t/RT_t$, together with $w_e = u_e/a_t$ and $a_t = \sqrt{\gamma RT_t}$, the Bernoulli equation becomes

$$P = P_t\left[1 - \frac{\gamma-1}{2}w_e^2\right]^{\frac{\gamma}{\gamma-1}} . \qquad (A-6)$$

Both sides of this equation are differentiated with respect to x, which gives

$$\frac{1}{P}\left(\frac{dP}{dx}\right) = \frac{-w_e\gamma}{\left[1-\frac{\gamma-1}{2}w_e^2\right]}\frac{dw_e}{dx} = \left(\frac{-1}{\phi_e}\right)\frac{dw_e}{dx} . \qquad (A-7)$$

Equation (A-7) is the desired form of the Bernoulli equation and is used in the following derivations.

In addition, the mean-temperature equation,

$$m = \frac{\rho \delta}{\phi_1} \quad , \tag{A-8}$$

and the Prandtl-Meyer relationship are needed to describe the flow. To complete the mathematical description of the problem, the three semi-empirical parameters F(K), C(K), and D(K) are introduced and are described by

$$F = F(K) = \frac{\phi_1 w_1 \gamma}{K^2} - \left(1 - \frac{\gamma-1}{2} w_e^2\right) = \frac{\phi_1 w_1 \gamma}{K^2} - t$$

$$k = \left(\frac{d\delta}{dx} - \tan\theta\right) = C(K) \frac{\mu_e a_t}{m} \tag{A-9}$$

$$c_f = \frac{D(K) \mu_e a_t}{m} \quad .$$

The five equations, (A-3), (A-4), (A-7), (A-8), and the Prandtl-Meyer expression, plus the three semi-empirical relationships (A-9), are sufficient to account for the eight variables involved in the problem.

The first step in the development of the differential equations requires expanding the momentum equation (A-3), collecting terms, and eliminating the pressure gradient term by using equation (A-7), thus giving

$$\frac{dK}{dx} = \left(1-K\right) \frac{1}{m} \frac{dm}{dx} + \left[\frac{\rho \gamma w_e \delta}{m w_e \left(1 - \frac{\gamma-1}{2} w_e^2\right)} - \frac{K}{w_e}\right] \frac{dw_e}{dx} - \frac{\rho c_f}{2 \phi_e m} \quad .$$

The definition for ϕ_e given above and the identity $\phi_1 = \frac{\rho\delta}{m}$ allows the second term on the right-hand side to be rewritten as

$$\frac{dK}{dx} = (1-K)\frac{1}{m}\frac{dm}{dx} + \left[\frac{\phi_1}{\phi_e} - K\right]\frac{1}{w_e}\frac{dw_e}{dx} - \frac{P c_f}{2\phi_e m} \quad .$$

The definition for F is used to show that $\left[\frac{\phi_1}{\phi_e} - K\right] = \frac{FK}{t}$.

In addition, $\frac{1}{w_e}\frac{dw_e}{dx}$ can be written as

$$\frac{1}{w_e}\frac{dw_e}{dx} = \frac{1}{\left(1+\frac{\gamma-1}{2}M_e^2\right)M_e}\frac{dM_e}{dx} = \frac{t}{M_e}\frac{dM_e}{dx} \quad .$$

After $\zeta = m/\mu_t a_t$ is rearranged and differentiated, it is easily shown that

$$\frac{1}{m}\frac{dm}{dx} = \frac{1}{\zeta}\frac{d\zeta}{dx} \quad .$$

These three substitutions transform the momentum equation into

$$\frac{dK}{dx} = (1-K)\frac{1}{\zeta}\frac{d\zeta}{dx} + \frac{FK}{M_e}\frac{dM_e}{dx} - \frac{P c_f}{2\phi_e m} \quad .$$

Finally, the definition of c_f from (A-9) is employed to obtain the desired form of the momentum equation

$$\frac{dK}{dx} = (1-K)\frac{1}{\zeta}\frac{d\zeta}{dx} + \frac{FK}{M_e}\frac{dM_e}{dx} - \frac{PD(K)\mu_e a_t}{2\phi_e m^2} \quad . \qquad \text{(A-10)}$$

By utilizing the definitions for C(K), $\frac{d\bar{m}}{dx}$, $\frac{1}{m}\frac{dm}{dx}$, m, and t, the continuity equation, (A-2), may be written as

$$\frac{1}{\zeta}\frac{d\zeta}{dx} = \frac{C(K)}{\zeta^2\mu_e}\rho_e u_e t^2. \qquad \text{(A-11)}$$

This form of the continuity equation is then inserted into the last term of the momentum equation, (A-10), to give

$$\frac{dK}{dx} - \frac{FK}{M_e}\frac{dM_e}{dx} = (1-K)\frac{1}{\zeta}\frac{d\zeta}{dx} - \sigma(1-K)\frac{1}{\zeta}\frac{d\zeta}{dx}$$

where $\sigma(K) = \dfrac{D(K)}{2(1-K)C(K)}$.

For convenience, this equation may be written as

$$\frac{dK}{dx} - \frac{FK}{M_e}\frac{dM_e}{dx} = (1-K)(1-\sigma)\frac{1}{\zeta}\frac{d\zeta}{dx} = (1-K)(1-\sigma)\frac{1}{m}\frac{dm}{dx} \quad . \qquad \text{(A-12)}$$

In addition to (A-12), another fundamental equation is developed; this one being derived from the definition of the boundary layer thickness. It is shown on page 658 of the original Crocco and Lees (2) paper that

$$\delta = \frac{mK(F+t)}{\gamma P W_e} \quad . \qquad \text{(A-13)}$$

After equation (A-13) is differentiated with respect to x,

$$\frac{d\delta}{dx} = \frac{\left\{mK\left[\frac{dF}{dK}\frac{dK}{dx} + \frac{dt}{dM_e}\frac{dM_e}{dx}\right] + (F+t)\left[m\frac{dK}{dx} + K\frac{dm}{dx}\right]\right\}\gamma P W_e}{(\gamma P W_e)^2}$$

$$- \frac{\gamma m K(F+t)\left[W_e\frac{dP}{dx} + P\frac{dW_e}{dx}\right]}{(\gamma P W_e)^2} \qquad \text{(A-14)}$$

is obtained. From the definition of mixing in (A-9), this can be written

$$\frac{d\delta}{dx} = \tan\theta + \frac{C(K)}{\zeta}\frac{T_e}{T_t} = \tan\theta + \frac{C(K)\,t}{\zeta} \quad .$$

This expression may be substituted into (A-14), and after substitution of the Bernoulli equation it becomes

$$K\frac{dF}{dK}\frac{dK}{dx} + \frac{K(1-\gamma)M_e}{(1+\frac{\gamma-1}{2}M_e^2)}\frac{dM_e}{dx} + \frac{(F+t)K}{m}\frac{dm}{dx} + \frac{K(F+t)w_e\gamma}{(1-\frac{\gamma-1}{2}w_e^2)}\frac{1}{w_e}\frac{dw_e}{dx}$$

$$-K(F+t)\frac{1}{w_e}\frac{dw_e}{dx} = \left[\tan\theta + \frac{C(K)\,t}{\zeta}\right]\frac{\gamma P w_e}{m} .$$

Similar terms are combined, and with the substitutions

$$\frac{1}{w_e}\frac{dw_e}{dx} = \frac{t}{M_e}\frac{dM_e}{dx} \qquad \text{and} \qquad w_e = \frac{M_e}{(1+\frac{\gamma-1}{2}M_e^2)^{1/2}} ,$$

this equation can be written

$$\left[F+t+K\frac{dF}{dK}\right]\frac{dK}{dx} - \left[K(F+t)(1-\frac{3\gamma-1}{2}w_e^2) + Kt(\gamma-1)w_e^2\right]\frac{1}{M_e}\frac{dM_e}{dx}$$

$$= \frac{-(F+t)K}{m}\frac{dm}{dx} + \left[\tan\theta + \frac{C(K)t}{\zeta}\right]\frac{\gamma P w_e}{m} .$$

The right-hand side is modified by making use of the relationships

$$m = \frac{\rho\delta}{\phi_1} , \qquad \phi_1 = \frac{K}{\gamma w_e}\left[F+t\right] ,$$

$$\frac{dm}{dx} = \frac{\rho}{\phi_e}\left(\frac{d\delta}{dx} - \tan\theta\right) , \qquad m = \zeta\mu_t a_t ,$$

and

$$t = \left(1 - \frac{\gamma-1}{2}w_e^2\right)$$

to obtain

$$\left[F+t+K\frac{dF}{dK}\right]\frac{dK}{dx} - \left[K(F+t)\left(1-\frac{3\gamma-1}{2}w_e^2\right) + Kt(\gamma-1)w_e^2\right]\frac{1}{M_e}\frac{dM_e}{dx}$$

$$= \frac{\rho_e u_e t^2}{\mu_e \zeta}\left[\tan\theta + \frac{C(K)}{\zeta}\left(t - K(F+t)\right)\right] \qquad \text{(A-15)}$$

which is the second fundamental equation.

Both equations (A-12) and (A-15) have x appearing only in the derivatives. By solving these two equations simultaneously, x may be eliminated, resulting in the desired set of non-linear first order ordinary differential equations. The two equations are multiplied by $dx/d\zeta$, where $dx/d\zeta$ is obtained from (A-11), and after some algebraic manipulations, are written as

$$\left[F+t+K\frac{dF}{dK}\right]\frac{dK}{d\zeta}-\frac{KF}{M_e}\left[F+t+K\frac{dF}{dK}\right]\frac{dM_e}{d\zeta}=\frac{(1-\sigma)(1-K)}{\zeta}\left[F+t+K\frac{dF}{dK}\right] \qquad \text{(A-12a)}$$

and

$$\left[F+t+K\frac{dF}{dK}\right]\frac{dK}{d\zeta}-\left[K(F+t)\left(1-\frac{3\gamma-1}{2}w_e^2\right)+Kt(\gamma-1)w_e^2\right]\frac{1}{M_e}\frac{dM_e}{d\zeta}$$
$$=\left[\frac{\tan\theta}{C(K)}+\frac{C(K)\left[t-K(F+t)\right]}{\zeta\,C(K)}\right]. \qquad \text{(A-15a)}$$

Equation (A-12a) is subtracted from (A-15a); the definition for t is used, and after manipulation, the desired expression for $dM_e/d\zeta$,

$$\frac{dM_e}{d\zeta}=\frac{-M_e}{C(K)}\left\{\frac{\frac{C(K)}{\zeta}\left[t-K(F+t)-(1-\sigma)(1-K)\left(F+t+K\frac{dF}{dK}\right)\right]+\tan\theta}{K(F+t)\left(1-\frac{(3\gamma-1)}{2}M_e^2t\right)+(\gamma-1)KM_e^2t^2-KF\left(F+t+K\frac{dF}{dK}\right)}\right\}, \qquad \text{(A-16)}$$

is obtained.

By dropping the common coefficient in (A-12a),

$$\frac{dK}{d\zeta}-\frac{KF}{M_e}\frac{dM_e}{d\zeta}=\frac{(1-\sigma)(1-K)}{\zeta} \qquad \text{(A-12b)}$$

remains. Equation (A-16) is substituted into (A-12b) and in solving for $dK/d\zeta$, the second desired differential equation,

$$\frac{dK}{d\zeta} = \frac{-KF}{C(K)} \left\{ \frac{\left\{ \frac{C}{S} \left[t - K(F+t) - \frac{(1-K)(1-\sigma)}{KF} \left(K(F+t)\left(1 - \frac{3\gamma-1}{2} M_e^2 t\right) + KM_e^2 t^2 (\gamma-1) \right) \right] + \tan\theta \right\}}{K(F+t)\left(1 - \frac{3\gamma-1}{2} M_e^2 t\right) + (\gamma-1)\left(KM_e^2 t^2\right) - KF\left(F + t + K\frac{dF}{dK}\right)} \right\} \qquad \text{(A-17)}$$

is obtained. These two differential equations, (A-16) and (A-17), form the basis for the numerical solutions. Prior to the beginning of reattachment, these equations are tailored to the particular region by specifying the behavior of the three semi-empirical parameters.

x-length Equation

To relate the solution of equations (A-16) and (A-17) to a meaningful pressure distribution, the numerical integration results must be transformed back into the real plane.

The derivation starts with the continuity equation (A-4). With the perfect gas relationship and definitions for ϕ_e, w_e, ζ, and t, this equation becomes

$$\frac{dm}{dx} = \frac{\rho_e u_e t C(K) a_t}{\zeta} \qquad \text{(A-18)}$$

This equation, after being integrated, results in an expression for determining x-distance locations. Since the separation point is the reference location for starting the interaction calculations, the integrations for x-distance must proceed upstream and downstream from this point. Substitution of $dm = \mu_t a_t d\zeta$ into (A-18) gives

$$dx = \frac{\zeta \mu_t \, d\zeta}{\rho_e u_e t C(K)} .$$

Both sides are divided by x_s, and with the definition $Re_{x_s} = \frac{\rho_\infty u_\infty x_s}{\mu_\infty}$,

$$\frac{dx}{x_s} = \frac{5d\varsigma\ \mu_t \rho_\infty u_\infty}{Re_{x_s} \rho_e u_e t C(K) \mu_\infty}$$

is obtained. The isentropic relationships,

$$\frac{T_e}{T_t} = \frac{1}{\left(1 + \frac{\gamma-1}{2} M_e^2\right)} \quad ,$$

$$\frac{P_e}{P_t} = \left(1 + \frac{\gamma-1}{2} M_e^2\right) \quad ,$$

and

$$\frac{\rho_\infty}{\rho_e} = \left[\frac{1+\frac{\gamma-1}{2} M_e^2}{1+\frac{\gamma-1}{2} M_\infty^2}\right]^{\frac{1}{\gamma-1}} \quad ,$$

together with the assumed temperature-viscosity relationship are used in transforming the previous equation into

$$\frac{dx}{x_s} = \frac{\left(1+\frac{\gamma-1}{2} M_\infty^2\right)^2}{Re_{x_s}} \frac{M_\infty}{M_e} \left[\frac{1+\frac{\gamma-1}{2} M_e^2}{1+\frac{\gamma-1}{2} M_\infty^2}\right]^{\frac{3\gamma-1}{2(\gamma-1)}} \frac{5d\varsigma}{C(K)} \quad . \qquad \text{(A-19)}$$

Equation (A-19) is now integrated between some arbitrary x-location and the separation point to give

$$\frac{1}{x_s}\int_x^{x_s} dx = \frac{\left(1+\frac{\gamma-1}{2} M_\infty^2\right)^2}{Re_{x_s}} \int_\varsigma^{\varsigma_s} \frac{M_\infty}{M_e C(K)} \left[\frac{1+\frac{\gamma-1}{2} M_e^2}{1+\frac{\gamma-1}{2} M_\infty^2}\right]^{\frac{3\gamma-1}{2(\gamma-1)}} 5d\varsigma$$

or

$$\frac{x_s - x}{x_s} = \frac{\left(1+\frac{\gamma-1}{2} M_\infty^2\right)^2}{Re_{x_s}} \int_{\zeta}^{\zeta_s} \frac{M_\infty}{M_e C(K)} \left[\frac{1+\frac{\gamma-1}{2} M_e^2}{1+\frac{\gamma-1}{2} M_\infty^2}\right]^{\frac{3\gamma-1}{2(\gamma-1)}} \zeta d\zeta . \quad \text{(A-20)}$$

Equation (A-20) is used to find the x-location which corresponds to each step in the numerical integration process.

Reattachment Equations

In keeping with the simplicity that was mentioned in Chapter III, it is assumed that the mixing and skin friction are negligible in the reattachment process. This means C(K) = 0, D(K) = 0, and consequently, $\sigma(K) = 0$. The generalization that the reattachment process is principally an inviscid flow is supported by Chapman, Kuehn, and Larson's (3) experiments. The only parameter left undefined is F(K), which we know to be associated with the velocity profile shape since it is related to the mean-temperature profile.

Rather than tailoring the generalized equations (A-16) and (A-17) to this region, it is easier to start from (A-12) and (A-15) and then to derive new simpler expressions. From the definition of the mixing parameter C(K), it is obvious that dm/dx = 0 when C(K) = 0. With this substitution, (A-12) becomes

$$\frac{dK}{dx} - \frac{FK}{M_e}\frac{dM_e}{dx} = 0$$

or

$$\frac{dM_e}{dK} = \frac{M_e}{KF} . \quad \text{(A-21)}$$

Equation (A-21) expresses the change in local Mach number throughout the reattachment process.

The second differential equation is obtained by substituting

$$\frac{dM_e}{dx} = -\frac{M_e}{KF}\frac{dK}{dx} \qquad \text{and} \qquad w_e^2 = M_e^2 t$$

into (A-15). After rearrangement, this gives

$$\frac{dx}{dK} = \frac{x_s\left[F+t+K\frac{dF}{dK} - \left(\frac{F+t}{F}\right)\left(1-\frac{3\gamma-1}{2}M_e^2 t\right) - \left(\frac{\gamma-1}{F}\right)M_e^2 t^2\right]}{Re_{x_s}\,\frac{t^2\tan\theta}{\zeta}}, \qquad \text{(A-22)}$$

which relates changes in K to changes in x-location. The value for F must be determined such that the desired pressure distribution is obtained. The selection of F is discussed in Chapters IV and V.

Hypersonic Limit Equations

Boundary layer calculations can commence from one of two general starting conditions, both of which depend on the characteristics of the external flow field. One of these, called the vorticity interaction, results from an effective blunting of the plate's leading edge and, as a result, affects the way the boundary layer grows initially. This type of interaction is important in the analysis of flows over blunted slender bodies and on blunt bodies at low values of Reynolds number. In this type of interaction the vorticity outside the boundary layer may be sufficiently large that it influences the boundary layer structure even though the layer is relatively thin. The vorticity interaction cannot be handled by the analysis presented in this thesis.

The second type, called the pressure interaction, results from the relatively large outward streamline deflection induced by a thick

boundary layer at hypersonic speeds. At high Reynolds numbers and subsonic or low supersonic speeds, the local streamline deflection induced by the boundary layer is of the order of the reciprocal of the square root of the local Reynolds number. At hypersonic speeds the streamline deflection is of the order of its value at low supersonic speeds multiplied by M_∞^2. On slender bodies, the induced pressure due to the interaction is of the order of the streamline deflection times M_∞. A pressure interaction of this order of magnitude may become very important when M_∞ is large.

Only the pressure interaction resulting from two-dimensional flow past a sharp leading-edge flat plate has been considered. A sharp leading edge implies that it has no essential affect on the inviscid pressure distribution along the surface. According to Hayes and Probstein (32), a sharp leading edge exists whenever the leading edge radius is small enough to make the Reynolds number based on this thickness on the order of 100 or less. In the case of high Mach numbers, the viscous effects far outweigh any inviscid effects associated with a finite leading edge radius.

The hypersonic interaction problem then becomes one of determining solutions for a classical Prandtl boundary layer which has been subjected to an initially unknown external pressure gradient and vorticity field, but which, through the hypersonic inviscid flow relations depends on the rate of growth of the boundary layer itself. The viscous boundary layer must be considered to be distinct from the inviscid shock layer. If the two were to coincide, the mass flow in the boundary layer would have to equal the mass flow passing through the shock.

Therefore, the shock layer contains both an inviscid region and the boundary layer.

Previous investigations have found that the pressure interaction could be divided quite naturally into two asymptotic regions, called strong and weak interaction zones respectively. On a flat plate the strong interaction zone would be close to the leading edge, while the weak interaction zone would be farther downstream. According to this concept, the effects produced in the weak interaction region by the self-induced pressure gradient are essentially perturbations superposed on an already existing uniform flow. The strong interaction region is characterized by the fact that the streamline inclination induced by the viscous layer becomes larger, and the pressure gradient and viscous stress gradient terms are of the same order of magnitude. The pressures along the plate for both types of interaction have been correlated in terms of an interaction parameter. This parameter varies directly with the cube of the Mach number and inversely as the square root of the local Reynolds number.

The values of ε and ζ are needed at the Blasius point in order to match the conditions at the beginning of the interaction. It has been shown by Crocco (33) that the value of ζ for Blasius type flow in a weak pressure interaction can be given by

$$\zeta_b = \frac{t\ Re_{\delta^{**}}}{(1-K_b)} \quad , \tag{A-23}$$

where $Re_{\delta^{**}} \approx \sqrt{A}\ \sqrt{Re_{x_b}}$. The undefined coefficient, A, has a numerical value of .44 and is called the momentum parameter. This value applies to both adiabatic and non-adiabatic flows with zero pressure gradient.

When there is a pressure gradient, the momentum parameter is defined by

$$N = A + B\,n$$

with $n \neq 0$ corresponding with a non-zero pressure gradient, and B is affected by the presence of heat transfer. Cohen and Reshotko (34) have tabulated the various heat transfer, wall shear, and momentum parameters.

The derivation of ε_b begins with the two general differential equations (A-16) and (A-17). The semi-empirical values for C(K) and D(K) at the Blasius point are substituted into the definition for $\sigma(K)$, giving

$$\sigma(K) = \frac{D(K)}{2(1-K)\,C(K)} = 0.974 \cong 1.0 \quad .$$

With the assumption that Blasius type flow can be represented by $\sigma(K)$ equal to unity, equations (A-16) and (A-17) become

$$\frac{dK}{d\xi} = \left(\frac{-K\,F}{C\,d}\right)\left\{\frac{C}{\xi}\left[t - K(F+t)\right] + \tan\theta\right\} \qquad \text{(A-24)}$$

and

$$\frac{dM_e}{d\xi} = \left(\frac{-M_e}{C\,d}\right)\left\{\frac{C}{\xi}\left[t - K(F+t)\right] + \tan\theta\right\}\left(\frac{M_e}{K\,F}\right)\frac{dK}{d\xi} \quad , \qquad \text{(A-25)}$$

where

$$d = K(F+t)\left(1 - \frac{3\gamma-1}{2}M_e^2 t\right) + K(\gamma-1)M_e^2 t^2 - KF\left(F+t+K\frac{dF}{dK}\right) .$$

When these two equations are combined and solved for tan θ, the following expression is obtained:

$$\tan\theta = \left.\frac{-C\left[t - K(F+t)\right]}{\xi}\right|_{K=K_b} . \qquad \text{(A-26)}$$

The streamline direction for the outer edge of the boundary layer at the Blasius point can also be given by the Prandtl-Meyer relationship. For convenience, at the small angles of θ which occur at the Blasius point, this quantity may be approximated by

$$\tan\theta \cong \theta \cong \frac{-\sqrt{M_\infty^2-1}\ \varepsilon_b}{M_\infty\left(1+\frac{\gamma-1}{2}M_\infty^2\right)} \quad . \tag{A-27}$$

The errors introduced by this assumption are small and can be ignored. For example, the largest error occurs at Mach 10 and corresponds to an ε of -.85 and $\theta = 2.5^\circ$. In this case, the approximate form of the Prandtl-Meyer relationship gives a value which is 7 percent smaller than the exact value. This error decreases rapidly with decreasing Mach number and is less than 1 percent below Mach 5.0.

Equations (A-26) and (A-27) are solved for ε_b to obtain the following expression:

$$\varepsilon_b = \frac{M_\infty\left(1+\frac{\gamma-1}{2}M_\infty^2\right)C(1-K)\left[\bar{t}-K(F+\bar{t})\right]}{\sqrt{M_\infty^2-1}\ \sqrt{A}\ \sqrt{Re_{x_b}}\ \bar{t}} \quad .$$

This equation, with the definition of t, may be reduced to

$$\varepsilon_b \left\{\frac{M_\infty\left(1+\frac{\gamma-1}{2}M_\infty^2\right)C\left(1-K_b\right)^2}{\sqrt{M_\infty^2-1}\ \sqrt{A}\ \sqrt{Re_{x_b}}}\right\}\left[1-\frac{KF}{(1-K)}\left(1+\frac{\gamma-1}{2}M_\infty^2\right)\right]. \tag{A-28}$$

The values of ζ and ε given by equations (A-23) and (A-28) are used as the quantities which must be matched at the start of the interaction. They apply only to plates with sharp leading edges and assume that a weak hypersonic pressure interaction exists.

APPENDIX B

NUMERICAL INTEGRATION OF THE DIFFERENTIAL EQUATIONS

Since the solution of this problem involves a numerical solution of two ordinary first-order differential equations, a discussion of the integration technique selected is warranted. If not carefully chosen, numerical integration schemes can result in erroneous answers, particularly at some distance from the start of the integration. The integration involved in this problem starts at the separation point and advances both upstream and downstream from this point. The downstream integration is subject to greater error, because of the considerable length in K over which the integration must be performed.

In order to choose the best method with which to effect the solution of a system of ordinary differential equations it is necessary to consider several factors. These include: 1.) The accuracy required. Are errors introduced by truncation and round-off in each step, and is the method stable, i.e., how is the error incurred at each step propagated to later steps? 2.) The ease with which the error at each step may be estimated. 3.) The speed of the computation., and 4.) The ease with which the method can be programmed for computer solution.

As a compromise of these requirements, a fourth-order Runge-Kutta method was selected. The Runge-Kutta methods are widely used and have an advantage in that they do not require the use of explicit definitions nor the evaluation of derivatives higher than the first. However, the

first derivative must be evaluated four times for each step in the fourth-order integration. Runge-Kutta methods are stable and are self-starting, i.e., only the function values at a single previous point are required to obtain the functional values at the next point. A chief disadvantage of the classical Runge-Kutta method is that neither the truncation errors nor estimates of them is obtained in the calculation procedure.

In order to apply the method on high-speed digital computers, Gill (19, 20) has developed a calculation procedure which controls the growth of round-off errors and gives the highest attainable accuracy. This method compensates for the round-off errors accumulated during each step without increasing the complexity of the procedure and with no increase in storage requirements. The quantities q_0 and q_4, which account for these errors, are introduced and are illustrated by the example given below. To start the calculation procedure, q_0 is taken initially as zero. If the step calculations are performed with no round-off errors, q_4 would be zero. This is not the case in practice, and q_4 represents approximately three times the round-off error in one step. To compensate for this accumulated round-off, q_4 is used as q_0 for the next step.

The following system of equations illustrates the method. The differential equation,

$$\frac{dM_e}{d\zeta} = f(\zeta, M_e) \quad , \tag{B-1}$$

represents the equation to be solved with the values at the starting point given by $M_e = M_{e_o}$ and $\zeta = \zeta_o$. The increment of ζ for one step of the numerical process is taken as $\Delta\zeta$.

$$K_1 = \Delta\zeta \; f(\zeta_0, M_{e_0})$$

$$M_{e_1} = M_{e_0} + \tfrac{1}{2}(K_1 - 2q_0)$$

$$q_1 = q_0 + 3\left[\tfrac{1}{2}(M_{e_1} - 2q_0)\right] - \tfrac{1}{2}K_1$$

$$K_2 = \Delta\zeta \; f\left(\zeta_0 + \frac{\Delta\zeta}{2}, M_{e_1}\right)$$

$$M_{e_2} = M_{e_1} + \left(1 - \sqrt{\tfrac{1}{2}}\right)(K_2 - q_1)$$

$$q_2 = q_1 + 3\left[\left(1 - \sqrt{\tfrac{1}{2}}\right)(K_2 - q_1)\right] - \left(1 - \sqrt{\tfrac{1}{2}}\right)K_2$$

$$K_3 = \Delta\zeta \; f\left(\zeta_0 + \frac{\Delta\zeta}{2}, M_{e_2}\right)$$

$$M_{e_3} = M_{e_2} + \left(1 + \sqrt{\tfrac{1}{2}}\right)(K_3 - q_2)$$

$$q_3 = q_2 + 3\left[\left(1 + \sqrt{\tfrac{1}{2}}\right)(K_3 - q_2)\right] - \left(1 + \sqrt{\tfrac{1}{2}}\right)K_3$$

$$K_4 = \Delta\zeta \; f(\zeta_0 + \Delta\zeta, M_{e_3})$$

$$M_{e_4} = M_{e_3} + \frac{1}{6}(K_4 - 2q_3) \qquad \text{(B-2)}$$

$$q_4 = q_3 + 3\left[\tfrac{1}{6}(K_4 - 2q_3)\right] - \tfrac{1}{2}K_4 \qquad \text{(B-3)}$$

At the end of a $\Delta\zeta$ step, M_e has the value given in equation (B-2) with the correction term, to be used as q_0 in the next step, given by (B-3).

The above system of equations is employed throughout the main program and subroutines whenever a numerical integration is required.

APPENDIX C

FLOW DIAGRAMS FOR COMPUTER PROGRAMS

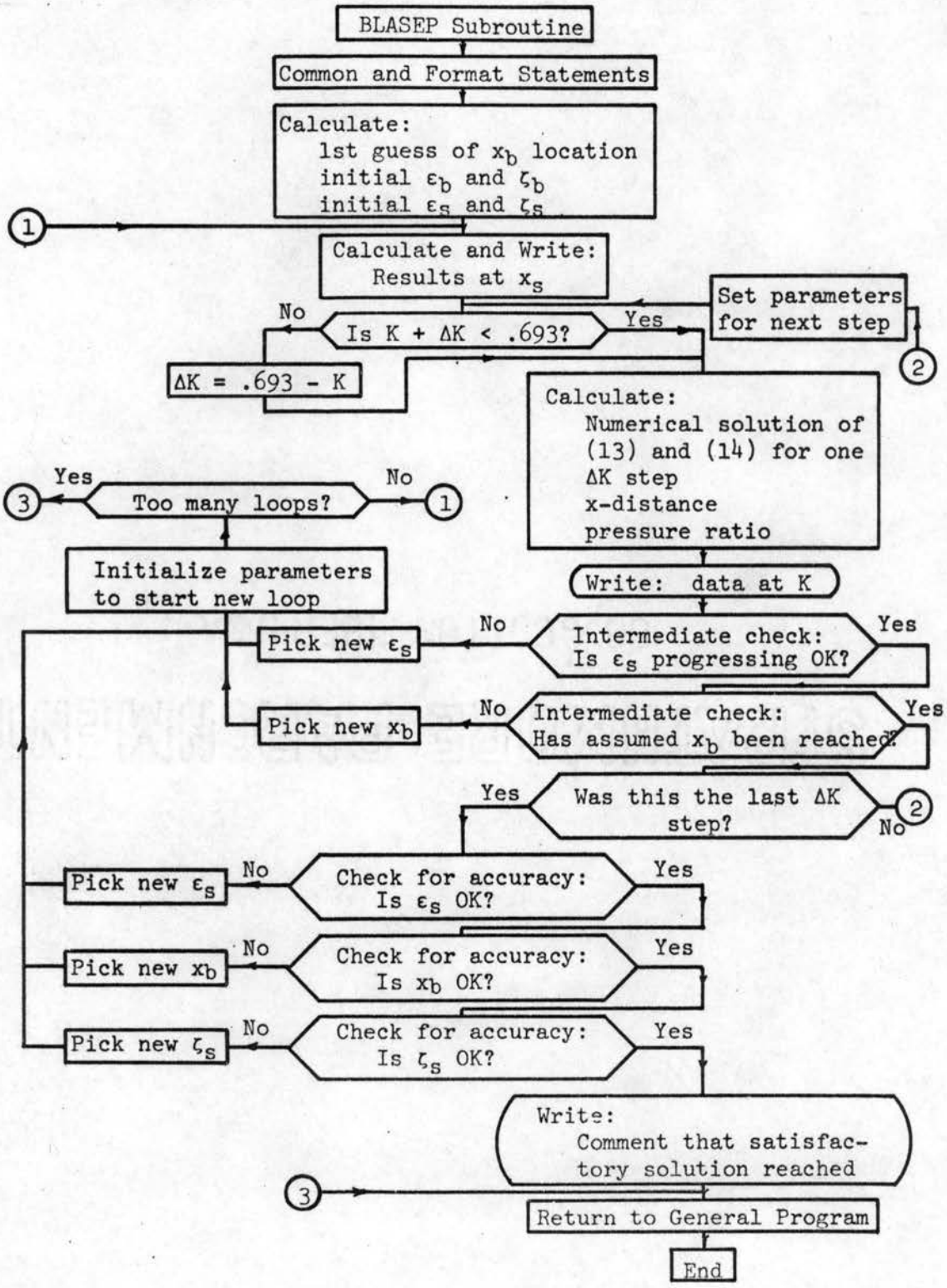

Figure 29. Computer Flow Diagram for BLASEP Subroutine

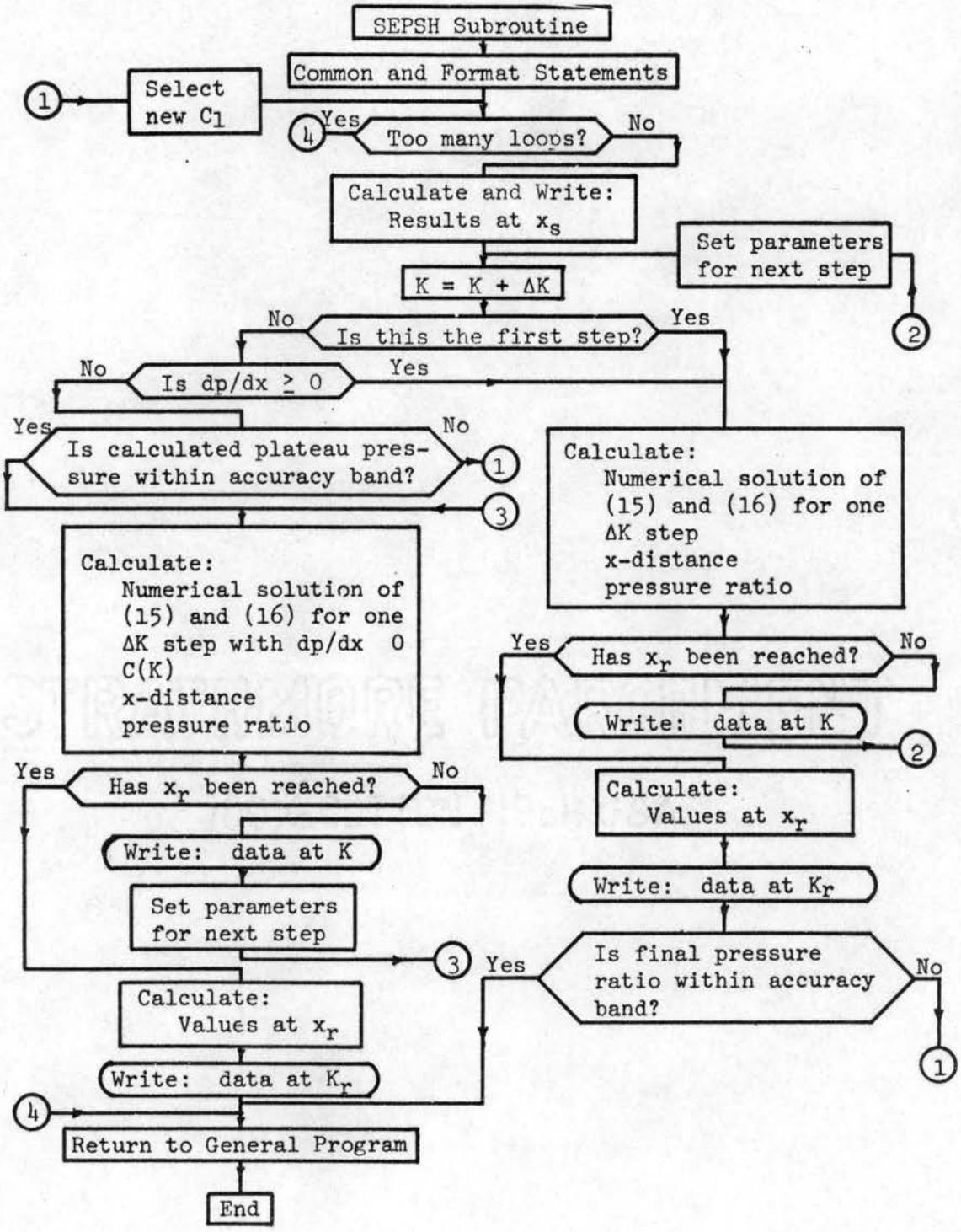

Figure 30. Computer Flow Diagram for SEPSH Subroutine

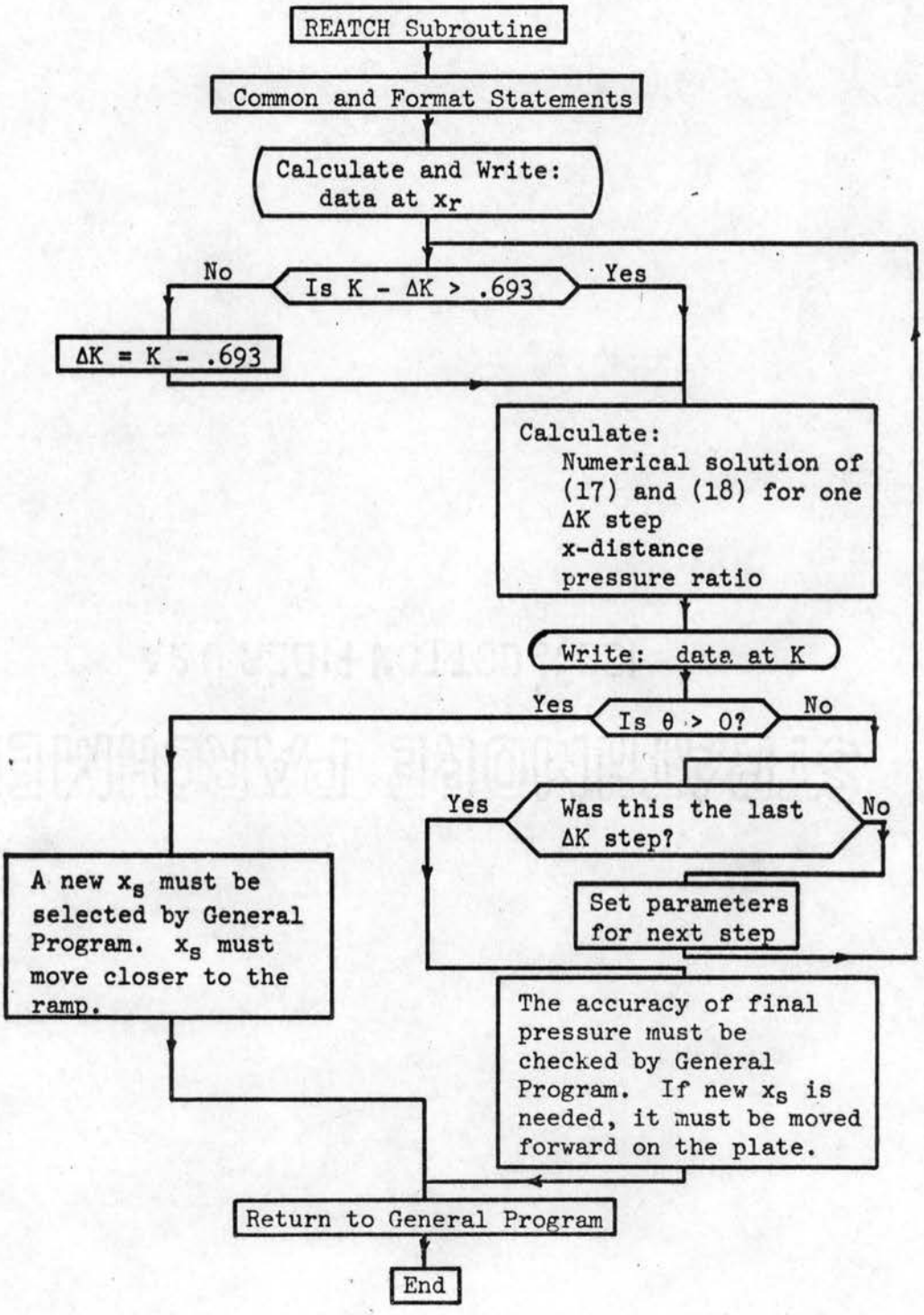

Figure 31. Computer Flow Diagram for REATCH Subroutine

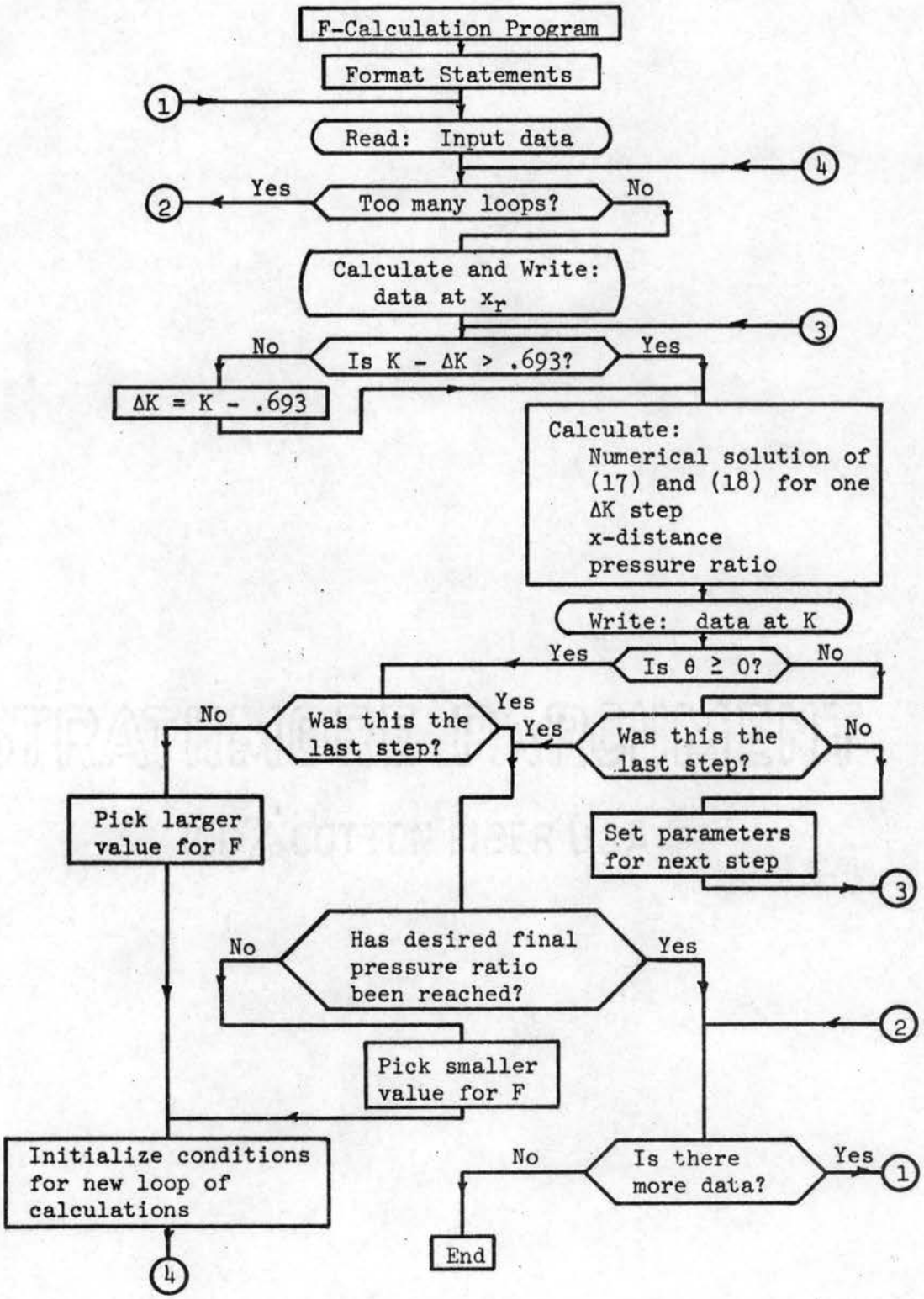

Figure 32. Computer Flow Diagram for F-Calculation Program

APPENDIX D

FORTRAN PROGRAM LISTINGS

COMPLETE INTERACTION (MAIN PROGRAM)

```
$ID          C-0001 ALEXANDER R. PETERS
$JOB                ALEXANDER R. PETERS            2527-50008
$IBJOB NAMEPR  DECK
$IBFTC DKNAME  DECK
C      LAMINAR BOUNDARY LAYER-SHOCK WAVE INTERACTION****MAIN PROGRAM
    1  FORMAT (7F10.2)
    2  FORMAT (4F10.2,8X,I2)
       COMMON XMACH,REY,XS,XSH,GAMMA,DELKI,PRP,A,XMB,XMS,ZS,ES,XB,XMDS,
      1XMF,XKSH,ZSH,XMSH,AANGLE,ANGLE,XP,C1,      PRF,XKP,PRS,PRDS,ZB,ZP,
      2FR,XRP,XKF,M1,M2,M3,M4
C      FORMAT STATEMENTS FOR FIRST PAGE OF PRINT-OUT
    4  FORMAT (1H1,///////////)
    5  FORMAT (30X,71HSHOCK WAVE-BOUNDARY LAYER INTERACTION SOLUTION FOR
      1FOLLOWING CONDITIONS/)
    6  FORMAT (39X,54H(USING A MODIFIED CROCCO-LEES MIXING PARAMETER METH
      1OD)///)
    7  FORMAT (34X,20HFREE STREAM MACH NO.,4X,3H = ,F10.2//)
    8  FORMAT (34X,21HREYNOLDS NO. PER INCH,3X,3H = ,F10.0//)
    9  FORMAT (34X,5HGAMMA,19X,3H = ,F10.3//)
   10  FORMAT (34X,17HDELTA K INCREMENT,7X,3H = ,F10.4//)
   11  FORMAT (34X,13HACCURACY TERM,11X,3H = ,F10.4//)
   12  FORMAT (34X,24HRAMP ANGLE OR EQUIVALENT)
   13  FORMAT (34X,23HSHOCK STRENGTH, RADIANS,2X,3H = ,F10.6,4H OR ,F6.2,
      18H DEGREES//)
   14  FORMAT (34X,16HSEPARATION POINT,8X,3H = ,F10.4,10H (A GUESS)//)
   15  FORMAT (34X,16HSEPARATION POINT,8X,3H = ,F10.4,35H (ADJUSTED BY PR
      1OGRAM CALCULATIONS)//)
   16  FORMAT (34X,20HCOMPLETE INTERACTION)
   17  FORMAT (34X,22HCALCULATIONS, LOOP NO.,2X,3H = ,8X,I2)
C      FORMAT STATEMENTS FOR FINAL PAGE OF PRINT-OUT
   18  FORMAT (1H1,////////)
   19  FORMAT (23X,85HA SATISFACTORY SOLUTION TO THE SHOCK WAVE-BOUNDARY
      1LAYER INTERACTION HAS BEEN REACHED////)
   20  FORMAT (10X,33HTHE PERTINENT RESULTS INCLUDE****///)
   21  FORMAT (14X,17HMACH, FREE STREAM,7X,13HMACH, BLASIUS,10X,10HMACH,
      1SEP,12X,11HMACH, SHOCK,4X,25HMACH, INVISCID DOWNSTREAM)
   22  FORMAT (17X,F10.5,12X,F10.5,12X,F10.5,12X,F10.5,12X,F10.5///)
   23  FORMAT (9X,27HMACH, ISENTROPIC DOWNSTREAM,5X,6HRE/IN.,14X,11HRE, B
      1LASIUS,15X,2HCI,13X,17HF(K)-REATTACHMENT)
   24  FORMAT (17X,F10.5,12X,F10.0,12X,F10.0,12X,F10.5,13X,F7.4///)
   25  FORMAT (17X,10HX, BLASIUS,14X,7HX, SEP.,13X,10HX, PLATEAU,13X,8HX,
      1 SHOCK,5X,26HX, REATTACHMENT STREAMLINE)
   26  FORMAT (18X,F8.4,14X,F8.4,14X,F8.4,14X,F8.4,14X,F8.4///)
   27  FORMAT (17X,11HP(SEP)/P(0),9X,15HP(PLATEAU)/P(0),8X,13HP(FINAL)/P(
      10),6X,18HP(DOWNSTREAM)/P(0),4X,19HRAMP ANGLE, DEGREES)
   28  FORMAT (18X,F9.5,13X,F9.5,13X,F9.5,13X,F9.5,14X,F6.2///)
   28  FORMAT (18X,F9.5,13X,F9.5,13X,F9.5,13X,F9.5,14X,F6.2///)
   28  FORMAT (18X,F9.5,13X,F*.5,13X,F9.5,13X,F9.5,14X,F6.2///)
   29  FORMAT (16X,13HZETA, BLASIUS,10X,10HZETA, SEP.,11X,13HZETA, PLATEA
      1U,10X,11HZETA, SHOCK,9X,14HKAPPA, PLATEAU)
   30  FORMAT (17X,F10.5,12X,F10.5,12X,F10.5,12X,F10.5,12X,F10.5///)
   31  FORMAT (16X,12HKAPPA, SHOCK)
   32  FORMAT (17X,F10.5///)
   44  FORMAT (10X,19HSOLUTION TERMINATED)
    3  READ (5,1) XMACH,REY,XSH,GAMMA,DELKI,ALPHA,XSP
       READ (5,2) A,XS,BETA1,FR,NL
       L=0
       M1=0
       M2=0
       M3=0
       M4=0
       ANGLE=ALPHA*.0174533
C      FINDING THE MACH ANGLE CORRESPONDING TO FREE STREAM MACH NO. AND
C      RAMP ANGLE ** USING THE NEWTON-RAPHSON METHOD.
   36  BETA11=BETA1
       A11=(((GAMMA+1.0)*(XMACH**2))/(2.0*((XMACH**2)*(SIN(BETA1)**2)-1.0
      1)))-1.0
       A12=((GAMMA+1.0)*(XMACH**4.0)*SIN(BETA1)*COS(BETA1))/(((XMACH**2)*
      1(SIN(BETA1)**2)-1.0)**2)
       FB1=TAN(BETA1)*A11-COTAN(ANGLE)
       FB1P=((1.0/COS(BETA1))**2)*A11-TAN(BETA1)*A12
       BETA1=BETA1-(FB1/FB1P)
       IF((ABS(BETA1-BETA11)).LT.0.00001) GO TO 37
       GO TO 36
   37  CONTINUE
   38  FORMAT (1H1,9X,7HBETA1 =,F10.6)
       WRITE (6,38) BETA1
C      CALCULATION OF DOWNSTREAM MACH NO. AND PRESSURE RATIO
       PRDS=(2.0*GAMMA*(XMACH**2)*(SIN(BETA1)**2)-(GAMMA-1.0))/(GAMMA+1.0
      1)
   53  FORMAT (10X,27HPRESSURE RATIO DOWNSTREAM =,F10.6)
       WRITE (6,53) PRDS
       A13=((GAMMA+1.0)**2)*(XMACH**4.0)*(SIN(BETA1)**2)
       A14=4.0*((XMACH**2)*(SIN(BETA1)**2)-1.0)*(GAMMA*(XMACH**2)*(SIN(BE
      1TA1)**2)+1.0)
       A15=(2.0*GAMMA*(XMACH**2)*(SIN(BETA1)**2)-(GAMMA-1.0))
       A16=((GAMMA-1.0)*(XMACH**2)*(SIN(BETA1)**2)+2.0)
       XMDS=SQRT((A13-A14)/(A15*A16))
   54  FORMAT (10X,24HDOWNSTREAM MACH NUMBER =,F10.6)
       WRITE (6,54) XMDS
C      BEGINNING OF EACH COMPLETE INTERACTION CALCULATIONS
   33  L=L+1
       IF (L.GE.NL) GO TO 3
C      WRITE FIRST PAGE OF OUTPUT
       WRITE (6,4)
       WRITE (6,5)
       WRITE (6,6)
       WRITE (6,7) XMACH
       WRITE (6,8) REY
       WRITE (6,9) GAMMA
       WRITE (6,10) DELKI
       WRITE (6,11) A
       WRITE (6,12)
       WRITE (6,13) ANGLE,ALPHA
       IF (L.EQ.1) GO TO 34
       WRITE (6,15) XS
       GO TO 35
   34  WRITE (6,14) XS
   35  WRITE (6,16)
       WRITE (6,17) L
C      CALL BLASIUS-SEPARATION SUBROUTINE
       CALL BLASEP
       IF(M1.EQ.0) GO TO 45
   46  FORMAT (10X,35HERROR IN BLASEP. SKIP TO NEXT DATA.)
       WRITE (6,46)
       GO TO 3
   45  CONTINUE
C      CALCULATION OF PLATEAU PRESSURE FROM SEMI-EMPIRICAL FORMULA
       REYXB=REY*XB
       A17=((XMB*((XMB**2)-1.0)*REYXB)**.25)
```

```
      PRP=1.0+(1.1207*GAMMA*(XMB**2))/A17
C     CALCULATING BREAKAWAY ANGLE FOR AN ASSUMED STRAIGHT DIVIDING
C     STREAMLINE
      SINBE3=SQRT((PRP*(GAMMA+1.0)+(GAMMA-1.0))/(2.0*GAMMA*(XMACH**2)))
      BETA3=ARSIN(SINBE3)
      COTBE2=TAN(BETA3)*(((GAMMA+1.0)*(XMACH**2))/(2.0*((XMACH**2)*(SIN(
     1BETA3))**2)-1.0))-1.0)
      TANBE2=1.0/COTBE2
      BETA2=ATAN(TANBE2)
   39 FORMAT (10X,4HBETA,I1,2H =,F9.6)
      N4=2
      N5=3
      WRITE (6,39)N4,BETA2
      WRITE (6,39)N5,BETA3
C     LOCATION OF REATTACHMENT POINT ON RAMP
      XRR=(XSH*TAN(ANGLE)-XS*TAN(BETA2))/(TAN(ANGLE)-TAN(BETA2))
      XRP=XSH+(XRR-XSH)/COS(ANGLE)
   55 FORMAT (10X,28HREATTACHMENT POINT ON RAMP =,F10.6)
      WRITE (6,55) XRP
C     CALL SEPARATION-SHOCK SUBROUTINE
      CALL SEPSH
      IF(M2.EQ.0) GO TO 47
   48 FORMAT (10X,34HERROR IN SEPSH. SKIP TO NEXT DATA.)
      WRITE (6,48)
      GO TO 3
   47 CONTINUE
C     CALCULATION OF EQUIVALENT TURN ANGLE FOR ISENTROPIC FLOW
      A18=1.0+((GAMMA-1.0)/2.0)*(XMB**2)
      XMF=SQRT((2.0/(GAMMA-1.0))*((A18/(PRDS**((GAMMA-1.0)/GAMMA)))-1.0)
     1)
      A3=SQRT(XMACH**2-1.0)
      TER=2.4495*ATAN(.40825*A3)-ATAN(A3)
      A19=SQRT(XMF**2-1.0)
      TEF=2.4495*ATAN(.40825*A19)-ATAN(A19)
      AANGLE=TER-TEF
      IF(XKSH.GT..693) GO TO 58
   59 FORMAT (1H0,29X,72HNOTE---KAPPA AT BEGINNING OF REATTACHMENT IS SM
     1ALLER THAN BLASIUS-KAPPA.)
   60 FORMAT (30X,69HIF A SOLUTION EXISTS, X-SEP MUST BE CLOSER TO THE P
     1LATE LEADING EDGE.)
      WRITE (6,59)
      WRITE (6,60)
      XS=.8*XS
      IF (L.GT.5) GO TO 3
      GO TO 33
   58 CONTINUE
C     CALL SHOCK-REATTACHMENT SUBROUTINE
      CALL REATCH
      IF(M3.EQ.0) GO TO 49
   50 FORMAT (10X,35HERROR IN REATCH. SKIP TO NEXT DATA.)
      WRITE (6,50)
      GO TO 3
   49 CONTINUE
      XS1=XS
      IF(M4.EQ.1) GO TO 51
      IF(ABS(PRDS-PRF).LT.(A*.5*(PRDS-1.0))) GO TO 42
      XS=XS-((PRDS-PRF)/(PRDS-1.0))*XS*.7
      GO TO 52
   51 XS=XS+XS*((XKF-.693)/(XKSH-.693))
   52 IF (XS.GE.XSH) GO TO 43
      GO TO 33
   43 XS=XS1+.5*(XSH-XS1)
      GO TO 33
C     WRITE FINAL PAGE OF PERTINENT RESULTS
   42 WRITE (6,18)
      WRITE (6,19)
      WRITE (6,20)
      WRITE (6,21)
      WRITE (6,22) XMACH,XMB,XMS,XMSH,XMDS
      WRITE (6,23)
      WRITE (6,24) XMF,REY,REYXB,CI,FR
      WRITE (6,25)
      WRITE (6,26) XB,XS,XP,XSH,XRP
      WRITE (6,27)
      WRITE (6,28) PPS,PRP,PRF,PRDS,ALPHA
      WRITE (6,29)
      WRITE (6,30) ZB,ZS,ZP,ZSH,XKP
      WRITE (6,31)
      WRITE (6,32) XKSH
      IF(XRP.LT.XEP) GO TO 56
   57 FORMAT (1H0,22X,86HNOTE---THE PROGRAM HAS FOUND A REATTACHMENT POI
     1NT WHICH IS BEYOND THE END OF THE FLAP.)
      WRITE (6,57)
   56 CONTINUE
      WRITE (6,44)
      GO TO 3
   41 STOP
      END
```

BLASEP SUBROUTINE

```
$IBFTC NAME1   DECK
      SUBROUTINE BLASEP
      COMMON XMACH,REY,XS,XSH,GAMMA,DELKI,PRP,A,XMB,XMS,ZS,ES,XB,XMDS,
     1XMF,XKSH,ZSH,XMSH,AANGLE,ANGLE,XP,C1,     PRF,XKP,PRS,PRDS,ZB,ZP,
     2FR,XRP,XKF,M1,M2,M3,M4
C     FORMAT STATEMENTS FOR STANDARD PRINT-OUT
  101  FORMAT (1H1,49X,34HBLASIUS TO SEPARATION CALCULATIONS)
  102  FORMAT (43X,45H(POINT 1 CORRESPONDS TO THE SEPARATION POINT)////)
  103  FORMAT (11X,8HLOOP NO.,10X,8HMACH NO.,8X,12HBLASIUS ZETA,4X,15HBLA
     1SIUS EPSILON,5X,12HINITIAL ZETA,4X,15HINITIAL EPSILON)
  104  FORMAT (13X,I3,14X,F6.3,10X,F10.4,8X,F10.6,8X,F10.4,8X,F10.6/)
  105  FORMAT (20X,10HX, BLASIUS,5X,13HX, SEPARATION,5X,8HX, SHOCK,7X,5HR
     1E/IN,8X,7HDELTA K,5X,18HPLAT. PRESS. RATIO)
  106  FORMAT (21X,F7.4,10X,F7.4,9X,F7.4,5X,F10.0,5X,F7.4,10X,F8.5///)
  107  FORMAT (21X,5HPOINT,5X,5HKAPPA,6X,7HEPSILON,7X,4HZETA,6X,8HMACH NO
     1.,3X,8HX-LENGTH,3X,11HPRESS RATIO,2X,7HME(AVE),5X,2HQ4,9X,3HQ14/)
  108  FORMAT (22X,I3,4X,F8.5,3X,F10.6,3X,F10.4,3X,F8.5,3X,F8.5,4X,F8.5,3
     1X,F8.5,2X,E10.3,2X,E10.3)
  109  FORMAT (1H0,3X,108HTHIS LOOP OF CALCULATIONS RESULTED IN A SATISFA
     1CTORY CONVERGENCE AT THE BLASIUS POINT.  AN ACCURACY TERM OF ,F7.4
     2,10H WAS USED.)
C     GUESS INITIAL VALUES FOR BLASIUS POINT
      XB= .8*XS
      REYXB=REY*XB
C     DEFINITION OF CONSTANTS APPEARING IN SUBROUTINE
      A1 =1.0-SQRT(.5)
      A2 =1.0+SQRT(.5)
      A3 = SQRT(XMACH**2-1.0)
      A4 =1.0+((GAMMA-1.0)/2.0)*(XMACH**2)
      A5 =(3.0*GAMMA-1.0)/2.0
      A6 =(GAMMA-1.0)/2.0
      A7 =(3.0*GAMMA-1.0)/(2.0*(GAMMA-1.0))
      A8 =GAMMA/(GAMMA-1.0)
      TER=2.4495*ATAN(.40825*A3)-ATAN(A3)
C     INITIAL VALUES FOR EPSILON AND ZETA
      EB=(((XMACH*A4)*2.2806*.094249)/(A3*SQRT(.44*REYXB)))*(1.0-((.693*
     11.59)/.307)*A4)
      XMB=XMACH +EB
      T =1.0/(1.0+A6*(XMB**2))
      A9 =1.0+((GAMMA-1.0)/2.0)*(XMB**2)
      ZB =(T*SQRT(.44*REYXB))/.307
C     SET INITIAL CONDITIONS FOR COMPUTATIONS
      Q4 =0.0
      Q14=0.0
      SUM=0.0
      L=0
      XKAPPA=.63
      N1=0
C     CALCULATION OF INITIAL GUESS FOR EPSILON AND ZETA AT THE SEP POINT
      DPR=PRP-1.0
      PRS=1.0+.5*DPR
      XME=SQRT((2.0/(GAMMA-1.0))*(A9*(PRS**((GAMMA-1.0)/(-GAMMA)))-1.0))
      XME1=XME
      EI=XME-XMACH
      T =1.0/(1.0+A6*(XME**2))
      Z1 =(T*SQRT(.44*REY*XS))/.37
      IF (ZI.GT.ZB) GO TO 156
      ZI=1.10*ZB
  156 Z1=ZI
C     CALCULATION OF INITIAL ROW OF DATA
  110 N=1
      L=L+1
      E1=EI
      B5=1.0+((GAMMA-1.0)/2.0)*(XME**2)
      PR=(A9/B5)**A8
      PR5=PR
      DELK= DELKI
C     WRITE HEADINGS AND FIRST ROW OF DATA
      WRITE (6,101)
      WRITE (6,102)
      WRITE (6,103)
      WRITE (6,104) L,XMACH,ZB,EB,ZI,EI
      WRITE (6,105)
      WRITE (6,106) XB,XS,XSH,REY,DELK,PRP
      WRITE (6,107)
      WRITE (6,108) N,XKAPPA,EI,ZI,XME,XS,PR,XME,Q4,Q14
C     BEGINNING OF STEPWISE CALCULATIONS
  111 IF (XKAPPA+DELK.LT.0.693) GO TO 112
      DELK =.693-XKAPPA
      N1=1
C     STEP-BY-STEP NUMERICAL INTEGRATION OF THE DIFFERENTIAL EQUATIONS.
C     USING GILLS RUNGE-KUTTA METHOD.
C     FINDING APPROX. AVERAGE VALUE FOR LOCAL MACH NUMBER TO USE IN
C     DZETA/DKAPPA CALCULATION.
  112 XK= XKAPPA+(DELK/2.0)
      XK1=XKAPPA
      XME=XME1
      Z=Z1
      N=N+1
      C =36.2*(XK-.63)
      D= 22.2*(XK-.63)
      F= (2.0*(1.0-XK))/(2.0*XK-1.0)
      SIGMA =D/(2.0*(1.0-XK)*C)
      E=XME-XMACH
      A10=SQRT(XME**2-1.0)
      TEP=2.4495*ATAN(.40825*A10)-ATAN(A10)
      TED=TER-TEP
      THETA=TAN(TED)
      T =1.0/(1.0+A6*(XME**2))
      DFDK = (-2.0)/((2.0*XK-1.0)**2)
      B1 =C*(XK*(F+T)*(1.0-A5*(XME**2)*T)+XK*(GAMMA-1.0)*(XME**2)*(T**2)
     1-XK*F*(F+T+XK*DFDK))
      B2 =(-XK*F)*((C/Z)*(T-XK*(F+T)-((1.0-XK)*(1.0-SIGMA)/(XK*F))*(XK*
     1(F+T)*(1.0-A5*(XME**2)*T)+XK*(XME**2)*(T**2)*(GAMMA-1.0)))+THETA)
      DZ=DELK*(B1/B2)
      Z=Z1+DZ/2.0
      B3 =-XME*((C/Z)*(T-XK*(F+T)-(1.0-SIGMA)*(1.0-XK)*(F+T+XK*DFDK))+
     1THETA)
      B4 = C*(XK*(F+T)*(1.0-A5*(XME**2)*T)+(GAMMA-1.0)*XK*(XME**2)*(T**2
     1) -XK*F*(F+T+XK*DFDK))
      DME = (B3/B4)*DZ
      XME=XME1 + DME/2.0
      XMEA=XME
C     RUNGE-KUTTA SOLUTION OF DZ/DK D.E. USING AVERAGE XME VALUE.
      I1=0
      Q0=Q4
      Z=Z1
      YG0=Z1
      XK=XK1
      E=XME-XMACH
```

```
      A10=SQRT(XME**2-1.0)
      TEP=2.4495*ATAN(.40825*A10)-ATAN(A10)
      TED=TFR-TEP
      THETA=TAN(TED)
      T =1.0/(1.0+A6*(XME**2))
  113 C =36.2*(XK-.63)
      D =22.2*(XK-.63)
      F =(2.0*(1.0-XK))/(2.0*XK-1.0)
      SIGMA=D/(2.0*(1.0-XK)*C)
      DFDK= (-2.0)/((2.0*XK-1.0)**2)
      B1 =C*(XK*(F+T)*(1.0-A5*(XME**2)*T)+XK*(GAMMA-1.0)*(XME**2)*(T**2)
     1-XK*F*(F+T+XK*DFDK))
      B2 =(-XK*F)*((C/Z)*(T-XK*(F+T)-((1.0-XK)*(1.0-SIGMA)/(XK*F))*(XK*(
     1F+T)*(1.0-A5*(XME**2)*T)+XK*(XME**2)*(T**2)*(GAMMA-1.0)))+THETA)
      DZDK=B1/B2
      I1=I1+1
      IF (I1-1.EQ.0) GO TO 114
      IF (I1-2.EQ.0) GO TO 115
      IF (I1-3.EQ.0) GO TO 116
      IF (I1-4.EQ.0) GO TO 117
  114 XKG1=DELK*DZDK
      YG1=YG0+.5*(XKG1-2.0*Q0)
      Q1=Q0+3.0*(.5*(XKG1-2.0*Q0))-.5*XKG1
      Z=YG1
      XK=XK1+DELK/2.0
      GO TO 113
  115 XKG2=DELK*DZDK
      YG2=YG1+A1*(XKG2-Q1)
      Q2 =Q1+3.0*(A1*(XKG2-Q1))-A1*XKG2
      Z=YG2
      XK= XK1+DELK/2.0
      GO TO 113
  116 XKG3 =DELK*DZDK
      YG3 =YG2+A2*(XKG3-Q2)
      Q3= Q2+3.0*(A2*(XKG3-Q2))-A2*XKG3
      Z=YG3
      XK=XK1+DELK
      GO TO 113
  117 XKG4=DELK*DZDK
      YG4 =YG3+(1.0/6.0)*(XKG4-2.0*Q3)
      Q4 =Q3+3.0*((1.0/6.0)*(XKG4-2.0*Q3))-.5*XKG4
      Z2=YG4
      XK2=XK1+DELK
      DZ=Z2-Z1
C     RUNGE-KUTTA SOLUTION OF DME/DZ D.E.
      I2=0
      Q10=Q14
      XK=XK1
      XME=XME1
      Z=Z1
      YG10=XME1
  118 C=36.2*(XK-.63)
      D=22.2*(XK-.63)
      F=(2.0*(1.0-XK))/(2.0*XK-1.0)
      SIGMA=D/(2.0*(1.0-XK)*C)
      E=XME-XMACH
      A10=SQRT(XME**2-1.0)
      TEP=2.4495*ATAN(.40825*A10)-ATAN(A10)
      TED=TFR-TEP
      THETA=TAN(TED)
      T =1.0/(1.0+A6*(XME**2))
      DFDK=(-2.0)/((2.0*XK-1.0)**2)
      B3 =-XME*((C/Z)*(T-XK*(F+T)-(1.0-SIGMA)*(1.0-XK)*(F+T+XK*DFDK))+
     1THETA)
      B4 =C*(XK*(F+T)*(1.0-A5*(XME**2)*T)+(GAMMA-1.0)*XK*(XME**2)*(T**2)
     1-XK*F*(F+T+XK*DFDK))
      DMEDZ=B3/B4
      I2=I2+1
      IF (I2-1.EQ.0) GO TO 119
      IF (I2-2.EQ.0) GO TO 120
      IF (I2-3.EQ.0) GO TO 121
      IF (I2-4.EQ.0) GO TO 122
  119 XKG11=DZ*DMEDZ
      YG11=YG10+.5*(XKG11-2.0*Q10)
      Q11 =Q10+3.0*(.5*(XKG11-2.0*Q10))-.5*XKG11
      XME=YG11
      Z=Z1+DZ/2.0
      XK= XK1+DELK/2.0
      GO TO 118
  120 XKG12=DZ*DMEDZ
      YG12 =YG11+A1*(XKG12-Q11)
      Q12 =Q11+3.0*(A1*(XKG12-Q11))-A1*XKG12
      XME =YG12
      Z=Z1+DZ/2.0
      XK =XK1+DELK/2.0
      GO TO 118
  121 XKG13 =DZ*DMEDZ
      YG13 =YG12+A2*(XKG13-Q12)
      Q13 =Q12+3.0*(A2*(XKG13-Q12))-A2*XKG13
      XME=YG13
      Z=Z2
      XK=XK2
      GO TO 118
  122 XKG14= DZ*DMEDZ
      YG14 =YG13+(1.0/6.0)*(XKG14-2.0*Q13)
      Q14 =Q13+3.0*((1.0/6.0)*(XKG14-2.0*Q13))-.5*XKG14
      XME2=YG14
      DME=XME2-XME1
      E2=XME2-XMACH
C     CALCULATION OF X-DISTANCE LOCATION.
      XME= XME1+DME/2.0
      XK =XK1+DELK/2.0
      C= 36.2*(XK-.63)
      REYXS =REY*XS
      B5 =1.0+((GAMMA-1.0)/2.0)*(XME**2)
      SX =(1.0/REYXS)*(A4**2)*(XMACH/(C*XME))*((B5/A4)**A7)*.5*((Z1**2)-
     1(Z2**2))
      SUM=SUM+SX
      X= XS*(1.0-SUM)
C     CALCULATION OF PRESSURE RATIO
      B6 =1.0+((GAMMA-1.0)/2.0)*(XME2**2)
      PR =(A9/B6)**A8
      XKAPPA=XKAPPA+DELK
C     WRITE ROW OF OUTPUT RESULTS
      WRITE (6,108) N,XKAPPA,E2,Z2,XME2,X,PR,XMEA,Q4,Q14
C     INTERMEDIATE CHECKS. TO SEE IF SATISFACTORY CONVERGENCE IS BEING
C     OBTAINED. (MODIFICATIONS INCLUDE DOWN TO STATEMENT 128)
      IF (E2.GE.EB) GO TO 127
      IF (X.LE.XB) GO TO 126
      IF (E2.GE.E1) GO TO 128
C     A NEW VALUE FOR INITIAL EPSILON IS NEEDED, SINCE A MAXIMUM IN
C     EPSILON VS. KAPPA HAS BEEN OBTAINED.
      E1 =EB-((E2-E1)/(XK2-.63))*1.05*.063
      XB1= XS-((XS-X)/(XK2-.63))*.063
      IF (XB1.GE.XB) GO TO 133
      XB=XB1
      IF(XB.GT.0.0) GO TO 163
      XB=.4*XS
  163 CONTINUE
  134 FORMAT (10X,77HINTERMEDIATE ADJUSTMENT -- EPSILON-SEPARATION (E-MA
     1X. OCCURRED) AND X-BLASIUS)
      WRITE (6,134)
```

```
      GO TO 150
  139 FORMAT (10X,63HINTERMEDIATE ADJUSTMENT -- EPSILON-SEPARATION (E-MA
     1X. OCCURRED))
  133 WRITE (6,139)
      GO TO 150
C     X-BLASIUS CORRECTION
  126 XB= XS-((XS-X)/(XK2-.63))*.063*1.05
      IF(XB.GT.0.0) GO TO 161
      XB=.4*XS
  161 CONTINUE
  135 FORMAT (10X,36HINTERMEDIATE ADJUSTMENT -- X-BLASIUS)
      WRITE (6,135)
      GO TO 150
C     EPSILON CORRECTION
  127 EI= EB-((E2-EI)/(XK2-.63))*1.05*.063
      XB1= XS-((XS-X)/(XK2-.63))*.063
      IF (XB1.GE.XB) GO TO 136
      XB=XB1
      IF(XB.GT.0.0) GO TO 162
      XB=.4*XS
  162 CONTINUE
  137 FORMAT (10X,59HINTERMEDIATE ADJUSTMENT -- EPSILON-SEPARATION AND X
     1-BLASIUS)
      WRITE (6,137)
      GO TO 150
  140 FORMAT (10X,45HINTERMEDIATE ADJUSTMENT -- EPSILON-SEPARATION)
  136 WRITE (6,140)
C     INITIALIZING PARAMETERS SO ANOTHER LOOP OF CALCULATIONS MAY BEGIN
C     AT THE SEPARATION POINT.
  150 IF (L.GE.25) GO TO 141
      REYXB =REY*XB
      EB= (((XMACH*A4)*2.2806*.094249)/(A3*SQRT(.44*REYXB)))*(1.0-((.693
     1*1.59)/.307)*A4)
      XMB=XMACH+EB
      T =1.0/(1.0+A6*(XMB**2))
      A9= 1.0+((GAMMA-1.0)/2.0)*(XMB**2)
      ZB =(T*SQRT(.44*REYXB))/.307
      IF (ZI.GT.ZB) GO TO 158
      ZI=1.10*ZB
  158 Q4=0.0
      Q14=0.0
      SUM=0.0
      N1=0
      XKAPPA=.63
      IF (EI.LT.EB) GO TO 157
      EI=EB*1.5
  157 XME=XMACH+EI
      Z1=Z1
      XME1=XME
      GO TO 110
  128 IF (N1.EQ.1) GO TO 130
C     SET INITIAL CONDITIONS FOR NEXT STEP IN THE NUMERICAL INTEGRATION
      Z1=Z2
      E1=E2
      XME1=XME2
      GO TO 111
C     CHECKING EPSILON, ZETA, AND X-BLASIUS FOR ACCURACY.
C     CHECKING EPSILON
  130 IF ((EB-E2).LT.(A*(EB-EI))) GO TO 148
      EI2=EI
      EI =EI +.7*(EB-E2)
  146 FORMAT (1H0, 9X,44HSOLUTION DID NOT RESULT IN DESIRED ACCURACY.)
      WRITE (6,146)
  147 FORMAT (10X,53HA NEW VALUE FOR EPSILON-SEPARATION HAS BEEN SELECTE
     1D.)
      WRITE (6,147)
      IF(L.LE.5) GO TO 164
      IF(ABS(EI-EI2).GT.(.5*EB)) GO TO 164
      IF(EI.GT.EI2) GO TO 168
      XB=XB-(((EI-EI2)/EB)**2)*XB
      GO TO 169
  168 XB=XB+(((EI-EI2)/EB)**2)*XB
  169 CONTINUE
  165 FORMAT (10X,29HADJUSTMENT MADE IN X-BLASIUS.)
      WRITE (6,165)
  164 CONTINUE
      GO TO 151
C     CHECKING X-BLASIUS
  148 IF (ABS(X-XB).LT.ABS(A*(XS-XB))) GO TO 143
      XB2=XB
      XB=X+.25*(XB-X)
      WRITE (6,146)
  155 FORMAT (10X,44HA NEW VALUE FOR X-BLASIUS HAS BEEN SELECTED.)
      WRITE (6,155)
      IF(L.LE.5) GO TO 166
      EI=EI-(1.0-SQRT(XB2/XB))*EB
  167 FORMAT (10X,38HADJUSTMENT MADE IN EPSILON-SEPARATION.)
      WRITE (6,167)
  166 CONTINUE
      GO TO 151
C     CHECKING ZETA
  143 IF (Z2.LT.ZB) GO TO 159
      IF ((Z2-ZB).LT.(A*(ZI-ZB))) GO TO 154
      ZI=ZI-.9*(Z2-ZB)
      GO TO 160
  159 ZI=ZI-1.1*(Z2-ZB)
  160 WRITE (6,146)
  153 FORMAT (10X,50HA NEW VALUE FOR ZETA-SEPARATION HAS BEEN SELECTED.)
      WRITE (6,153)
  151 GO TO 150
C     RETURN OR TERMINATION OF SUBROUTINE
  154 WRITE (6,109) A
      ES=E2
      ZS=Z2
      XMS=XMACH+EI
      XB=X
  170 RETURN
  141 CONTINUE
  142 FORMAT (1H0,10X,63HCONVERGENCE HAS NOT BEEN REACHED. SUBROUTINE BL
     1ASEP TERMINATED.)
      WRITE (6,142)
      M1=1
      GO TO 170
  171 STOP
      END
```

SEPSH SUBROUTINE

```
$IBFTC NAME2   DECK
      SUBROUTINE SEPSH
      COMMON XMACH,REY,XS,XSH,GAMMA,DELKI,PRP,A,XMB,XMS,ZS,ES,XB,XMDS,
     1XMP,XKSH,ZSH,XMSH,AANGLE,ANGLE,XP,C1,     PRF,XKP,PRS,PRDS,ZB,ZP,
     2PR,XAP,XKP,M1,M2,M3,M4
C     FORMAT STATEMENTS FOR STANDARD PRINT-OUT
  200 FORMAT (1H1,44X,44HSEPARATION TO SHOCK (OR CORNER) CALCULATIONS)
  201 FORMAT (44X,45H(POINT 1 CORRESPONDS TO THE SEPARATION POINT)////)
  202 FORMAT (34X,8HLOOP NO.,I3,5X,4HC1 =,F7.3,5X,24HPLATEAU PRESSURE RA
     1TIO =,F7.3//)
  203 FORMAT(7X,8HMACH NO.,7X,6HRE/IN.,8X,5HX-SEP,6X,8HX-CORNER,5X,8HZET
     1A SEP,6X,11HEPSILON SEP,5X,16HBLASIUS MACH NO.,5X,13HSEP. MACH NO.
     2)
  204 FORMAT (8X,F6.3,3X,F10.1,5X,F7.4,5X,F7.4,5X,F10.4,6X,F8.5,11X,F9.5
     1,10X,F9.5//)
  205 FORMAT (58X,15HTABLE OF VALUES//)
  206 FORMAT (11X,5HPOINT,6X,5HKAPPA,10X,4HZETA,9X,7HEPSILON,6X,13HLOCL.
     1MACH NO.,5X,10HX-LOCATION,5X,12HPRESS. RATIO,7X,4HC(K)/)
  207 FORMAT (12X,I3,6X,F8.5,5X,F10.4,5X,F9.5,7X,F9.5,7X,F9.5,7X,F9.5,7X
     1,F8.3)
  208 FORMAT (1H0, 9X,54HCORRECT PLATEAU PRESSURE RATIO REACHED USING C1
     1 SHOWN.)
  209 FORMAT (10X,15HACCURACY TERM =,F7.4/)
  210 FORMAT (1H0,10X,59HINCORRECT PLATEAU PRESSURE RATIO. NEW VALUE OF
     1C1 SELECTED.)
  211 FORMAT (1H0, 9X,64HX-SHOCK HAS BEEN REACHED BEFORE ESTABLISHING A
     1PRESSURE PLATEAU.)
  212 FORMAT (10X,45HC1 PRODUCED TOO LOW A PRESS RATIO AT X-SHOCK.)
  213 FORMAT (10X,46HC1 PRODUCED TOO HIGH A PRESS RATIO AT X-SHOCK.)
  214 FORMAT (10X,63HCORRECT PLATEAU PRESS RATIO REACHED AT X-SHOCK.  AC
     1CURACY TERM=,F7.4)
  215 FORMAT (10X,36HSEPARATION-SHOCK SOLUTION COMPLETED.)
  216 FORMAT (1H0, 9X,36HSEPARATION-SHOCK SOLUTION COMPLETED.)
C     DEFINITION OF CONSTANTS APPEARING IN SUBROUTINE
      A1 =1.0-SQRT(.5)
      A2 =1.0+SQRT(.5)
      A3 =SQRT(XMACH**2-1.0)
      A4 =1.0+((GAMMA-1.0)/2.0)*(XMACH**2)
      A5 =(3.0*GAMMA-1.0)/2.0
      A6 =(GAMMA-1.0)/2.0
      A7 =(3.0*GAMMA-1.0)/( 2.0*(GAMMA-1.0))
      A8 =GAMMA/(GAMMA-1.0)
      A9 =1.0+((GAMMA-1.0)/2.0)*(XMB**2)
      TER=2.4495*ATAN(.40825*A3)-ATAN(A3)
      L=0
      F=2.84615
      C1= 1/.8398-2.4114*XMACH+.1143*(XMACH**2)
C     SET INITIAL CONDITIONS FOR COMPUTATIONS
  217 IF (L.GE.10) GO TO 218
      Q4=0.0
      Q14=0.0
      SOM=0.0
      XKAPPA=.63
      XME1=XMS
      XK1=XKAPPA
      X=XS
      C=C1
      Z1=ZS
      N=1
      L=L+1
      XME=XMS
      DELK=DELKI
C     CALCULATIONS FOR INITIAL ROW OF DATA
      B5= 1.0+((GAMMA-1.0)/2.0)*(XME**2)
      PR =(A9/B5)**A8
      PR2=PR
C     WRITE HEADINGS AND FIRST ROW OF DATA
      WRITE (6,200)
      WRITE (6,201)
      WRITE (6,202) L,C1,PRP
      WRITE (6,203)
      WRITE (6,204) XMACH,REY,XS,XSH,ZS,ES,XMP,XMS
      WRITE (6,205)
      WRITE (6,206)
      WRITE (6,207) N,XKAPPA,ZS,ES,XMS,XS,PR,C1
C     BEGINNING OF STEPWISE CALCULATIONS
  219 IF (N.EQ.1) GO TO 220
      IF (DPDX.LE.0.0) GO TO 221
  220 N=N+1
C     STEP-BY-STEP NUMERICAL INTEGRATION OF THE DIFFERENTIAL EQUATIONS,
C     USING GILLS RUNGE-KUTTA METHOD.
C     FINDING APPROX. AVERAGE VALUE FOR LOCAL MACH NUMBER TO USE IN
C     DZETA/DKAPPA CALCULATION.
      XK=XKAPPA+(DELK/2.0)
      XK1=XKAPPA
      XME=XME1
      Z=Z1
      E=XME-XMACH
      A10=SQRT(XME**2-1.0)
      TEP=2.4495*ATAN(.40825*A10)-ATAN(A10)
      TED=TER-TEP
      THETA=TAN(TED)
      T =1.0/(1.0+A6*(XME**2))
      B1 =C*(XK*(F+T)*(1.0-A5*(XME**2)*T)+XK*(GAMMA-1.0)*(XME**2)*(T**2)
     1-XK*F*(F+T))
      B2 =(-XK*F)*((C/Z)*(T-XK*(F+T)-((1.0-XK)/(XK*F))*(XK*(F+T)*(1.0-A5
     1*(XME**2)*T)+XK*(XME**2)*(T**2)*(GAMMA-1.0)))+THETA)
      DZ=DELK*(B1/B2)
      Z= Z1+DZ/2.0
      B3 =-XME*((C/Z)*(T-XK*(F+T)-(1.0-XK)*(F+T))+THETA)
      B4 =C*(XK*(F+T)*(1.0-A5*(XME**2)*T)+(GAMMA-1.0)*XK*(XME**2)*(T**2)
     1-XK*F*(F+T))
      DME= (B3/B4)*DZ
      XME= XME1+DME/2.0
      XMEA=XME
C     RUNGE-KUTTA SOLUTION OF DZ/DK D.E. USING AVERAGE XME VALUE.
      I1=0
      QC=Q4
      Z=Z1
      YGO=Z1
      XK=XK1
      E=XME-XMACH
      A10=SQRT(XME**2-1.0)
      TEP=2.4495*ATAN(.40825*A10)-ATAN(A10)
      TED=TER-TEP
      THETA=TAN(TED)
      T =1.0/(1.0+A6*(XME**2))
  222 B1 =C*(XK*(F+T)*(1.0-A5*(XME**2)*T)+XK*(GAMMA-1.0)*(XME**2)*(T**2)
     1-XK*F*(F+T))
      B2 =(-XK*F)*((C/Z)*(T-XK*(F+T)-((1.0-XK)/(XK*F))*(XK*(F+T)*(1.0-A5
```

```
     1*(XME**2)*T)+XK*(XME**2)*(T**2)*(GAMMA-1.0)))+THETA)
      DZDK=B1/B2
      I1=I1+1
      IF (I1-1.EQ.0) GO TO 223
      IF (I1-2.EQ.0) GO TO 224
      IF (I1-3.EQ.0) GO TO 225
      IF (I1-4.EQ.0) GO TO 226
  223 XKG1=DELK*DZDK
      YG1=YG0+.5*(XKG1-2.0*Q0)
      Q1=Q0+3.0*(.5*(XKG1-2.0*Q0))-.5*XKG1
      Z=YG1
      XK=XK1+DELK/2.0
      GO TO 227
  224 XKG2=DELK*DZDK
      YG2=YG1+A1*(XKG2-Q1)
      Q2 =Q1+3.0*(A1*(XKG2-Q1))-A1*XKG2
      Z=YG2
      XK=XK1+DELK/2.0
      GO TO 222
  225 XKG3 =DELK*DZDK
      YG3 =YG2+A2*(XKG3-Q2)
      Q3= Q2+3.0*(A2*(XKG3-Q2))-A2*XKG3
      Z=YG3
      XK=XK1+DELK
      GO TO 222
  226 XKG4=DELK*DZDK
      YG4= YG3+(1.0/6.0)*(XKG4-2.0*Q3)
      Q4 =Q3+3.0*((1.0/6.0)*(XKG4-2.0*Q3))-.5*XKG4
      Z2=YG4
      XK2=XK1+DELK
      DZ=Z2-Z1
C     RUNGE-KUTTA SOLUTION OF DME/DZ D.E.
      I2=0
      Q10=Q14
      XK=XK1
      XME=XME1
      Z=Z1
      YG10=XME1
  227 E=XME-XMACH
      A10=SQRT(XME**2-1.0)
      TEP=2.4495*ATAN(.40825*A10)-ATAN(A10)
      TED=TER-TEP
      THETA=TAN(TED)
      T= 1.0/(1.0+A6*(XME**2))
      B3= -XME*((C/Z)*(T-XK*(F+T)-(1.0-XK)*(F+T))+THETA)
      B4= C*(XK*(F+T)*(1.0-A5*(XME**2)*T)+(GAMMA-1.0)*XK*(XME**2)*(T**2)
     1-XK*F*(F+T))
      DMEDZ=B3/B4
      I2=I2+1
      IF (I2-1.EQ.0) GO TO 228
      IF (I2-2.EQ.0) GO TO 229
      IF (I2-3.EQ.0) GO TO 230
      IF (I2-4.EQ.0) GO TO 231
  228 XKG11=DZ*DMEDZ
      YG11=YG10+.5*(XKG11-2.0*Q10)
      Q11 =Q10+3.0*(.5*(XKG11-2.0*Q10))-.5*XKG11
      XME=YG11
      Z=Z1+DZ/2.0
      XK= XK1+DELK/2.0
      GO TO 227
  229 XKG12=DZ*DMEDZ
      YG12 =YG11+A1*(XKG12-Q11)
      Q12= Q11+3.0*(A1*(XKG12-Q11))-A1*XKG12
      XME =YG12
      Z=Z1+DZ/2.0
      XK=XK1+DELK/2.0
      GO TO 227
  230 XKG13 =DZ*DMEDZ
      YG13 =YG12+A2*(XKG13-Q12)
      Q13 =Q12+3.0*(A2*(XKG13-Q12))-A2*XKG13
      XME=YG13
      Z=Z2
      XK=XK2
      GO TO 227
  231 XKG14=DZ*DMEDZ
      YG14 =YG13+(1.0/6.0)*(XKG14-2.0*Q13)
      Q14 =Q13+3.0*((1.0/6.0)*(XKG14-2.0*Q13))-.5*XKG14
      XME2=YG14
      DME=XME2-XME1
      E2=XME2-XMACH
C     CALCULATION OF X-DISTANCE LOCATION
      XME=XME1+DME/2.0
      XK=XK1+DELK/2.0
      REYXS=REY*XS
      B5= 1.0+((GAMMA-1.0)/2.0)*(XME**2)
      SX =(1.0/REYXS)*(A4**2)*(XMACH/(C*XME))*((B5/A4)**A7)*.5*((Z1**2)-
     1(Z2**2))
      SUM1=SUM
      SUM=SUM+SX
      X1=X
      X=XS*(1.0-SUM)
C     CALCULATION OF PRESSURE RATIO
      B6= 1.0+A6*(XME2**2)
      PR1=PR
      PR=(A9/B6)**A8
      XKAPPA=XKAPPA+DELK
      DPDX=(PR-PR1)/(X-X1)
C     CHECK TO SEE IF X-SHOCK HAS BEEN REACHED.
      IF (X.GE.XRP) GO TO 232
C     WRITE ROW OF OUTPUT RESULTS
      WRITE (6,207) N,XKAPPA,Z2,E2,XME2,X,PR,C
C     SET INITIAL CONDITIONS FOR NEXT STEP IN THE NUMERICAL INTEGRATION
      Z1=Z2
      E1=E2
      XME1=XME2
      GO TO 219
C     ADJUSTMENTS BECAUSE X-SHOCK HAS BEEN REACHED.
  232 IF (X.GT.XRP) GO TO 233
      WRITE (6,207) N,XKAPPA,Z2,E2,XME2,X,PR,C
      WRITE (6,211)
      GO TO 234
C     CALCULATING CONDITIONS FOR THE FINAL STEP WHICH ENDS AT X-SHOCK
  233 SUM=1.0-(XRP/XS)
      SX=SUM-SUM1
      Z2= SQRT((Z1**2)-(SX)/((.5/REYXS)*(A4**2)*(XMACH/(C*XME))*((B5/A4)
     1**A7)))
      DZ=Z2-Z1
      DME=DMEDZ*DZ
      XME2=XME1+DME
      E2=XME2-XMACH
      DK=DZ/DZDK
      XK2=XK1+DK
      B6= 1.0+A6*(XME2**2)
      PR=(A9/B6)**A8
      XKAPPA=XK1+DK
      X=XRP
      ZP=Z2
      XKP=XKAPPA
      XP=XRP
C     WRITE FINAL ROW OF RESULTS AT X-SHOCK
      WRITE (6,207)    N,XKAPPA,Z2,E2,XME2,X,PR,C
      WRITE (6,211)
C     CHECKING FINAL PRESSURE RATIO FOR ACCURACY
  234 IF(ABS(PR-PRP).LT.ABS(A*(PRP-PR2))) GO TO 235
      IF (PR.GT.PRP) GO TO 237
      WRITE (6,212)
      C1 =(1.0+((PRP-PR)/(PRP-PR2))*.7)*C1
C     SET NEW INITIAL CONDITIONS
```

```
      GO TO 217
  237 WRITE (6,213)
      C1 =(1.0+((PRP-PR)/(PRP-PR2))*.7)*C1
C     SET NEW INITIAL CONDITIONS
      GO TO 217
C     CHECKING THE CALCULATED PLATEAU PRESSURE FOR ACCURACY
  221 IF(ABS(PR-PRP).LT.ABS(A*(PRP-PR2))) GO TO 238
      WRITE (6,210)
      IF (PR.GT.PRP) GO TO 239
      IF((PRP-PR2).LT.0.1) GO TO 249
      C1= (1.0+((PRP-PR)/(PRP-PR2))*.7)*C1
      GO TO 217
  249 C1= (1.0+((PRP-PR)/(PRP-PR2))*.25)*C1
      GO TO 217
  239 CONTINUE
      IF((PRP-PR2).LT.0.1) GO TO 250
      C1 =(1.0+((PRP-PR)/(PRP-PR2))*.7)*C1
      GO TO 217
  250 C1= (1.0+((PRP-PR)/(PRP-PR2))*.25)*C1
      GO TO 217
  238 WRITE (6,208)
      WRITE (6,209) A
      XP=X
      XKP=XKAPPA
      ZP=Z2
C     SOLUTION IN THE PRESSURE PLATEAU REGION
C     SOLVING DZ/DK D.E. USING GILLS RUNGE-KUTTA METHOD.
  240 XK1=XKAPPA
      XME=XME1
      E=XME-XMACH
      B5= 1.0+((GAMMA-1.0)/2.0)*(XME**2)
      A10=SQRT(XME**2-1.0)
      TEP=2.4495*ATAN(.40825*A10)-ATAN(A10)
      TED=TER-TEP
      THETA=TAN(TED)
      T= 1.0/(1.0+A6*(XME**2))
      Q4=0.0
C     BEGIN STEPWISE CALCULATIONS.
  241 I3=0
      N=N+1
      Q0=Q4
      Z=Z1
      YG0=Z1
      XK=XK1
  242 C= (-THETA*Z)/(T-XK*(F+T)-(1.0-XK)*(F+T))
      B1= C*(XK*(F+T)*(1.0-A5*(XME**2)*T)+XK*(GAMMA-1.0)*(XME**2)*(T**2)
     1-XK*F*(F+T))
      B2= (-XK*F)*((C/Z)*(T-XK*(F+T)-((1.0-XK)/(XK*F))*(XK*(F+T)*(1.0-A5
     1*(XME**2)*T)+XK*(XME**2)*(T**2)*(GAMMA-2.0)))+THETA)
      DZDK=B1/B2
      I3=I3+1
      IF (I3-1.EQ.0) GO TO 243
      IF (I3-2.EQ.0) GO TO 244
      IF (I3-3.EQ.0) GO TO 245
      IF (I3-4.EQ.0) GO TO 246
  243 XKG1=DELK*DZDK
      YG1=YG0+.5*(XKG1-2.0*Q0)
      Q1=Q0+3.0*(.5*(XKG1-2.0*Q0))-.5*XKG1
      Z=YG1
      XK=XK1+DELK/2.0
      C2=C
      GO TO 242
  244 XKG2=DELK*DZDK
      YG2=YG1+A1*(XKG2-Q1)
      Q2=Q1+3.0*(A1*(XKG2-Q1))-A1*XKG2
      Z=YG2
      XK=XK1+DELK/2.0
      C3=C
      GO TO 242
  245 XKG3=DELK*DZDK
      YG3 =YG2+A2*(XKG3-Q2)
      Q3= Q2+3.0*(A2*(XKG3-Q2))-A2*XKG3
      Z=YG3
      XK=XK1+DELK
      C4=C
      GO TO 242
  246 XKG4=DELK*DZDK
      YG4=YG3+(1.0/6.0)*(XKG4-2.0*Q3)
      Q4= Q3+3.0*((1.0/6.0)*(XKG4-2.0*Q3))-.5*XKG4
      Z2=YG4
      XK2=XK1+DELK
      XKAPPA=XK2
      C5=C
      DZ=Z2-Z1
C     CALCULATION OF X-DIXTANCE LOCATION
      XK=XK1+DELK/2.0
      C=(C2+C3+C4+C5)/4.0
      REYXS=REY*XS
      B5= 1.0+(A6*(XME**2))
      SX= (1.0/REYXS)*(A4**2)*(XMACH/(C*XME))*((B5/A4)**A7)*.5*((Z1**2)-
     1(Z2**2))
      SUM1=SUM
      SUM=SUM+SX
      X1=X
      X=XS*(1.0-SUM)
C     CHECKING TO SEE IF X-SHOCK HAS BEEN REACHED.
      IF (X.GE.XRP) GO TO 247
      WRITE (6,207)  N,XKAPPA,Z2,E2,XME2,X,PR,C5
C     SET INITIAL CONDITIONS FOR NEXT STEP IN THE NUMERICAL INTEGRATION.
      Z1=Z2
      XK1=XKAPPA
      GO TO 241
C     CALCULATING CONDITIONS FOR THE FINAL STEP WHICH ENDS AT X-SHOCK.
  247 SUM=1.0-(XRP/XS)
      SX=SUM-SUM1
      Z2= SQRT((Z1**2)-(SX)/((.5/REYXS)*(A4**2)*(XMACH/(C*XME))*((B5/A4)
     1**A7)))
      DZ=Z2-Z1
      XME2=XME
      DK=DZ/DZDK
      XK2=XK1+DK
      XKAPPA=XK2
      X=XRP
      C=C2+((C5-C2)/2.0)*((XK2-XK1)/DELK)
C     WRITE FINAL ROW OF RESULTS AT X-SHOCK.
      WRITE (6,207) N,XKAPPA,Z2,E2,XME2,X,PR,C
  235 WRITE (6,216)
      WRITE (6,209) A
      XKSH=XKAPPA
      ZSH=Z2
      XMSH=XME2
  251 RETURN
  218 CONTINUE
  248 FORMAT (1H0,10X,62HCONVERGENCE HAS NOT BEEN REACHED. SUBROUTINE SE
     1PSH TERMINATED.)
      WRITE (6,248)
      M2=1
      GO TO 251
  252 STOP
      END
```

REATCH SUBROUTINE

```
$IBFTC NAME3   DECK
      SUBROUTINE REATCH
      COMMON XMACH,REY,XS,XSH,GAMMA,DELKI,PRP,A,XMB,XMS,ZS,ES,XB,XMDS,
     1XMF,XKSH,ZSH,XMSH,AANGLE,ANGLE,XP,C1,      PRF,XKP,PRS,PPDS,ZB,ZP,
     2FR,XRP,XKF,M1,M2,M3,M4
C     REATTACHMENT SOLUTION, F(K) AS PARAMETER
C     FORMAT STATEMENTS FOR PRINT-OUT
  302 FORMAT (1H1,46X,40HREATTACHMENT SOLUTION, F(K) AS PARAMETER///)
  303 FORMAT (15X,10HMACH NO. =,F6.3,3X,8HRE/IN. =,F9.0,3X,6HZETA =,F8.3
     1,3X,3HF =,F7.4,3X,8HX,SEP. =,F7.3,3X,7HANGLE =,F8.5///)
  304 FORMAT (60X,12HTABULAR DATA//)
  305 FORMAT (20X,5HPOINT,6X,5HKAPPA,5X,7HEPSILON,6X,12HLCL MACH NO.,5X,
     110HX-DISTANCE,5X,12HPRESS. RATIO,6X,5HTHETA/)
  306 FORMAT (21X,I3,6X,F7.4,5X,F8.5,6X,F9.5,9X,F8.4,8X,F8.4,7X,F8.5)
C     CALCULATION OF CONSTANTS
      A1=1.0-SQRT(.5)
      A2=1.0+SQRT(.5)
      A3=SQRT(XMACH**2-1.0)
      A4=1.0+((GAMMA-1.0)/2.0)*(XMACH**2)
      A5=(3.0*GAMMA-1.0)/2.0
      A6=(GAMMA-1.0)/2.0
      A7=(3.0*GAMMA-1.0)/(2.0*(GAMMA-1.0))
      A8=GAMMA/(GAMMA-1.0)
      A9=1.0+A6*(XMB**2)
      TER=2.4495*ATAN(.40825*A3)-ATAN(A3)
C     CALCULATION OF INITIAL ROW OF DATA
      N=1
      M4=0
      XKAPPA=XKSH
      XME=XMSH
      E=XME-XMACH
      B5=1.0+A6*(XME**2)
      PR=(A9/B5)**A8
      PRSH=PR
C     SEMI-EMPIRICAL FORMULA FOR F(K)
      F=FR
      A10=SQRT(XME**2-1.0)
      TEP=2.4495*ATAN(.40825*A10)-ATAN(A10)
      TED=(TER-TEP)-AANGLE
      THETA=TAN(TED)
C     WRITE HEADINGS AND INITIAL ROW OF DATA
      WRITE (6,302)
      WRITE (6,303) XMACH,REY,ZSH,F,XS,AANGLE
      WRITE (6,304)
      WRITE (6,305)
      WRITE (6,306) N,XKAPPA,E,XME,XRP,PR,THETA
C     SET INITIAL CONDITIONS FOR COMPUTATIONS
      DELK=-DELKI
      XME1=XMSH
      Q4=0.0
      Q14=0.0
      E1=XME1-XMACH
      XK1=XKAPPA
      X1=XRP
      Z=ZSH
      DFDK=0.0
      REYXS=REY*XS
      N1=0
C     CHECKING IF BLASIUS FLOW REACHED
  308 IF (XKAPPA+DELK.GT.0.693) GO TO 309
      DELK=.693-XKAPPA
      N1=1
C     NUMERICAL SOLUTION FOR ONE STEP IN INTEGRATION
C     SOLUTION OF DME/DK AND DX/DK EQUATIONS
  309 I1=0
      Q0=Q4
      YG0=XME1
      XK=XK1
      X=X1
      Q10=Q14
      YG10=X1
      XME=XME1
      N=N+1
  310 A10=SQRT(XME**2-1.0)
      TEP=2.4495*ATAN(.40825*A10)-ATAN(A10)
      TED=(TER-TEP)-AANGLE
      THETA=TAN(TED)
      T=1.0/(1.0+A6*(XME**2))
      DMEDK=XME/(XK*F)
      B1=XS*(F+T+XK*DFDK-((F+T)/F)*(1.0-A5*(XME**2)*T)-((GAMMA-1.0)/F)*(
     1XME**2)*(T**2) )
      B2=REYXS*(T**2)*(THETA/Z)
      DXDK=B1/B2
      I1=I1+1
      IF(I1-1.EQ.0) GO TO 311
      IF(I1-2.EQ.0) GO TO 312
      IF(I1-3.EQ.0) GO TO 313
      IF(I1-4.EQ.0) GO TO 314
  311 XKG1=DELK*DMEDK
      YG1=YG0+.5*(XKG1-2.0*Q0)
      Q1=Q0+3.0*(.5*(XKG1-2.0*Q0))-.5*XKG1
      XME=YG1
      XKG11=DELK*DXDK
      YG11=YG10+.5*(XKG11-2.0*Q10)
      Q11=Q10+3.0*(.5*(XKG11-2.0*Q10))-.5*XKG11
      X=YG11
      XK=XK1+DELK/2.0
      GO TO 310
  312 XKG2=DELK*DMEDK
      YG2=YG1+A1*(XKG2-Q1)
      Q2=Q1+3.0*(A1*(XKG2-Q1))-A1*XKG2
      XME=YG2
      XKG12=DELK*DXDK
      YG12=YG11+A1*(XKG12-Q11)
      Q12=Q11+3.0*(A1*(XKG12-Q11))-A1*XKG12
      X=YG12
      XK=XK1+DELK/2.0
      GO TO 310
  313 XKG3=DELK*DMEDK
      YG3=YG2+A2*(XKG3-Q2)
      Q3=Q2+3.0*(A2*(XKG3-Q2))-A2*XKG3
      XME=YG3
      XKG13=DELK*DXDK
      YG13=YG12+A2*(XKG13-Q12)
      Q13=Q12+3.0*(A2*(XKG13-Q12))-A2*XKG13
      X=YG13
      XK=XK1+DELK
      GO TO 310
  314 XKG4=DELK*DMEDK
      YG4=YG3+(1.0/6.0)*(XKG4-2.0*Q3)
```

```
      Q4=Q3+3.0*((1.0/6.0)*(XKG4-2.0*Q3))-.5*XKG4
      XME2=YG4
      XKG14=DELK*DXDK
      YG14=YG13+(1.0/6.0)*(XKG14-2.0*Q13)
      Q14=Q13+3.0*((1.0/6.0)*(XKG14-2.0*Q13))-.5*XKG14
      X2=YG14
      DME=XME2-XME1
      E2=XME2-XMACH
      DX=X2-X1
      X=X1+DX
C     CALCULATION OF PRESSURE RATIO
      B6=1.0+A6*(XME2**2)
      PR=(A9/B6)**A8
      XKAPPA=XKAPPA+DELK
      IF (THETA.GE.0.0) GO TO 315
      WRITE (6,306) N,XKAPPA,E2,XME2,X,PR,THETA
      IF (N1.EQ.1) GO TO 315
      E1=E2
      XME1=XME2
      X1=X
      XK1=XKAPPA
      IF (N.GT.100) GO TO 316
      IF (N1.EQ.1) GO TO 315
      GO TO 308
C     THETA=0 REACHED BEFORE K-BLASIUS WAS REACHED. THIS IMPLIES F(K)
C     WAS TOO SMALL. THEREFORE, A X-SEP. CLOSER TO THE HINGE CORNER IS
C     NEEDED.
 315  XKF=XKAPPA
      FR=F
      PRF=PR
      IF (N1.EQ.1) GO TO 317
      M4=1
 317  CONTINUE
      GO TO 318
 316  M3=1
 318  CONTINUE
      RETURN
      END
$ENTRY
$IBSYS
```

F - CALCULATION PROGRAM

```
$ID         B-0001 ALEXANDER R. PETERS
$JOB                ALEXANDER R. PETERS          2527-50008
$IBJOB NAMEPR  DECK
$IBFTC DKNAME  DECK
C      REATTACHMENT SOLUTION, F(K) AS PARAMETER
  300  FORMAT (7F10.2)
  301  FORMAT (7F10.2)
C      FORMAT STATEMENTS FOR PRINT-OUT
  302  FORMAT (1H1,46X,40HREATTACHMENT SOLUTION, F(K) AS PARAMETER///)
  303  FORMAT (15X,10HMACH NO. =,F6.3,3X,8HRE/IN. =,F9.0,3X,6HZETA =,F8.3
     1,3X,3HF =,F7.4,3X,8HX,SEP. =,F7.3,3X,7HANGLE =,F8.5///)
  304  FORMAT (60X,12HTABULAR DATA//)
  305  FORMAT (20X,5HPOINT,6X,5HKAPPA,5X,7HEPSILON,6X,12HLCL MACH.NO.,5X,
     110HX-DISTANCE,5X,12HPRESS. RATIO,6X,5HTHETA/)
  306  FORMAT (21X,I3,6X,F7.4,5X,F8.5,6X,F9.5,9X,F8.4,8X,F8.4,7X,F8.5)
  323  FORMAT (10X,8HLOOP NO.,I3/)
C      READ INPUT DATA
  307  READ (5,300) XMACH,REY,GAMMA,XMSH,XMB,XS,XSH
       READ (5,301) XKSH,DELK1,F,ANGLE,ZSH,PRDS,A
C      CALCULATION OF CONSTANTS
       A1=1.0-SQRT(.5)
       A2=1.0+SQRT(.5)
       A3=SQRT(XMACH**2-1.0)
       A4=1.0+((GAMMA-1.0)/2.0)*(XMACH**2)
       A5=(3.0*GAMMA-1.0)/2.0
       A6=(GAMMA-1.0)/2.0
       A7=(3.0*GAMMA-1.0)/(2.0*(GAMMA-1.0))
       A8=GAMMA/(GAMMA-1.0)
       A9=1.0+A6*(XMB**2)
       TER=2.4495*ATAN(.40825*A3)-ATAN(A3)
       L=0
C      CALCULATION OF INITIAL ROW OF DATA
  318  N=1
       L=L+1
       IF (L.GT.15) GO TO 307
       XKAPPA=XKSH
       XME=XMSH
       E=XME-XMACH
       B5=1.0+A6*(XME**2)
       PR=(A9/B5)**A8
       PRSH=PR
       A10=SQRT(XME**2-1.0)
       TEP=2.4495*ATAN(.40825*A10)-ATAN(A10)
       TED=(TER-TEP)-ANGLE
       THETA=TAN(TED)
C      WRITE HEADINGS AND INITIAL ROW OF DATA
       WRITE (6,302)
       WRITE (6,303) XMACH,REY,ZSH,F,XS,ANGLE
       WRITE (6,323) L
       WRITE (6,304)
       WRITE (6,305)
       WRITE (6,306) N,XKAPPA,F,XME,XSH,PR,THETA
C      SET INITIAL CONDITIONS FOR COMPUTATIONS
       DELK=-DELK1
       XME1=XMSH
       Q4=0.0
       Q14=0.0
       E1=XME1-XMACH
       XK1=XKAPPA
       X1=XSH
       Z=ZSH
       DFDK=0.0
       REYXS=REY*XS
       N1=0
C      CHECKING IF BLASIUS FLOW REACHED
  308  IF (XKAPPA+DELK.GT.0.693) GO TO 309
       DELK=.693-XKAPPA
       N1=1
C      NUMERICAL SOLUTION FOR ONE STEP IN INTEGRATION
C      SOLUTION OF DME/DK AND DX/DK EQUATIONS
  309  I1=0
       Q0=Q4
       YG0=XME1
       XK=XK1
       X=X1
       Q10=Q14
       YG10=X1
       XME=XME1
       N=N+1
  310  A10=SQRT(XME**2-1.0)
       TEP=2.4495*ATAN(.40825*A10)-ATAN(A10)
       TED=(TER-TEP)-ANGLE
       THETA=TAN(TED)
       T=1.0/(1.0+A6*(XME**2))
       DMEDK=XME/(XK*F)
       B1=XS*(F+T+XK*DFDK-((F+T)/F)*(1.0-A5*(XME**2)*T)-((GAMMA-1.0)/F)*(
     1XME**2)*(T**2) )
       B2=REYXS*(T**2)*(THETA/Z)
       DXDK=B1/B2
       I1=I1+1
       IF(I1-1.EQ.0) GO TO 311
       IF(I1-2.EQ.0) GO TO 312
       IF(I1-3.EQ.0) GO TO 313
       IF(I1-4.EQ.0) GO TO 314
  311  XKG1=DELK*DMEDK
       YG1=YG0+.5*(XKG1-2.0*Q0)
       Q1=Q0+3.0*(.5*(XKG1-2.0*Q0))-.5*XKG1
       XME=YG1
       XKG11=DELK*DXDK
       YG11=YG10+.5*(XKG11-2.0*Q10)
       Q11=Q10+3.0*(.5*(XKG11-2.0*Q10))-.5*XKG11
       X=YG11
       XK=XK1+DELK/2.0
       GO TO 310
  312  XKG2=DELK*DMEDK
       YG2=YG1+A1*(XKG2-Q1)
       Q2=Q1+3.0*(A1*(XKG2-Q11))-A1*XKG2
       XME=YG2
       XKG12=DELK*DXDK
       YG12=YG11+A1*(XKG12-Q11)
       Q12=Q11+3.0*(A1*(XKG12-Q11))-A1*XKG12
       X=YG12
       XK=XK1+DELK/2.0
       GO TO 310
  313  XKG3=DELK*DMEDK
       YG3=YG2+A2*(XKG3-Q2)
       Q3=Q2+3.0*(A2*(XKG3-Q2))-A2*XKG3
       XME=YG3
       XKG13=DELK*DXDK
       YG13=YG12+A2*(XKG13-Q12)
```

```
      Q13=Q12+3.0*(A2*(XKG13-Q12))-A2*XKG13
      X=YG13
      XK=XK1+DELK
      GO TO 310
  314 XKG4=DELK*DMEDK
      YG4=YG3+(1.0/6.0)*(XKG4-2.0*Q3)
      Q4=Q3+3.0*((1.0/6.0)*(XKG4-2.0*Q3))-.5*XKG4
      XME2=YG4
      XKG14=DELK*DXDK
      YG14=YG13+(1.0/6.0)*(XKG14-2.0*Q13)
      Q14=Q13+3.0*((1.0/6.0)*(XKG14-2.0*Q13))-.5*XKG14
      X2=YG14
      DME=XME2-XME1
      E2=XME2-XMACH
      DX=X2-X1
      X=X1+DX
C     CALCULATION OF PRESSURE RATIO
      B6=1.0+A6*(XME2**2)
      PR=(A9/B6)**A8
      XKAPPA=XKAPPA+DELK
      IF (THETA.GE.0.0) GO TO 315
      WRITE (6,306) N,XKAPPA,E2,XME2,X,PR,THETA
      IF (N1.EQ.1) GO TO 315
      E1=E2
      XME1=XME2
      X1=X
      XK1=XKAPPA
      IF (N.GT.100) GO TO 307
      IF (N1.EQ.1) GO TO 315
      GO TO 308
  315 CONTINUE
C     CHECKING TO SEE IF THE CORRECT F(K) HAS BEEN SELECTED.
C     CONVERGENCE SCHEME REQUIRES THAT THE CORRECT F(K) BE APPROACHED
C     FROM THE HIGH SIDE.
      IF (N1.EQ.1) GO TO 317
      F =F+ F *((XKAPPA-.693)/(XKSH-.693))*1.25
  319 FORMAT (1HO,9X,44HF(K) WAS TOO SMALL TO OBTAIN DESIRED RESULT.)
      WRITE (6,319)
      GO TO 318
  317 IF((PRDS-PR).LT.(.5*A*(PRDS-PRSH))) GO TO 321
      F=F-F*((PRDS-PR)/(PRDS-PRSH)) *1.25
  320 FORMAT (1HO,9X,44HF(K) WAS TOO LARGE TO OBTAIN DESIRED RESULT.)
      WRITE (6,320)
      GO TO 318
  322 FORMAT (1HO,9X,46HF(K) PRODUCED DESIRED RESULTS. ACCURACY TERM =,F
     16.3)
  321 WRITE (6,306) N,XKAPPA,E2,XME2,X,PR,THETA
      WRITE (6,322) A
      GO TO 307
  318 STOP
      END
$ENTRY
$IBSYS
```

VITA

Alexander Robert Peters

Candidate for the Degree of

Doctor of Philosophy

Thesis: ANALYTICAL INVESTIGATIONS OF LAMINAR SEPARATIONS USING THE "CROCCO-LEES MIXING PARAMETER" METHOD

Major Field: Mechanical Engineering

Biographical:

Personal Data: Born in Pender, Nebraska, November 17, 1936, the son of Alexander and Maude L. Peters.

Education: Received the Bachelor of Science degree from the University of Nebraska, Lincoln, Nebraska, with a major in Mechanical Engineering, in January, 1959; received the Master of Science degree from the University of Nebraska, Lincoln, Nebraska, with a major in Mechanical Engineering, in June, 1963; completed requirements for the Doctor of Philosophy degree in May, 1967.

Professional experience: Served with the United States Marine Corps as an officer-pilot from February, 1959, through June, 1962; Engineer, Aerodynamics, with the Space and Information Systems Division of North American Aviation, Downey, California, from July, 1963, to August, 1964.

Professional organizations: The author is a member of the following honorary and professional organizations: Lambda Delta Lambda, Pi Tau Sigma, Sigma Tau, Society of the Sigma Xi, American Society of Mechanical Engineers, and American Institute of Aeronautics and Astronautics.